UNIVERSIDADE ESTADUAL PAULISTA
"JÚLIO DE MESQUITA FILHO"
Câmpus de Ilha Solteira

CARLOS FRANCISCO SABILLON ANTUNEZ

MATHEMATICAL OPTIMIZATION OF UNBALANCED NETWORKS OPERATION WITH SMART GRID DEVICES

Ilha Solteira
2018

UNIVERSIDADE ESTADUAL PAULISTA
"JÚLIO DE MESQUITA FILHO"
Câmpus de Ilha Solteira

CARLOS FRANCISCO SABILLON ANTUNEZ

MATHEMATICAL OPTIMIZATION OF UNBALANCED NETWORKS OPERATION WITH SMART GRID DEVICES

Ph.D. thesis presented to the Faculty of Engineering, Campus of Ilha Solteira – UNESP, as part of the requirements for obtaining the title of PhD in Electrical Engineering. Field of knowledge: Automation.

Prof. Dr. Marcos Julio Rider Flores
Supervisor

Prof. Dr. John Fredy Franco Baquero
Co-Supervisor

Ilha Solteira

2018

FICHA CATALOGRÁFICA
Desenvolvido pelo Serviço Técnico de Biblioteca e Documentação

S116m

Sabillón Antúnez, Carlos Francisco.
Mathematical optimization of unbalanced networks operation with smart grid devices / Carlos Francisco Sabillón Antúnez. -- Ilha Solteira: [s.n.], 2018
153 f. : il.

Tese (doutorado) - Universidade Estadual Paulista. Faculdade de Engenharia de Ilha Solteira. Área de conhecimento: Automação, 2018

Orientador: Marcos Julio Rider Flores
Coorientador: John Fredy Franco Baquero
Inclui bibliografia

1. Dispositivos de redes inteligentes. 2. Operação de rede de distribuição. 3. Otimização matemática. 4. Ponto de operação em regime permanente. 5. Programação linear inteira mista.

Raiane da Silva Santos

Raiane da Silva Santos
Supervisora Técnica de Seção
Seção Técnica de Referência, Atendimento ao usuário e Documentação
Diretoria Técnica de Biblioteca e Documentação
CRB/8 - 9999

UNIVERSIDADE ESTADUAL PAULISTA

Câmpus de Ilha Solteira

CERTIFICADO DE APROVAÇÃO

TÍTULO DA TESE: Mathematical Optimization of Unbalanced Networks Operation with Smart Grid Devices

AUTOR: CARLOS FRANCISCO SABILLON ANTUNEZ
ORIENTADOR: MARCOS JULIO RIDER FLORES
COORIENTADOR: JOHN FREDY FRANCO BAQUERO

Aprovado como parte das exigências para obtenção do Título de Doutor em ENGENHARIA ELÉTRICA, área: AUTOMAÇÃO pela Comissão Examinadora:

Prof. Dr. MARCOS JULIO RIDER FLORES
Departamento de Engenharia Elétrica / Universidade Estadual de Campinas

Prof. Dr. RUBEN AUGUSTO ROMERO LAZARO
Departamento de Engenharia Elétrica / Faculdade de Engenharia de Ilha Solteira

Prof. Dr. JOSE ROBERTO SANCHES MANTOVANI
Departamento de Engenharia Elétrica / Faculdade de Engenharia de Ilha Solteira

Prof. Dr. MARIANA RESENER
Departamento de Sistemas Elétricos de Automação de Energia / Universidade Federal do Rio Grande do Sul

José Carlos de Melo Vieira Júnior
Prof. Dr. JOSE CARLOS DE MELO VIEIRA JUNIOR
Departamento de Engenharia Elétrica e de Computação / Universidade Estadual de Campinas

Ilha Solteira, 26 de março de 2018

“A mis padres Santiago y Mabel por todo el amor, la entrega y el cariño.”

Acknowledgements

Foremost, I would like to express my sincere gratitude to my supervisor Prof. Dr. Marcos J. Rider, for the continuous support on my Ph.D study and related research, for his patience, motivation, and immense knowledge. His guidance helped me in all the time of research and writing of this thesis.

I am highly in debt with my dear friend and co-supervisor Prof. Dr. John Fredy Franco, for his guidance and constant supervision as well as for providing necessary information regarding this research and also his support in completing this endeavor.

I would like to express my special gratitude and thanks to Prof. Dr. Ruben Romero, for his invaluable help since my arrival to Ilha Solteira, for his guidance, and for providing me the opportunity of joining his research team.

My sincere thanks also go to Dr. Bala Venkatesh, for offering me the internship opportunity at the Centre for Urban Energy and leading me working on diverse exciting projects.

To the ones with whom I spent the longest journeys and the best cups of coffee:

Thanks to my great buddy Ozy, not only for agreeing to work with me, but also for being a fantastic colleague, for all the help, for all those journeys of hard work together, for the ideas shared, and the effort given to our work.

Also, to my dear chum Naty many thanks for all the humongous journeys at the lab, for all the thoughts, ideas, and experiences, for the trips, for the time shared, for teaming up with me, and for all the effort and dedication to our team.

I also thank all the professors that participated in the thesis committee, especially to Prof. Dr. Jose Roberto Mantovani, for all the advice and nice wishes.

I would like to thank my friends, Miller, Melisa, and Elias, Augusto, Camila, and Angelo, Flavilene, Patricia, Laura, and Esaú, for all the nice memories.

To those with whom I have shared my house and tons of adventures, my family in Ilha Solteira: Luis and Natasha, Fredy and Lilian, Ozy, Darwin, Hector, and Juan Jose, thank you. Also sharing this stories and part of this family, to my love Julia for her patience, love, and companionship, thank you! And to our Teo for his endless happiness.

To my siblings, thank you for being such an important part of my life. Also, I would like to thank my parents Mabel and Santiago, for giving birth to me at the first place and supporting me spiritually throughout my life.

And finally, last but by no means least, to everyone in the LaPSEE... it was great sharing laboratory with all of you during the last four years.

Thanks God!

“Todo depende del punto de vista”
H. M. O. C. - “El Bambino”

Resumo

As redes de distribuição de energia elétrica devem estar preparadas para fornecer um serviço econômico e confiável a todos os clientes, bem como para integrar tecnologias relacionadas à geração distribuída, armazenamento de energia e veículos elétricos. Uma representação adequada da operação das redes de distribuição, considerando as tecnologias de redes inteligentes, é fundamental para atingir esses objetivos. Este trabalho apresenta formulações matemáticas para a operação em regime permanente das redes de distribuição, que consideram o desequilíbrio de redes trifásicas. Modelos matemáticos da operação de dispositivos relacionados à redes inteligentes presentes em redes de distribuição são desenvolvidos (e.g., dispositivos de controle volt-var, sistemas de armazenamento de energia e veículos elétricos). Além disso, características relacionadas à dependência da tensão das cargas, geração distribuída e limites térmico e de tensão também estão incluídos. Essas formulações constituem um marco matemático para a análise de otimização da operação das redes de distribuição de energia elétrica, o que possibilita modelar os processos de tomada de decisões. Objetivos diferentes relacionados a aspectos técnicos e/ou econômicos podem ser almejados dentro deste marco; Além disso, a extensão para otimização multi-período e multi-cenário é discutida. Os modelos apresentados são construídos com base em formulações de programação linear inteira mista, evitando o uso de formulações não-lineares inteiras mistas convencionais. A aplicação do marco apresentado é ilustrada em abordagens de controle para coordenação de carregamento de veículos elétricos, controle de magnitude de tensão e controle de geração distribuída renovável. Diversos métodos são desenvolvidos, com base no marco de otimização matemática, para otimizar a operação de sistemas de distribuição desbalanceados, considerando não apenas diferentes penetrações de veículos elétricos e fontes de energia renováveis, mas também a presença de sistemas de armazenamento e dispositivos de controle volt-var. A este respeito, o agendamento dinâmico e a otimização multi-período de janela rolante são frequentemente usados para alcançar uma operação ótima na rede. A eficácia e robustez das metodologias, bem como a confiabilidade do marco de otimização matemática, são verificados usando vários sistemas de teste (e.g., 123-node, 34-node e 178-node) com nós de média e baixa tensão, diferentes janelas de controle e várias disponibilidades de controle relacionadas aos dispositivos de rede inteligente.

Palavras-chave: Dispositivos de redes inteligentes. Operação de rede de distribuição. Otimização matemática. Ponto de operação em regime permanente. Programação linear inteira mista.

Abstract

Electric distribution networks should be prepared to provide an economic and reliable service to all customers, as well as to integrate technologies related to distributed generation, energy storage, and plug-in electric vehicles. A proper representation of the electric distribution network operation, taking into account smart grid technologies, is key to accomplish these goals. This work presents mathematical formulations for the steady-state operation of electric distribution networks, which consider the unbalance of three-phase grids. Mathematical models of the operation of smart grid-related devices present in electric distribution networks are developed (e.g., volt-var control devices, energy storage systems, and plug-in electric vehicles). Furthermore, features related to the voltage dependency of loads, distributed generation, and voltage and thermal limits are also included. These formulations constitute a mathematical framework for optimization analysis of the electric distribution network operation, which could assist planners in decision-making processes. Different objectives related to technical and/or economic aspects can be pursued within the framework; in addition, the extension to multi-period and multi-scenario optimization is discussed. The presented models are built based on mixed integer linear programming formulations, avoiding the use of conventional mixed integer nonlinear formulations. The application of the presented framework is illustrated throughout control approaches for plug-in electric vehicle charging coordination, voltage magnitude control, and renewable distributed generation control. Several methods are developed, based on this framework, to optimize the operation of unbalanced distribution systems considering not only different penetrations of electric vehicles and renewable energy sources but also the presence of storage systems and volt-var control devices. In this regard, dynamic scheduling and rolling multi-period optimization are often used to achieve optimal economic operation in the grid. The effective and robustness of the methodologies, as well as the reliability of the mathematical framework, are verified using many test systems (e.g., 123-node, 34-node, and 178-node) with medium and low voltage nodes, different operation control time frames, and several control availabilities related to the smart grid devices.

Keywords: Distribution network operation. Mathematical optimization. Mixed integer linear programming. Smart grids devices. Steady-state operation point.

List of Figures

List of Tables

Contents

Part I

Mathematical Modeling

1 Introduction

At the present time, high levels of reliability are demanded to power systems, as electricity is depended, among others, for industry, communication, lightning, heating and entertainment. Smart grids emerged from earlier attempts of power utilities to use the improvements on electronic technologies in order to bring a reliable supply of good quality electricity to their customers. Nowadays, smart grids stand out as the current responses in order to cope with the challenges brought by a rising electrical demand.

Since the early 1990's many authors have introduced smart grid basic concepts and techniques (ZHU, 2015). For example, in the United States, the definition of smart grids was officialized by the Energy Independence and Security Act of 2007, where is stated the following:

"It is the policy of the United States to support the modernization of the Nation's electricity transmission and distribution system to maintain a reliable and secure electricity infrastructure that can meet future demand growth and to achieve each of the following, which together characterize a Smart Grid:

1. Increased use of digital information and controls technology to improve reliability, security, and efficiency of the electric grid.
2. Dynamic optimization of grid operations and resources, with full cyber–security.
3. Deployment and integration of distributed resources and generation, including renewable resources.
4. Development and incorporation of demand response, demand-side resources, and energy-efficiency resources.
5. Deployment of 'smart' technologies (real-time, automated, interactive technologies that optimize the physical operation of appliances and consumer devices) for metering, communications concerning grid operations and status, and distribution automation.
6. Integration of 'smart' appliances and consumer devices.
7. Deployment and integration of advanced electricity storage and peak-shaving technologies, including plug-in electric and hybrid electric vehicles, and thermal storage air conditioning.
8. Provision to consumers of timely information and control options.

9. Development of standards for communication and interoperability of appliances and equipment connected to the electric grid, including the infrastructure serving the grid.

10. Identification and lowering of unreasonable or unnecessary barriers to adoption of smart grid technologies, practices, and services."

In short, all new technologies and equipment, computers, automation, and controls, working with the electrical grid in order to allow a two-way communication between utilities and customers will make up the so-called smart grids (ENERGY, 2016).

Several researchers all over the world, related to the power system area, devote their efforts to fulfill the aforementioned. Nevertheless, research has just kick started in several issues related to smart grids, and yet, its features and characteristics continue to be build and defined. Hereby, this work will focus in items 1, 2, 3 and 7 from the above, particularly in the Electric Distribution Network (EDN).

1.1 IMPACT OF THE SMART GRIDS ON THE DISTRIBUTION SYSTEMS

The EDN is the final stage in the transfer of power to individual consumers. The EDN routes power from small energy sources nearby or power substation fed by transmission lines, to residential, industrial, and commercial customers, through power lines, switches, and transformers (MOMOH., 2009). Nowadays, EDN utilities are in charge of operating the distribution network, maintaining a reliable supply of electric power to all customers connected into the grid. Traditionally, the EDN has been designed to carry the power from the sources downstream to the consumers, but lately this one-way electricity delivery model has been changing.

With the evolution of the smart grids, the distributed generation (DG) growth, and the introduction of renewable sources and energy storage systems (ESS), the classic distribution network model is evolving. All of these factors impact directly over the planning, engineering, construction, operation, and maintenance of the network. As smart grids technologies continue to strengthen, the current EDN will become a more intelligent and real-time optimized grid; in consequence, the complexity of the planning, operation, and maintenance of the EDN will increase, as new technologies and distribution practices, which offer greater efficiency, sustainability, and cost savings, are provided. Thereupon, the EDN must evolve in order to engage all network elements and participants including consumer, generators, and those that do both, in an active management seeking to fulfill technical, economic, and environmental objectives (ALEIXO et al., 2013).

EDNs, which may vary in size, topology, and structural components, must have a proper representation of all features through mathematical models in order to successfully analyze their behavior. Veritable formulations that represent:

- the operation of the EDN;
- constraints related to load conditions, DG features, and voltage and thermal limits, among others; and
- the operation of new smart grid devices,

are key to mathematically formalize decision–making regarding countless objectives related to technical and/or economic constraints.

1.2 MATHEMATICAL MODELING ON DISTRIBUTION SYSTEMS

Since mid-1960s optimization concepts and techniques have been part of the power system planning and operation. The development of strong optimization methods and algorithms and their proper application to the power system depends on a suitable representation of the EDN behavior under smart grid schemes. Hence, mathematical modeling is crucial to achieve an enhanced representation of the EDN operation, endorsing the decision-making of optimization algorithms.

Once a problem has been properly represented, it is up to the planners/operators to choose the most appropriate method in order to solve it. Heuristic and metaheuristic techniques, as well as mathematical optimization have foregrounded among those techniques to become the most commonly applied methods to problem solving in power systems. In the latest years, the accelerated advent of efficient commercial solvers based on mathematical optimization has increased the interest of researchers in the development of complex and realistic mathematical models for optimization problems in power systems. Therefore, once the mathematical model is properly defined, the commercial solver finds the best solution; i.e., the planner/operator does not need to take care of the development of the solution method.

According to the nature of the adopted formulation for the optimization problem, the corresponding mathematical model may be classified as follows:

- Linear Programming (LP), where the term 'linear' indicates that all constraints, as well as the objective function, are barren of any nonlinearity.
- Nonlinear Programming (NLP), which aims to deal with problems involving nonlinear constraints or objective function.

- Mixed Integer Linear Programming (MILP), which are a special type of LP, where all or some of the decision variables are confined to only integer values.
- Mixed Integer Nonlinear Programming (MINLP), a special type of NLP (analogue to MILP).

For each type of mathematical model there are several well-known optimization techniques. For example, LP problems can be solved by using simplex or interior point algorithms. For NLP problem one can use several traditional optimization techniques (gradient-based techniques, Lagrangian relaxation, Newton's method, successive linear programming, etc.) or an interior point algorithm. To solve MILP problems, a branch and bound algorithm, improved versions of branch and bound such as branch and price or branch and cut, Benders' decomposition, Gomory's cutting planes, among others, might be used. Finally, solving an MINLP problem is a very complicated task and there is few theory related to classical optimization in this regard. Thus, commercial solvers are assumed to solve this type of problems based on branch and bound algorithms, sensitivity and barrier methods, and interior point methods.

In the decade of 2000, commercial solvers based on classical optimization techniques excelled to become extremely efficient, taking advantage of the improvement on resolution techniques. Since then, solvers that target LP and MILP problems such as CPLEX ILOG Inc. (2009), MOSEK ApS (2009), GUROBI Inc. (2014), and similar, had become extremely efficient compared to prior versions. In counterpart, the development of specialized solvers on NLP and MINLP problems is still in progress.

Due to the aforementioned, the interest in the development of mathematical models to represent the operation and planning of power systems grew among the area-related researchers. Thereby, commercial solvers such as CPLEX have been used when the problem is represented by a LP or MILP mathematical model. On the other hand, for those cases in which the problems are represented by NLP or MINLP formulations, these formulations have been transformed into equivalent or approximated LP problems, if possible, or have been solved using solvers for NLP or MINLP problems such as KNITRO Byrd, Nocedal e Waltz (2006) or BONMIN Bonami e Lee (2007), even though NLP specialized software are not equally efficient (i.e., they cannot guarantee the global optimum of the problem and they usually demand high computational efforts).

In EDN, mathematical modeling has become an important tool, as it is widely used in operation and expansion planning problems, especially those including mixed integer programming. This is due to the fact that commonly planners and operators of power systems have to meet specific goals with limited sources. Hence, a great share of the optimization problems in power systems can be classified as 'yes' or 'no' problems, which may be represented by binary variables. Specifically, in EDN, decisions such as:

- *schedule/not schedule*, e.g., electric vehicle charging;
- *build/not build*, e.g., the construction of a distribution line;
- *K out of N*, e.g., the number of capacitors operating in a bank; and
- *N-possible values*, e.g., the tap–position of a voltage regulator;

can be optimized using mathematical models (MOMOH., 2009).

Moreover, the inclusion of smart grid devices and technologies into the EDN urge improvements in mathematical formulations previously employed to model the grid. The flexibility offered by smart grid devices demand higher levels of accuracy and resolution in the problem formulations, leading to more realistic but also more complex models. In this regard, the utilization of a three-phase representation has become crucial in the solution of problems related to EDN operation. A three-phase representation, in despite of the commonly used single-phase, takes into account the imbalance in the EDN and allows the inclusion of mutual coupling effects, conveying to a more accurate determination of the steady-state operation point.

1.3 LITERATURE REVIEW

In this section some highlighted works and articles related to mathematical optimization in EDNs are presented. Several solutions for different optimization problems on both balanced and unbalanced systems are shown.

A widely studied problem in EDNs is the expansion planning, commonly called distribution system expansion planning (DSEP) problem. Its purpose is to develop strategies in order to meet new demand, while fulfilling all technical constraints in the EDN. When solving the DSEP problem several objectives might be pursued, such as costs for new equipment, operating costs for the EDN and substation, energy losses, and reliability. Therefore, several techniques have been proposed over the years aiming to optimally solve this problem, as presented by Ganguly, Sahoo e Das (2013).

In despite of the type of planning developed (e.g., static, dynamic or pseudo–dynamic), mathematical optimization is commonly used as a solution technique. For example in Franco, Rider e Romero (2014), an MIQP problem was proposed to the DSEP, while the steady state operation of a single–phase EDN is represented by a set of linear and quadratic constraints. Later, on Tabares et al. (2016), an MILP model to solve the multistage long–term expansion planning of EDNs considering multiple alternatives was presented. Here, linearization techniques were applied to the quadratic constraints in order to represent the steady state operation of the system using only linear equations.

Further works that solve the DSEP problem, classified by the type of programming model chose, are as follows:

- Lavorato et al. (2012), Ravadanegh e Roshanagh (2014), Gomez et al. (2004), Aghaei et al. (2014), and Souza e Almeida (2010), among others that chose MINLP models. It is important to highlight that, due to high complexity in the solution of this type of problem, several works pick meta–heuristic techniques or fuzzy logic over mathematical optimization.
- Besides Franco, Rider e Romero (2014), Jabr (2013) also uses MIQP in order to model the DSEP.
- Finally, Ramirez-Rosado e Gonen (1991), Haffner et al. (2008), Tang (1996), Gonen e Ramirez-Rosado (1986), Delgado, Contreras e Arroyo (2015), and Goncalves (2013), propose MILP models to solve the DSEP problem.

All of the aforementioned use a single–phase representation of the EDN. On the other hand, in some approaches which aim to solve problems regarding the operation of the EDN, this single–phase representation may not be accurate enough. Therefore, the mutual coupling between phases is to be considered in order to avoid breaches in the EDN operation constraints.

Similarly to those works presented for DSEP, solution methodologies for the EDN operation problems use a NLP model to represent the steady state of the grid. Later, linearizations and approximations techniques are often applied to nonlinear constraints to cope with the difficulties previously foregrounded. Below, some examples are presented.

Padilha (2010) aimed to optimally determine the operation of voltage regulators (VRs) installed in the EDN with presence of DG. It shows how treating the VR tap position as an optimization problem can lead to improvements in the EDN operation, satisfiying technical solutions. MINLP models representing the single–phase EDN operation were presented, and AMPL (FOURER; GAY; KERNIGHAN, 2003) and KNITRO (BYRD; NOCEDAL; WALTZ, 2006) were used to determine the best solution.

In Melgar et al. (2014) a mixed integer second order programming formulation is presented for the operation of the EDN. This work considers the presence of DG units, switched capacitor banks CBs, VRs, and of remotely controlled switches. The mathematical formulation aims to minimize the cost of energy losses during a period of 24 hours for each level of demand by setting the appropriate adjustments, such as the injection of active and reactive power by DG units, the number of modules of switched capacitors in operation, the tap position of the VRs, and the operation of remotely controlled switches. Furthermore, this approach also considers the occurrence of a disturbance in EDNs in which DG units go out of operation. The model also represents a single–phase EDN. It was written in AMPL (FOURER; GAY; KERNIGHAN, 2003) and solved using the solver CPLEX (ILOG INC., 2009), which is specialized on solving LP problems but can also deal with second order cone representations.

Similar to Melgar et al. (2014), Goncalves, Alves e Rider (2012) presents a mathematical formulation to define the active and reactive power generation of the DG units, the number of capacitor modules in operation and the tap position of the RTs in order to minimize the daily losses on the EDN. In this work, the steady state operation of a single–phase EDN was represented by LP constraints. The resultant problem was modeled by a MILP formulation, as the tap positions and number of capacitors operating were integer values. A MILP formulation for the original model was also presented in order to show the accuracy, and both formulations were tested on an 11-node single-phase and a 42-node single-phase real test system.

An additional mixed integer second order cone programming model was presented in Macedo et al. (2015). In this work, the objective is to solve the optimal operation problem of radial EDNs considering ESSs; i.e., to minimize the total cost of energy purchased from the distribution substation and the dispatchable DGs.

A further MILP formulation was proposed by Resener et al. (2016). In this work, the objective is to minimize energy losses and voltage violations, while optimally allocating capacitor banks. The solution of the optimization problem provides site and size of the capacitor banks, the number of automatic capacitors to be connected for each load level, and the best operation point for DGs. The approach was tested in four different test systems, assuming balanced three-phase systems and loads, which are represented by equivalent single-phase circuits.

Another widely studied problem in the EDN operation is the reconfiguration of the network. This problem consists in modifying the system topology by opening or closing interconnection switches strategically allocated, keeping the EDN with a radial topology. Interconnection switches enable the reconfiguration of the system aiming to reduce energy losses, to isolate faults (system protection), and in some cases to allow preventive maintenance. In order to solve the problem of reconfiguration one has to fulfill the operational limits in the EDN. Therefore, it is necessary to know the steady state operation of the system. Hereby, several works have used mathematical optimization to solve the reconfiguration problem.

For example, Lavorato et al. (2012) represented the problem of reconfiguration of the EDN considering the presence of DG units. This work presents a literature review, a critical analysis, and a proposal for incorporating the radiality constraints in mathematical models of optimization problems for radial distribution systems. Furthermore, Borges, Franco e Rider (2014) presents a MINLP model for the reconfiguration problem of a single–phase EDNs, aiming to reduce the active power losses. Linearization techniques are later applied to achieve a MILP model, which represents, with a suitable degree of accuracy, the steady state operation of the EDN. In Franco et al. (2013), a MILP model was also used, but the presence of DG units were taken into account. Finally, Romais, Borges e Rider (2014) presented a second order conic representation to solve the reconfiguration problem.

It can be seen that the aforementioned researches used single–phase representations of the EDN. This may be due to the complexity associated to the inclusion of the mutual coupling. Although using a single–phase representation might be enough in order to solve some problems related to the EDNs, some problems require a better and more realistic representation. In this regard, fewer works are found in literature that have solved through mathematical optimization problems related to the EDN operation including a three–phase representation of the system. Some examples of this works are cited below.

In Antunez et al. (2016a), a MILP formulation is proposed to optimally control the Volt-VAr control devices installed in a balanced EDN, taking into account the presence of dispatchable DG units. The approach considers a voltage dependent load model and aims to reduce the cost of the energy purchased. It analyzes a three–phase balanced and symmetrical EDN, and it states that under these conditions, each phase may be analyzed independently as a single-phase system, assuming each circuit impedance to be the positive sequence impedance in the mathematical model.

In Robbins e Dominguez-Garcia (2016), a method to optimally define the reactive power contributions of distributed energy resources in EDN aiming to regulate bus voltages is presented. For a balanced EDN, a branch power flow quadratic programming formulation is introduced as base of the optimal power flow used to solve the voltage regulation problem. This formulation is later extended for the unbalanced three–phase case. This formulation is solved through a distributed algorithm based on the alternating direction method of multipliers. This method solves convex optimization problems by breaking them into smaller pieces, each of which are then easier to handle (BOYD et al., 2011).

Moreover, in Franco, Rider e Romero (2015) a MILP model for the electric vehicle charging coordination problem in unbalanced EDNs is proposed. Linearization techniques are applied over a MINLP model to obtain the proposed MILP formulation based on current injections. More details on this approach will be later discussed in this work.

1.4 OBJECTIVES AND CONTRIBUTIONS

EDNs should be prepared to provide an economic and reliable service to all customers, as well as to integrate technologies related to DG, ESSs, and plug-in electric vehicles (EVs). A proper representation of the EDN operation, taking into account smart grid technologies, is key to accomplish these goals. Therefore, the main objective and contribution of this work is to constitute a mathematical framework for optimization analysis of the EDN operation, which makes it possible to model decision-making processes.

Besides, to present not only mathematical formulations for the steady-state operation of EDN (which consider the unbalance of three-phase grids), but also mathematical models for the operation of smart grid-related devices present in EDN (e.g., volt-var control devices, ESSs, and plug-in EVs). Moreover, features related to the voltage dependency of loads, DG, and voltage and thermal limits are included.

Different objectives related to technical and/or economic aspects can be pursued within the framework. In addition, the extension of this framework for multi-period and multi-scenario optimization is discussed and implemented. Models are built based on mixed integer linear programming formulations, avoiding the use of conventional mixed integer nonlinear formulations.

The application of the presented framework is illustrated throughout control approaches for plug-in EV charging coordination, voltage magnitude control, and renewable DG control. Several methodologies are developed, based on this framework, to optimize the operation of unbalanced distribution systems considering not only different penetrations of EVs and renewable energy sources but also the presence of ESSs and volt-var control devices.

Aiming to meet the stated, this work is divided into two parts. Part I focuses in the study, development, and improvement of tools for the representation and analysis of the EDN operation. While Part II focuses on the development of control algorithms based on these tools, aiming to optimize the EDN operation. Here, independent algorithms are presented in each chapter, aiming to optimize the EDN operation taking advantage of different devices associated to the smart grid advent.

1.5 THESIS STRUCTURE

Specific objectives and contributions of this work are separately presented in each chapter along the document. This manuscript is organized as follows.

- Chapter 2 presents mathematical formulations that represent the steady state operation of unbalanced EDNs. The presented models are built based on linear programming formulations, enabling the use of commercial software to find optimal solutions. Besides, the mathematical representation for smart grid devices (e.g., volt-var control devices, ESSs, and plug-in EVs) is also shown. **NOTE: Results of this chapter had been accepted for publication as a chapter of**

Shahnia, A e Ledwich (2018)

- Chapter 3 proposes an algorithm to solve the optimal charging coordination of EVs considering vehicle-to-grid technology. The developed method defines an optimal charging schedule for the EVs. This charging schedule considers the EVs' arrival and departure times and their arrival state of charge, along with the energy contribution of EVs equipped with V2G technology. **NOTE: Results of this chapter had been published in Antunez et al. (2016b)**

- Chapter 4 proposes the inclusion of Volt-VAr control devices and ESSs to optimize the EDN operation. A new approach is presented, solving the EV charging coordination (EVCC) problem, while considering Volt-VAr control, ESSs operation and dispatchable DG. **NOTE: Results of this chapter had been published in Sabillon-Antunez et al. (2017), Antunez et al. (2016a)**

- Chapter 5 proposes a dynamic scheduling algorithm in order to determine the optimal operation of PV units and EVs in residential EDNs, considering ESSs. A rolling multi–period strategy based on an MILP model is used to dynamically optimize a centralized decision making in order to determine control actions for on-load tap changers (OLTCs), ESSs, PV units, and EVs connected to the network. **NOTE: Results of this chapter had been accepted for publication to the International Journal of Electrical Power and Energy Systems.**

Finally, general conclusions and future works are addressed in Chapter 6.

2 MATHEMATICAL REPRESENTATION OF UNBALANCED EDNs

Traditionally, the evaluation of the EDN state has been determined by solving a power flow (PF). The objective of the PF is to determine, given a set of specific values, the steady-state operation point of the network, i.e., obtain the voltage magnitudes, phase angles in all nodes, and derived quantities (e.g., active and reactive power flows, current magnitudes in the circuits, and power losses). The PF is a useful tool for the analysis of networks in steady-state, being widely utilized in real time operation, as well as in the EDN planning of expansion and operation. This problem is typically modeled as a system of nonlinear equations, solved through iterative methods Shirmohammadi et al. (1988), Cespedes (1990).

In this chapter, two approaches are presented aiming to model the operation of an unbalanced EDN. In contradistinction to the iterative trait proper of commonly used PF methods, these formulations can be solved using mathematical optimization; and they can be extended in order to be used as tools in optimization analysis in order to mathematically formalize decision–making regarding different objectives related to technical and/or economic constraints. Thereupon, to determine the steady-state operation point of an EDN using mathematical optimization, the operation of the grid must be modeled as a conventional mathematical programming problem (1). These problems have as a common feature the involvement of optimization. A goal is established and defined as an objective function (f) which has to be maximized or minimized by the setting of a set of control variables (x) and subject to a set of constraints.

$$\max / \min \quad f(x) \tag{1}$$

subject to:

$$g(x) \leq 0;$$
$$h(x) = 0;$$

Although the behavior of an EDN follows a set of nonlinear constraints, it is desired to reach LP representations, which avoid the complexity related to the solution of NLP problems. For this, the nonlinear set of equations is initially presented; later, linearization and approximation techniques are applied to reach an LP model, in each approach. The presented LP formulations are tested in a 123-node distribution system. The results are compared to those obtained from the specialized software OpenDSS.

2.1 CURRENT-BASED MATHEMATICAL FORMULATION

This formulation is based on the real and imaginary parts of currents through circuits and node voltages in the network. A single branch of an unbalanced EDN is depicted in Fig. 1. Each vector of voltages and currents represent the sum of the corresponding real and imaginary parts, e.g., $\overrightarrow{I} = I^{re} + jI^{im}$. Hence, the set of nonlinear mathematical relationships that represent the steady-state operation of an unbalanced EDN are written in terms of the current and voltages real and imaginary parts, the active and reactive power demanded by loads, and the circuit impedance, resistance, and reactance.

In the following formulation, consider the sets F, L, and N representing phases, circuits, and nodes, respectively. Furthermore, $V_{n,f}^{re/im}$are the real/imaginary parts of the voltage at node n and phase f, while $I_{n,f}^{Gre/im}$ and $I_{n,f}^{Dre/im}$ are the real/imaginary parts of the generated and demanded currents, respectively. $P_{n,f}^{G/D}$and $Q_{n,f}^{G/D}$ are the generated/demanded active and reactive powers. In addition, $I_{mn,f}^{re/im}$ represents the real/imaginary parts of the current through the circuit connecting nodes m and n, while $B_{mn,f}$ represents its shunt susceptance for phase f. Finally, $R_{mn,f,h}$ and $X_{mn,f,h}$ are the resistance and reactance for circuit mn between phases f and h, respectively.

From Fig. 1, we can assure that the voltage drop from node m to node n is:

$$\begin{aligned}
\begin{bmatrix} \Delta\vec{V}_{mn,a} \\ \Delta\vec{V}_{mn,b} \\ \Delta\vec{V}_{mn,c} \end{bmatrix} &= \begin{bmatrix} Z_{mn,a} & Z_{mn,a,b} & Z_{mn,a,c} \\ Z_{mn,a,b} & Z_{mn,b} & Z_{mn,b,c} \\ Z_{mn,a,c} & Z_{mn,b,c} & Z_{mn,c} \end{bmatrix} \begin{bmatrix} \vec{I}_{mn,a} \\ \vec{I}_{mn,b} \\ \vec{I}_{mn,c} \end{bmatrix} \\
&= \begin{bmatrix} Z_{mn,a}\vec{I}_{mn,a} + Z_{mn,a,b}\vec{I}_{mn,b} + Z_{mn,a,c}\vec{I}_{mn,c} \\ Z_{mn,a,b}\vec{I}_{mn,a} + Z_{mn,b}\vec{I}_{mn,b} + Z_{mn,b,c}\vec{I}_{mn,c} \\ Z_{mn,a,c}\vec{I}_{mn,a} + Z_{mn,b,c}\vec{I}_{mn,b} + Z_{mn,c}\vec{I}_{mn,c} \end{bmatrix}
\end{aligned} \tag{2}$$

Analyzing the individual case for phase a, (3) is formulated:

$$\Delta\vec{V}_{mn,a} = Z_{mn,a}\vec{I}_{mn,a} + Z_{mn,a,b}\vec{I}_{mn,b} + Z_{mn,a,c}\vec{I}_{mn,c} \tag{3}$$

Extending (3), considering that $Z_{mn,f,h} = R_{mn,f,h} + jX_{mn,f,h}$ and separating currents and voltages in their real and imaginary parts, (4) and (5) are obtained.

Figure 1 – Current-based representation of a single branch of an unbalanced EDN.

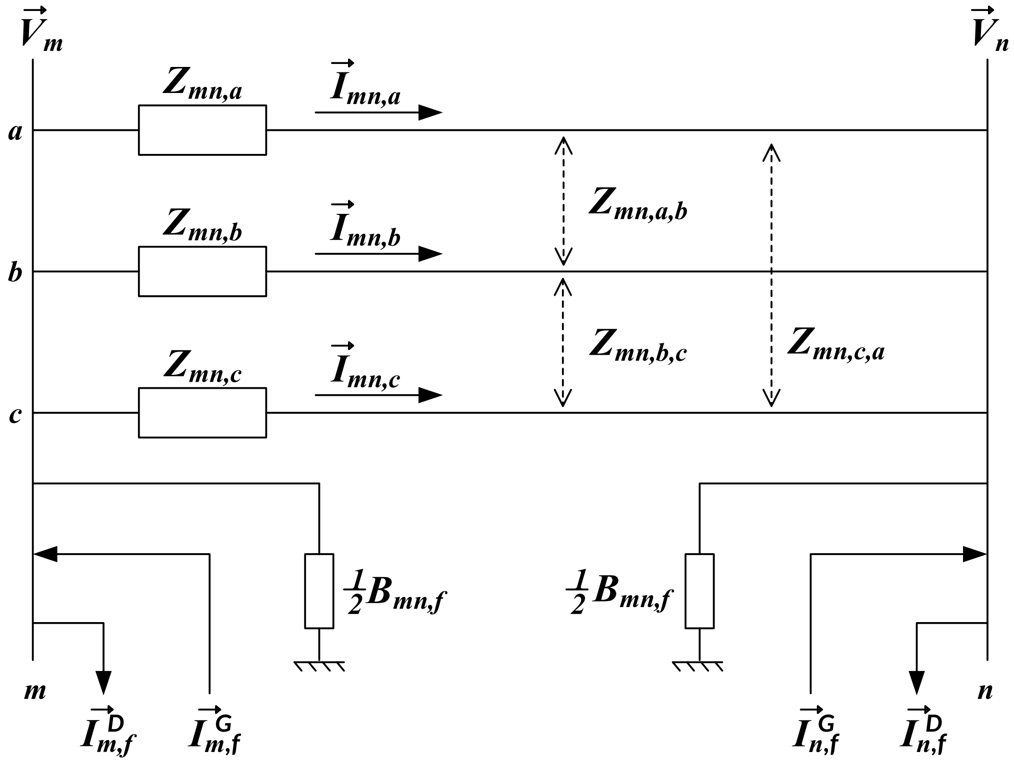

Source: Created by the author.

$$V^{re}_{m,a} - V^{re}_{n,a} = R_{mn,a}I^{re}_{mn,a} + R_{mn,a,b}I^{re}_{mn,b} + \\ R_{mn,a,c}I^{re}_{mn,c} - X_{mn,a}I^{im}_{mn,a} - X_{mn,a,b}I^{im}_{mn,b} - X_{mn,a,c}I^{im}_{mn,c} \tag{4}$$

$$V^{im}_{m,a} - V^{im}_{n,a} = R_{mn,a}I^{im}_{mn,a} + R_{mn,a,b}I^{im}_{mn,b} + \\ R_{mn,a,c}I^{im}_{mn,c} + X_{mn,a}I^{re}_{mn,a} + X_{mn,a,b}I^{re}_{mn,b} + X_{mn,a,c}I^{re}_{mn,c} \tag{5}$$

Generalizing these expressions, the voltage drop of an unbalanced EDN, written in terms of the real and imaginary parts of the voltages and currents, can be expressed by (6) and (7).

$$V^{re}_{m,f} - V^{re}_{n,f} = \sum_{h \in F} \left(R_{mn,f,h}I^{re}_{mn,h} - X_{mn,f,h}I^{im}_{mn,h} \right) \qquad \forall mn \in L, f \in F \tag{6}$$

$$V^{im}_{m,f} - V^{im}_{n,f} = \sum_{h \in F} \left(X_{mn,f,h}I^{re}_{mn,h} + R_{mn,f,h}I^{im}_{mn,h} \right) \qquad \forall mn \in L, f \in F \tag{7}$$

Furthermore, to model the complete steady-state operation of an unbalanced EDN, the first Kirchhoff's Law for the real and imaginary parts of the currents in each node is applied, as shown in (8) and (9). Hereupon, (10) and (11) establish the relationship between power, voltage and current for the loads.

$$I^{Gre}_{m,f} + \sum_{km \in L} I^{re}_{km,f} - \sum_{mn \in L} I^{re}_{mn} - \left(\sum_{km \in L} B_{km,f} + \sum_{mn \in L} B_{mn,f} \right) \frac{V^{im}_{m,f}}{2} = I^{Dre}_{m,f} \qquad \forall m \in N, f \in F \tag{8}$$

$$I^{Gim}_{m,f} + \sum_{km \in L} I^{im}_{km,f} - \sum_{mn \in L} I^{im}_{mn} - \left(\sum_{km \in L} B_{km,f} + \sum_{mn \in L} B_{mn,f} \right) \frac{V^{re}_{m,f}}{2} = I^{Dim}_{m,f} \qquad \forall m \in N, f \in F \tag{9}$$

$$P^{D}_{n,f} = V^{re}_{n,f} I^{Dre}_{n,f} + V^{im}_{n,f} I^{Dim}_{n,f} \qquad \forall n \in N, f \in F \tag{10}$$

$$Q^{D}_{n,f} = -V^{re}_{n,f} I^{Dim}_{n,f} + V^{im}_{n,f} I^{Dre}_{n,f} \qquad \forall n \in N, f \in F \tag{11}$$

Equation (12) presents the complete NLP formulation developed to determine the steady–state operation point of an unbalanced EDN.

$$\min \alpha \tag{12}$$

$$\text{subject to: (6)–(11)}$$

where, α is the objective function of the NLP model, and can be designed to minimize or maximize the network operator best interests (e.g., power losses, voltage deviation, or reliability).

Aiming to achieve a LP model based on (12), linearization techniques and approximations must be applied to the nonlinearities shown in (10) and (11). In this regard, Franco, Rider e Romero (2015) proposed the application of Taylor's approximation around an estimated point $(V^{re^*}_{n,f}, V^{im^*}_{n,f})$. Hence, (10) and (11) are rewritten, expressing the real and imaginary currents in terms of the power and voltages, as shown in (13) and (14). Those equations represent the nonlinear expressions for the real and imaginary demanded currents as the functions $g(P^D_{n,f}, Q^D_{n,f}, V^{re}_{n,f}, V^{im}_{n,f})$ and $h(P^D_{n,f}, Q^D_{n,f}, V^{re}_{n,f}, V^{im}_{n,f})$, respectively.

$$I^{Dre}_{n,f} = \frac{P^D_{n,f}V^{re}_{n,f} + Q^D_{n,f}V^{im}_{n,f}}{{V^{re}_{n,f}}^2 + {V^{im}_{n,f}}^2} = g(P^D_{n,f}, Q^D_{n,f}, V^{re}_{n,f}, V^{im}_{n,f}) \qquad \forall n \in N, f \in F \tag{13}$$

$$I^{Dim}_{n,f} = \frac{P^D_{n,f}V^{im}_{n,f} - Q^D_{n,f}V^{re}_{n,f}}{{V^{re}_{n,f}}^2 + {V^{im}_{n,f}}^2} = h(P^D_{n,f}, Q^D_{n,f}, V^{re}_{n,f}, V^{im}_{n,f}) \qquad \forall n \in N, f \in F \tag{14}$$

Hereupon, taking advantage of the relatively small and limited variation range of the voltage magnitude in a distribution network, (15) and (16) present the Taylor's approximation used to linearize (10) and (11).

$$I^{Dre}_{n,f} = g^* + \left.\frac{\partial g}{\partial V^{re}}\right|^* (V^{re}_{n,f} - V^{re^*}_{n,f}) + \left.\frac{\partial g}{\partial V^{im}}\right|^* (V^{im}_{n,f} - V^{im^*}_{n,f}) \qquad \forall n \in N, f \in F \tag{15}$$

$$I^{Dim}_{n,f} = h^* + \left.\frac{\partial h}{\partial V^{re}}\right|^* (V^{re}_{n,f} - V^{re^*}_{n,f}) + \left.\frac{\partial h}{\partial V^{im}}\right|^* (V^{im}_{n,f} - V^{im^*}_{n,f}) \qquad \forall n \in N, f \in F \tag{16}$$

Therefore, the LP model that represents the steady-state operation of an unbalanced EDN is shown in (17).

$$\min \alpha \tag{17}$$

subject to: (6)–(9), (15), and (16)

2.2 POWER-BASED MATHEMATICAL FORMULATION

An additional representation to determine the steady-state operation point of an unbalanced EDN using mathematical optimization is presented. This formulation is based on the active and reactive power flow through the circuits and the voltage magnitudes in the network. Similarly to Fig. 1, Fig. 2 shows a single branch of an unbalanced EDN, depicting the power flows through the circuits. Thus, each vector of complex power represents the sum of the active and reactive powers, i.e., $\overrightarrow{S} = P + jQ$.

For the following formulation let the sets F, L, and N, represent phases, circuits, and nodes, respectively. Besides, $\vec{V}_{n,f}$ is the voltage vector at node n and phase f, with magnitude $V_{n,f}$ and angle $\theta_{n,f}$; while, $V^{qdr}_{n,f}$ is the squared voltage magnitude at node n and

Figure 2 – Power-based representation of a single branch of an unbalanced EDN.

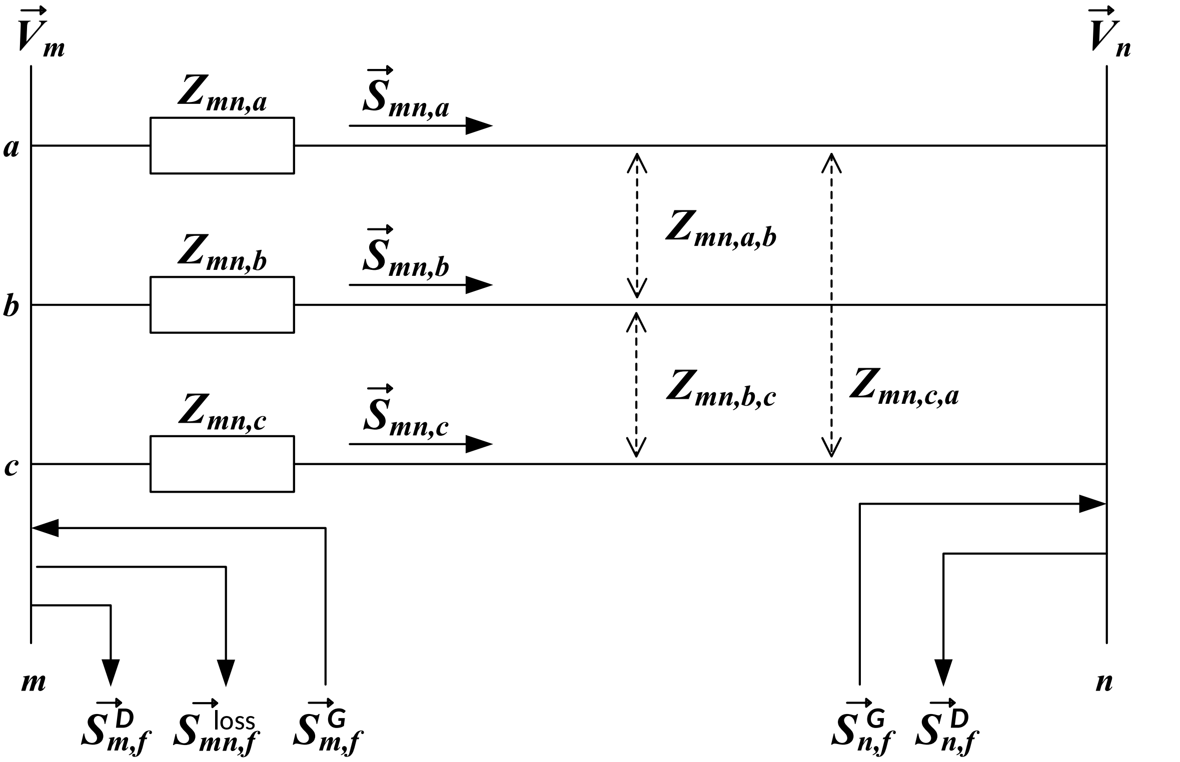

Source: Created by the author.

phase f. Furthermore, $I_{mn,f}$ and $I^{qdr}_{mn,f}$ are the current magnitude and the squared current magnitude through circuit mn and phase f, respectively; while $P_{mn,f}$and $Q_{mn,f}$ are the active and reactive power flows arriving at node n, respectively. $S^{G/D}_{n,f}$,$P^{G/D}_{n,f}$and $Q^{G/D}_{n,f}$ are the generated/demanded apparent, active, and reactive powers, respectively. Finally, $Z_{mn,f,h}$, $R_{mn,f,h}$, and $X_{mn,f,h}$ are the impedance, resistance, and reactance for circuit mn between phases f and h, respectively.

Hereby, $\vec{I}_{mn}$ in (2) must be expressed in terms of the active and reactive powers as shown in (18).

$$\vec{I}_{f,mn} = \left(\frac{\vec{S}_{f,mn}}{\vec{V}_{f,n}}\right)^* = \left(\frac{P_{f,mn} + jQ_{f,mn}}{\vec{V}_{f,n}}\right)^* \tag{18}$$

Analyzing only phase A from (2), Fig. 3 presents a simplified equivalent which divides the voltage drop considering two fictitious nodes m' and n'.

Therefore, the mathematical equations for each branch-segment are shown in (19).

Figure 3 – Single branch equivalent for phase a.

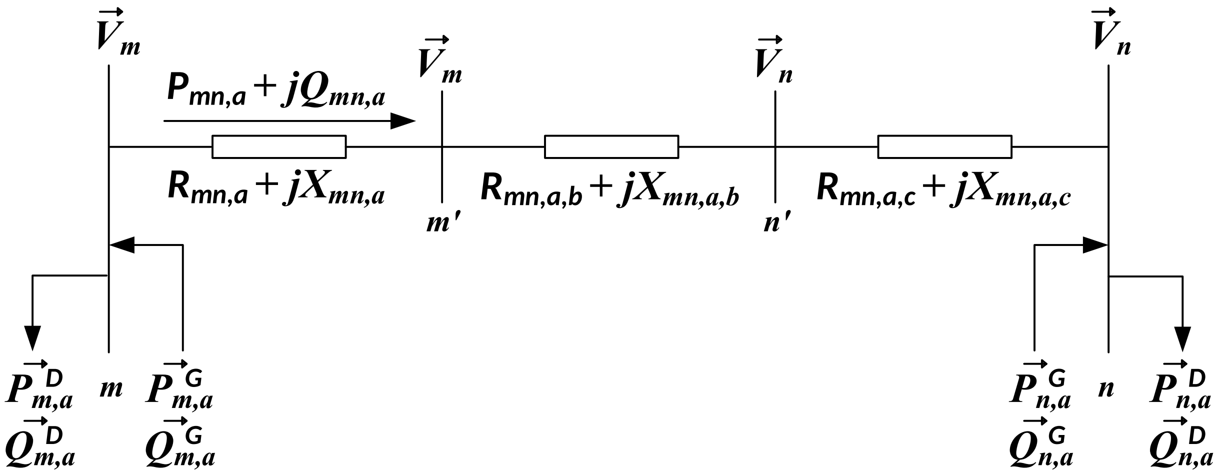

Source: Created by the author.

$$\begin{aligned}\vec{V}_{m,a} - \vec{V}_{m',a} &= Z_{mn,a,b}\vec{I}_{mn,b}\\ \vec{V}_{m',a} - \vec{V}_{n',a} &= Z_{mn,a,c}\vec{I}_{mn,c}\\ \vec{V}_{n',a} - \vec{V}_{n',a} &= Z_{mn,a}\vec{I}_{mn,a}\end{aligned} \tag{19}$$

In order to reach a general expression for the voltage drop, each term of (19) is analysed separately. Initially, the first term can be written as shown in (20). Where the term $\vec{V}^*_{m',a}/\vec{V}^*_{m',a}$ is added to enable some algebraic manipulations aiming to reach a approximated linear expression for the voltage drop.

$$\left(\vec{V}_{m,a} - \vec{V}_{m',a}\right) = \left(R_{mn,a,b} + jX_{mn,a,b}\right)\frac{P_{mn,b} - jQ_{mn,b}}{\vec{V}^*_{n,b}}\left(\frac{\vec{V}^*_{m',a}}{\vec{V}^*_{m',a}}\right) \tag{20}$$

Applying the simplification shown in (21), and replacing ($R_{mn,a,b}$ and $X_{mn,a,b}$) as presented in (22), constraint (23) is reached.

$$\frac{\vec{V}^*_{m',a}}{\vec{V}^*_{n,b}} \approx \frac{V_{m',a}}{V_{n,b}}\angle\left(\theta_{m,b} - \theta_{m,a}\right) \approx \frac{V_{m',a}}{V_{n,b}}\angle - 120° \tag{21}$$

$$\left(\tilde{R}_{mn,a,b} + j\tilde{X}_{mn,a,b}\right) = \left(R_{mn,a,b} + jX_{mn,a,b}\right)\left(1\angle - 120°\right) \tag{22}$$

$$\vec{V}_{m,a}\vec{V}^*_{m',a} - V^2_{m',a} = \frac{V_{m',a}}{V_{n,b}}\left(\tilde{R}_{mn,a,b} + j\tilde{X}_{mn,a,b}\right)\left(P_{mn,b} - jQ_{mn,b}\right) \tag{23}$$

By separating (23) into its real and imaginary parts, (24) and (25) are obtained.

$$V_{m,a}V_{m',a}\cos\left(\theta_{m,a}-\theta_{m',a}\right)=\frac{V_{m',a}}{V_{n,b}}\left(\tilde{R}_{mn,a,b}P_{mn,b}+\tilde{X}_{mn,a,b}Q_{mn,b}\right)+V_{m',a}^{2} \tag{24}$$

$$V_{m,a}V_{m',a}\sin\left(\theta_{m,a}-\theta_{m',a}\right)=\frac{V_{m',a}}{V_{n,b}}\left(\tilde{X}_{mn,a,b}P_{mn,b}-Q_{mn,b}\tilde{R}_{mn,a,b}\right) \tag{25}$$

Later, by adding the square power of (24) and (25), the expression for the voltage drop corresponding to the first segment of Fig. 3 is shown in (26).

$$V_{m,a}^{2}-V_{m',a}^{2}=2\frac{V_{m',a}}{V_{n,b}}\left(\tilde{R}_{mn,a,b}P_{mn,b}+\tilde{X}_{mn,a,b}Q_{mn,b}\right)+\tilde{Z}_{mn.a.b}^{2}I_{mn,b}^{2} \tag{26}$$

Therefore, in order to avoid the nonlinearities shown in (26), we assume $V_{m',a}/V_{n,b}\approx 1$, and the variables V^2 and I^2 are replaced by V^{sqr} and I^{sqr}, respectively. Hence, (27) is reached.

$$V_{m,a}^{sqr}-V_{m',a}^{sqr}=2\left(\tilde{R}_{mn,a,b}P_{mn,b}+\tilde{X}_{mn,a,b}Q_{mn,b}\right)+\tilde{Z}_{mn.a.b}^{2}I_{mn,b}^{sqr} \tag{27}$$

For the second term of (19), an analogue expression is obtained as shown in (27).

$$\left(\vec{V}_{n',a}-\vec{V}_{n,a}\right)=\left(R_{mn,a}+jX_{mn,a}\right)\frac{P_{mn,a}-jQ_{mn,a}}{\vec{V}_{n,a}^{*}} \tag{28}$$

Finally, for the last term of (19), the voltage drop is given by:

$$\left(\vec{V}_{n',a}-\vec{V}_{n,a}\right)=\left(R_{mn,a}+jX_{mn,a}\right)\frac{P_{mn,a}-jQ_{mn,a}}{\vec{V}_{n,a}^{*}} \tag{29}$$

For this segment it is considered that $R_{mn,a}+jX_{mn,a}=\tilde{R}_{mn,a}+j\tilde{X}_{mn,a}$, reaching the expression presented in (30).

$$V_{n',a}^{sqr} - V_{n,a}^{sqr} = 2\left(\tilde{R}_{mn,a}P_{mn,a} + \tilde{X}_{mn,a}Q_{mn,a}\right) + \tilde{Z}_{mn.a}^{2}I_{mn,a}^{sqr} \tag{30}$$

Therefore, the whole voltage drop in circuit mn is defined by (31), which considers coupling effects between the phases.

$$V_{m,f}^{sqr} - V_{n,f}^{sqr} = \sum_{h \in F}\left\{2 * \left(\tilde{R}_{mn,fh}P_{mn,f} + \tilde{X}_{mn,fh}Q_{mn,f}\right) + \tilde{Z}_{mn,fh}^{2}I_{mn,f}^{sqr}\right\} \tag{31}$$

$$\forall mn \in L, f \in F$$

In addition, the active and reactive power balances for each node are represented by (32) and (33), respectively. The calculation of the circuit current is given by (34).

$$\sum_{km \in L} P_{km,f} - \sum_{mn \in L}\left(P_{mn,f} + P_{mn,f}^{L}\right) + P_{m,f}^{G} = P_{m,f}^{D} \qquad \forall m \in N, f \in F \tag{32}$$

$$\sum_{km \in L} Q_{km,f} - \sum_{mn \in L}\left(Q_{mn,f} + Q_{mn,f}^{L}\right) + Q_{m,f}^{G} = Q_{m,f}^{D} \qquad \forall m \in N, f \in F \tag{33}$$

$$V_{n,f}^{sqr}I_{mn,f}^{sqr} = P_{mn,f}^{2} + Q_{mn,f}^{2} \qquad \forall mn \in L, f \in F \tag{34}$$

To determine the power losses (P^L and Q^L), the complex power losses are initially expressed as follows:

$$S_{mn,f}^{L} = \sum_{h \in \Omega_f} Z_{mn,f,h}\left(\frac{P_{mn,h} + jQ_{mn,h}}{\vec{V}_{n,h}}\right)^{*}\left(\frac{P_{mn,f} + jQ_{mn,f}}{\vec{V}_{n,f}}\right) \tag{35}$$

Equation (35) can be also written as:

$$S_{mn,f}^{L} = \sum_{h \in \Omega_f} Z_{mn,f,h}\frac{\left(P_{mn,h} + jQ_{mn,h}\right)^{*}\left(P_{mn,f} + jQ_{mn,f}\right)}{\vec{V}_{n,f}\vec{V}_{n,h}\angle\left(\theta_{n,f} - \theta_{n,h}\right)} \tag{36}$$

Furthermore, by replacing (22) in (36), it is obtained:

$$S^L_{mn,f} \approx \sum_{h\in\Omega_f} \tilde{Z}_{mn,f,h} \frac{(P_{mn,h} + jQ_{mn,h})^* \, (P_{mn,f} + jQ_{mn,h})}{\vec{V}_{n,f}\vec{V}_{n,h}} \tag{37}$$

Later, (37) and (38) are reached by separating the real and imaginary parts of (37). These constraints represent the active and reactive power losses in an unbalanced EDN.

$$\begin{aligned} P^L_{mn,f} = \sum_{h\in\Omega_f} \tilde{R}_{mn,f,h} & \frac{(P_{mn,f}P_{mn,h} + Q_{mn,f}Q_{mn,h})}{V_{n,f}V_{n,h}} \\ + \tilde{X}_{mn,f,h} & \frac{(-Q_{mn,f}P_{mn,h} + P_{mn,f}Q_{mn,h})}{V_{n,f}V_{n,h}} \qquad \forall mn \in L, f \in F \end{aligned} \tag{38}$$

$$\begin{aligned} Q^L_{mn,f} = \sum_{h\in\Omega_f} \tilde{X}_{mn,f,h} & \frac{(P_{mn,f}P_{mn,h} + Q_{mn,f}Q_{mn,h})}{V_{n,f}V_{n,h}} \\ + \tilde{R}_{mn,f,h} & \frac{(Q_{mn,f}P_{mn,h} - P_{mn,f}Q_{mn,h})}{V_{n,f}V_{n,h}} \qquad \forall mn \in L, f \in F \end{aligned} \tag{39}$$

Finally, (40) represents the complete NLP model for the steady-state operation of an unbalanced EDN.

$$\min \alpha \tag{40}$$

$$\text{subject to: (31)–(34), (38), and (39)}$$

The NLP model (40) contain nonlinearities (in constraints (34), (38), and (39)) that must be addressed to reach a LP model. Equation (34) has a product of two variables ($V^{sqr}_{n,f}$ and $I^{sqr}_{mn,f}$) in the left-hand side and the square of two variables ($P_{mn,f}$ and $Q_{mn,f}$) in the right-hand side. The left-hand side of (34) is linearized replacing the variable $V^{sqr}_{n,f}$ by an estimated value $\tilde{V}^2_{n,f}$. On the other hand, the right-hand side is approximated using a piecewise linearization technique (see Section 2.11). Hence, (41) shows the complete linear expression used to approximate (34).

$$\tilde{V}^2_{n,f} I^{sqr}_{mn,f} = f\left(P_{mn,f}, \overline{P_{mn,f}}, \Lambda\right) + f\left(Q_{mn,f}, \overline{Q_{mn,f}}, \Lambda\right) \qquad \forall mn \in L, f \in F \tag{41}$$

Furthermore, as represented by (38) and (39), power losses can be approximated by any of the following options:

Option–A: Use actual, historic, or estimated values for the voltages and the power flows, in order to reach approximated values for P^L and Q^L in (32) and (33), disregarding (38) and (39), as shown in (42) and (43).

$$\sum_{km \in L} P_{km,f} - \sum_{mn \in L} \left(P_{mn,f} + \tilde{P}^L_{mn,f} \right) + P^G_{m,f} = P^D_{m,f} \qquad \forall m \in N, f \in F \tag{42}$$

$$\sum_{km \in L} Q_{km,f} - \sum_{mn \in L} \left(Q_{mn,f} + \tilde{Q}^L_{mn,f} \right) + Q^G_{m,f} = Q^D_{m,f} \qquad \forall m \in N, f \in F \tag{43}$$

In not fully observable distribution networks, a two-stage approach is recommended to estimate the power losses $\tilde{P}^L_{km,f}$ and $\tilde{Q}^L_{km,f}$. In the first stage, the LP is solved disregarding the power losses, i.e., $\tilde{P}^L_{km,f}$ and $\tilde{Q}^L_{km,f}$ are equal to zero. Later, the solution of stage one is used to initialize stage two and the LP model is once again solved.

If option A is chosen, the complete LP model will have the following form:

$$\min \alpha \tag{44}$$

$$\text{subject to: (31), and (41)–(43)}$$

Option–B: Use Taylor's approximation around an estimated point for the power flows and voltages ($P^*_{mn,f}$, $P^*_{mn,h}$, $V^*_{m,f}$, and $V^*_{m,h}$). Let the functions $g(P^*_{mn,f}, P^*_{mn,h}, Q^*_{mn,f}, Q^*_{mn,h}, V^*_{m,f}, V^*_{m,h})$ and $h(P^*_{mn,f}, P^*_{mn,h}, Q^*_{mn,f}, Q^*_{mn,h}, V^*_{m,f}, V^*_{m,h})$ be equal to the right part of (38) and (39), respectively. Equations (45) and (46) show the Taylor's approximation used in order to determine the power losses in the EDN.

$$\begin{aligned} P^L_{mn,f} = g^* &+ \left.\frac{\partial g}{\partial P_{mn,f}}\right|^* (P_{mn,f} - P^*_{mn,f}) + \left.\frac{\partial g}{\partial P_{mn,h}}\right|^* (P_{mn,h} - P^*_{mn,h}) \\ &+ \left.\frac{\partial g}{\partial Q_{mn,f}}\right|^* (Q_{mn,f} - Q^*_{mn,f}) + \left.\frac{\partial g}{\partial Q_{mn,h}}\right|^* (Q_{mn,h} - Q^*_{mn,h}) \\ &+ \left.\frac{\partial g}{\partial V_{n,f}}\right|^* (V_{n,f} - V^*_{n,f}) + \left.\frac{\partial g}{\partial V_{n,h}}\right|^* (V_{n,h} - V^*_{n,h}) \qquad \forall mn \in L, f \in F \end{aligned} \tag{45}$$

$$
\begin{aligned}
Q^L_{mn,f} = h^* &+ \left.\frac{\partial h}{\partial P_{mn,f}}\right|^* (P_{mn,f} - P^*_{mn,f}) + \left.\frac{\partial h}{\partial P_{mn,h}}\right|^* (P_{mn,h} - P^*_{mn,h}) \\
&+ \left.\frac{\partial h}{\partial Q_{mn,f}}\right|^* (Q_{mn,f} - Q^*_{mn,f}) + \left.\frac{\partial h}{\partial Q_{mn,h}}\right|^* (Q_{mn,h} - Q^*_{mn,h}) \\
&+ \left.\frac{\partial h}{\partial V_{n,f}}\right|^* (V_{n,f} - V^*_{n,f}) + \left.\frac{\partial h}{\partial V_{n,h}}\right|^* (V_{n,h} - V^*_{n,h}) \qquad \forall mn \in L, f \in F
\end{aligned} \tag{46}
$$

Hence, the complete LP model is given by (47).

$$
\min \alpha \tag{47}
$$

subject to: (31)–(33), (41), (45), and (46)

2.3 PERFORMANCE AND ACCURACY

Two LP formulations to determine the steady-state operation point of an unbalanced EDN via mathematical optimization were presented. These representations are the base of the complete mathematical optimization framework for the distribution network operation. Different objectives related to technical and/or economic constraints can be pursued embedding these formulations in multi-period and multi-scenario optimization. Therefore, the quality of studies developed hereinafter will rely on their level of accuracy.

The performance and accuracy of both formulations is evaluated in the IEEE123–node test system IEEE/PES (). All LP models were written in the mathematical language AMPL Fourer, Gay e Kernighan (2003), and solved using CPLEX ILOG Inc. (2009). The case study had the following characteristics:

- The whole conventional demand of the distribution network was 1.62 MVA (40.61%), 1.05 MVA (26.36%), and 1.32 MVA (33.03%), connected to phases A, B, and C, respectively.
- All loads were connected in wye configuration.
- All demands were considered as constant power loads.

The LP formulations presented (17) and (44) are expressed as shown in (48) and (49), aiming to minimize the total active power generation; considering nominal voltage at the substation node. Moreover, as the accuracy of both unbalanced formulations depends on the precision of the assumed operation point (i.e., V^{re^*}, V^{im^*} for the current-based formulation, and P^L and Q^L for the power-based formulation), a two-stage approach was used for both formulations to obtain a better approximation for the operation point.

$$\min \sum_{f \in F} \left(V^{re}_{S,f} I^{Gre}_{S,f} + V^{im}_{S,f} I^{Gim}_{S,f} \right) \tag{48}$$

subject to: (6)–(9), (15), and (16)

$$\min \sum_{f \in F} P^{G}_{S,f} \tag{49}$$

subject to: (31), and (41)–(43)

A comparison of the two methods (Current-based and power-based PF) was made analyzing the voltage magnitude profile obtained from each when compared to the one obtained from the solution of a conventional PF. To solve this conventional PF, the specialized software OpenDSS was selected. For both formulations, Table 1 shows the maximum error percentage in the voltage magnitude, for each phase, compared against the OpenDSS; as well as the minimum voltage magnitude in the system.

Table 1 – Comparison of the LP formulations against OpenDSS

Phase	A		B		C	
LP Formulation	Current Based	Power Based	Current Based	Power Based	Current Based	Power Based
Error (%)	0.01	0.02	0.01	0.05	0.11	0.3
Vmin (p.u.)	0.8996	0.8997	0.9599	0.9595	0.9241	0.9223

Source: Created by the author.

Although both formulations show high accuracy when compared with OpenDSS results, it can be seen from Table 1, that the current-based LP formulation outperforms the power-based representation. This is an important fact to be taken under consideration by the distribution network optimizer when choosing one LP formulation for an EDN optimization algorithm. Nevertheless, the complexity due to troublesome constraints associated with operational limits and the inclusion of different technologies and devices should be thoroughly analyzed.

2.4 MULTI-PERIOD AND MULTI-SCENARIO EXTENSION

Typically, optimization analyses in EDN operation are done along a time window in which several control actions have to be defined and they may be dependent among them; this is known as multi-period optimization. For example, the day-ahead operation planning is typically divided in one-hour time windows, and the decisions from one hour may or may not affect the decisions regarding the next time intervals. Thus, mathematical formulations for the distribution network operation should be able to handle multi-period optimization analyses. In this regard, the LP formulations presented can be easily adapted to handle several time intervals. Hence, a new index associated to the time interval is added to the variables that represent the distribution network operation (e.g., voltages, currents, and power flows).

Furthermore, adaptability to multi-scenario optimizations is also required in an optimization framework for EDN to model the uncertainty in the grid. The multi-scenario optimization is a method usually employed to solve stochastic programming problems in which some of the variables or parameters are of uncertain nature (e.g., EV behavior, renewable DG availability, and demand variations). The uncertainties are represented through a set of scenarios and each one with an associated probability, i.e., a multi-scenario model will provide an optimal solution on average, considering all the scenarios simultaneously. Analogue to the multi-period case, a new index is added to the uncertain variables associated to each scenario. Thereby, the objective function of the problem is calculated as the expected value due to the inclusion of the probabilities related to each scenario.

2.5 ESTIMATED STEADY-STATE OPERATION POINT

As mentioned, the accuracy of the presented three-phase formulations relies on the precision of the estimated operation point. High quality estimations will minimize the error corresponding to some approximations in voltage magnitudes and some linearization techniques (e.g., Taylor's linearization). In order to obtain a suitable estimated operation point, the following techniques might be employed:

1. A two-stage approach, in which a first stage solves the LP model using a flat start (e.g., assuming nominal voltages and disregarding power). Later, the solution of the first stage is used to initialize the second stage in which the LP model is once again solved from the already calculated operating point.

2. Using historical data, where historical data is used in order to determine the estimated values. Typically, the operator's knowledge and experience are crucial to select previous operating points which have occurred under similar loading and generation scenarios.

3. Using the previous time interval operating point is another technique for the estimation of the operating point. This approach is commonly used on small time

interval optimization approaches in which abrupt changes in the demand are not expected (e.g., EVCC problems).

It is important to remark, that the estimation of the operation point is an important issue to be taken into account when applying the presented formulations. Furthermore, the technique chosen to determine the estimated operation point will depend on the information available and the characteristics of the problem that is being tackled.

2.6 OPERATIONAL CONSTRAINTS

The LP formulations presented in (17) and (44) are expected to serve as the central engine of optimization analysis, mathematically formalizing decision–making processes regarding several objectives. Hereby, an essential component of any optimization strategy or algorithm related to electricity distribution is the service quality. Although several electrical quantities can be measured and limited to guarantee good quality in the service, voltage magnitude limits and thermal limits in conductors and transformers are the most commonly used in steady-state studies to ensure the proper operation of the EDN. Therefore, the mathematical representation of these limits and their inclusion in the LP formulations are presented below.

2.6.1 Voltage Magnitude

Ensuring a good quality service in the EDN, the voltage magnitude is limited within a range established by regulatory policies. This range is mathematically expressed as shown in (50), in terms of the minimum and maximum values of the voltage magnitude ($\underline{V}$ and $\bar{V}$, respectively). Therefore, the inclusion of (50) in the LP formulations is presented below.

$$\underline{V} \leqslant \left|\vec{V}\right| \leqslant \bar{V} \tag{50}$$

Current-Based Representation – Voltage Magnitude Limits: The current-based representation is written in terms of the currents and voltages real and imaginary parts. Hence, (50) is rewritten in (51), limiting the square power of the voltage magnitude. Nevertheless, (51) presents nonlinearities which have to be dealt with in order to include this limit in the LP model.

$$\underline{V}^2 \leqslant {V_{n,f}^{re}}^2 + {V_{n,f}^{im}}^2 \leqslant \bar{V}^2 \qquad \forall n \in N, f \in F \tag{51}$$

To reach a linear approximation for (51), a set of linear constraints limiting the feasible region for the voltage real and imaginary components is implemented. Fig. 4 depicts the sets of lines used to approximate the upper and lower voltage limits (red lines and blue lines, respectively). In each phase, the upper limit is replaced by a set of $2*\ell$ line segments; where, ℓ lines are built clockwise starting from an estimated operation angle θ^*, and ℓ lines are built counterclockwise. For the lower limit, a single line is used for each phase also built around θ^*. Equations (52) and (53) are the mathematical expressions for the linear approximations of the upper and lower voltage limits, respectively.

$$V^{im}_{n,f} \leqslant \frac{\sin(\varphi^{+}_{n,f,i}) - \sin(\varphi^{-}_{n,f,i})}{\cos(\varphi^{+}_{n,f,i}) - \cos(\varphi^{-}_{n,f,i})}\left[V^{re}_{n,f} - \bar{V}\cos(\varphi^{-}_{n,f,i})\right] + \bar{V}\sin(\varphi^{-}_{n,f,i}) \tag{52}$$

$$\forall i \in -\ell \ldots \ell, n \in N, f \in F$$

$$V^{im}_{n,f} \leqslant \frac{\sin(\varphi^{o+}_{n,f}) - \sin(\varphi^{o-}_{n,f})}{\cos(\varphi^{o+}_{n,f}) - \cos(\varphi^{o-}_{n,f})}\left[V^{re}_{n,f} - \underline{V}\cos(\varphi^{o+}_{n,f})\right] + \underline{V}\sin(\varphi^{o+}_{n,f}) \qquad \forall n \in N, f \in F \tag{53}$$

Where, $\varphi^{+}_{n,f,i} = \theta^*_{n,f} + \ell_i\phi$; $\varphi^{-}_{n,f,i} = \theta^*_{n,f} + (\ell_i - 1)\,\phi$; $\theta^*_{n,f}$ is the operation angle for bus n in phase f; ℓ_i is the i-element from the set of line segments; and ϕ is the angle of the arc corresponding to each line segment. Finally, $\varphi^{o+}_{n,f,i} = \theta^*_{n,f} + \phi$; and $\varphi^{o-}_{n,f,i} = \theta^*_{n,f} - \phi$.

Power-Based Representation – Voltage Magnitude Limits: On the other hand, to include the voltage magnitude limits in the power-based representation, (50) is rewritten in order to limit the square power of the voltage magnitude, as shown in (54).

$$\underline{V}^2 \leqslant V^{sqr}_{n,f} \leqslant \bar{V}^2 \qquad \forall n \in N, f \in F \tag{54}$$

2.6.2 Circuit Currents

Thermal limits are often the main constraint in power systems. Hence, a proper operation of the EDN must maintain the current in all circuits within the conductor thermal limitations; i.e., the magnitude of the current in all circuits must be held under their ampacities. Constraint (55) shows the general mathematical expression for the current limit, which will be added to each LP formulation as follows.

Figure 4 – Constraints for voltage limits in the current-based formulation.

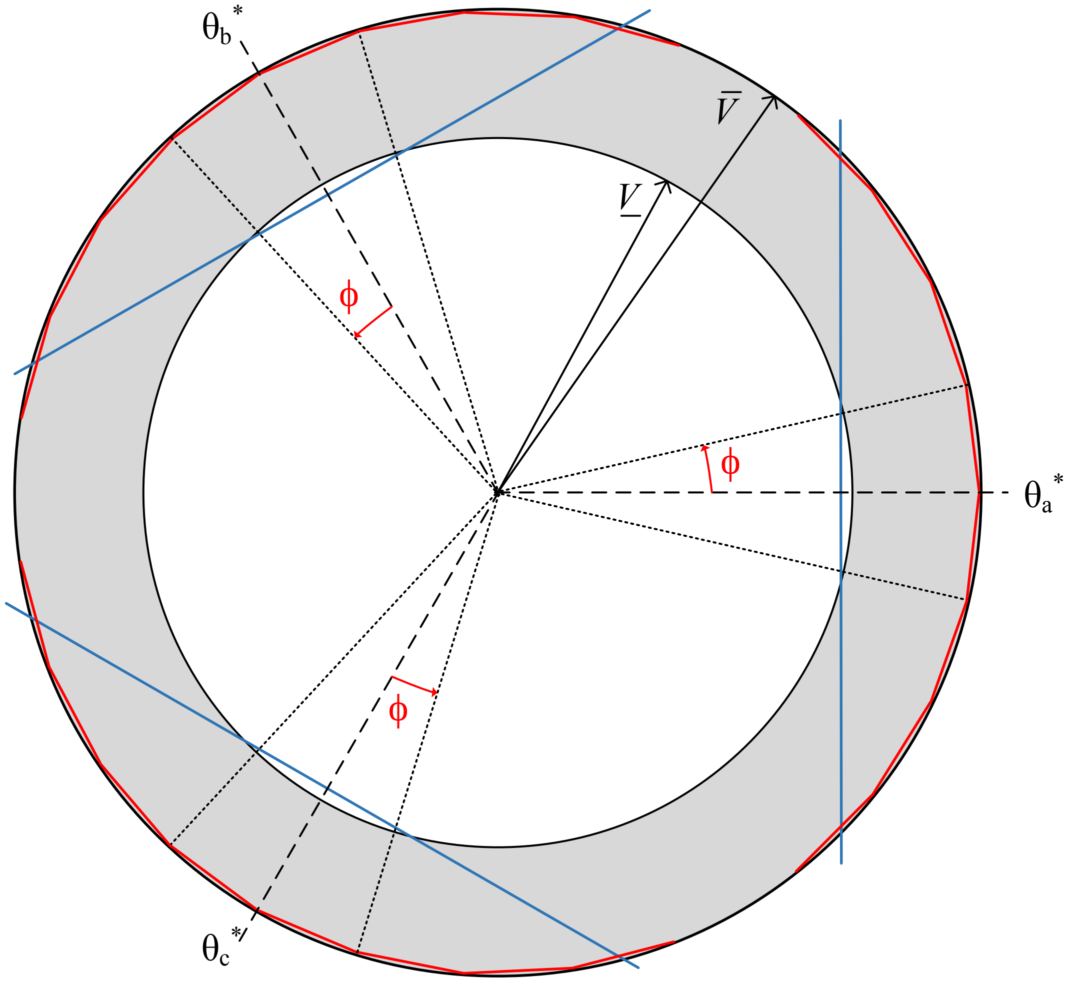

Source: Created by the author.

$$\left|\vec{I}\right| \leqslant \bar{I} \tag{55}$$

Current-Based Representation – Circuit Current Limits: Similar to the voltage magnitude limit, (55) is squared and expressed in terms of the real and imaginary parts of the circuit currents, as shown in (56). Later, the nonlinearities are avoided through a piecewise linearization technique, reaching a linear expression for the circuit current limit in terms of the real and imaginary parts of the current (57).

$${I^{re}_{mn,f}}^2 + {I^{im}_{mn,f}}^2 \leqslant \bar{I}^2_{mn} \qquad \forall mn \in L, f \in F \tag{56}$$

$$f\left(I^{re}_{mn,f}, \bar{I}, \Lambda\right) + f\left(I^{im}_{mn,f}, \bar{I}, \Lambda\right) \leqslant \bar{I}^2_{mn} \qquad \forall mn \in L, f \in F \tag{57}$$

Power-Based Representation – Circuit Current Limits: Analogous to (50), (58) must be added to the power-based LP formulation to limit the current in each circuit.

$$I^{sqr}_{mn,f} \leqslant \bar{I}^2_{mn} \qquad \forall mn \in L, f \in F \tag{58}$$

2.6.3 Transformer Capacity

In steady-state studies of the EDN where different voltage levels are taken into account, thermal limits regarding the distribution and substation transformers are a key aspect. Therefore, the inclusion of the transformer capacity in the mathematical optimization framework for the distribution network operation is presented below. Hence, the mathematical expression (59) limiting the transformer apparent power must be fulfilled for each transformer.

$$\left|\vec{S}\right| \leqslant \bar{S} \tag{59}$$

Hereby, let $TR \subseteq N$ be the set of nodes where a transformer is installed; while $P^{TR}_{\wp}$ and $Q^{TR}_{\wp}$ the active and reactive power, respectively, for transformer $\wp$. Thus, the general expression for each transformer capacity is presented in (60), and linearized in (61) through piecewise linearization technique.

$${P^{TR}_{\wp}}^2 + {Q^{TR}_{\wp}}^2 \leqslant \overline{S^{TR}_{\wp,t}}^2 \qquad \forall \wp \in TR \tag{60}$$

$$f(P^{TR}_{\wp}, \overline{S^{TR}_{\wp}}, \Lambda) + f(Q^{TR}_{\wp}, \overline{S^{TR}_{\wp}}, \Lambda) \leqslant \overline{S^{TR}_{\wp,t}}^2 \qquad \forall \wp \in TR \tag{61}$$

Current-Based Representation – Transformer Capacity: Besides (61), for the current-based formulation, $P^{TR}_{\wp}$ and $Q^{TR}_{\wp}$ have to be calculated. Equation (62) and (63) calculate, for transformer $\wp$, the active and reactive powers in terms an operation point for the real and imaginary voltages ($V^{re/im*}_{\wp,f}$) and the currents ($I^{re/im}_{\wp,f}$) at the secondary windings.

$$P_{\wp}^{TR} = \sum_{f \in F} V_{\wp,f}^{re^*} I_{\wp,f}^{re} + V_{\wp,f}^{im^*} I_{\wp,f}^{im} \qquad \forall \wp \in TR \tag{62}$$

$$Q_{\wp}^{TR} = \sum_{f \in F} -V_{\wp,f}^{re^*} I_{\wp,f}^{im} + V_{\wp,f}^{im^*} I_{\wp,f}^{re} \qquad \forall \wp \in TR \tag{63}$$

Power-Based Representation – Transformer Capacity: Likewise, for the power-based formulation, (64) and (65) show the mathematical expression for $P_{\wp}^{TR}$ and $Q_{\wp}^{TR}$ in terms of the active and reactive power flowing through each phase of the transformer ($P_{\wp,f}$ and $Q_{\wp,f}$, respectively).

$$P_{\wp}^{TR} = \sum_{f \in F} P_{\wp,f} \qquad \forall \wp \in TR \tag{64}$$

$$Q_{\wp}^{TR} = \sum_{f \in F} Q_{\wp,f} \qquad \forall \wp \in TR \tag{65}$$

Finally, the complete LP formulations, considering operational limits are presented in (66) and (67), for the current-based and power-based representations, respectively.

$$\min \alpha \tag{66}$$

subject to: (6)–(9), (15), (16), (52), (53), (57), and (61)- (63)

$$\min \alpha \tag{67}$$

subject to: (31), (41)–(43), (54), (58), (61), (64), and (65)

2.7 LOAD REPRESENTATION

Nowadays, EDNs must deal with social, technical and environmental challenges in order to successfully satisfy present-day consumers. The world's electrical energy consumption is expected to have an annual growth rate of about 2.2% until 2040 (U.S. DEPARTMENT OF ENERGY, 2013), which will substantially impact the operation of future EDNs. Hence, network operators are continuously challenged as they are in charge of meeting customer demands and optimize energy sources, while guaranteeing a reliable service. As a result, improvements in the network load modelling are continuously demanded within the grid operator efforts for predicting system behavior.

Besides the rapid growth of the conventional demand, EDNs face issues related to the progressive integration of new technologies. The rise of new loads (e.g., EVs), which cannot be pigeonholed in traditional classifications, require a special attention. Thus, this section presents the load modelling and the inclusion of special loads within the mathematical optimization framework.

2.7.1 Type of Loads: Voltage Dependent Load Models

In EDNs, loads are traditionally classified as residential, industrial or commercial. This rough classification was elaborated in order to group loads that share features related to usage patterns. These well-studied patterns are commonly affected by factors such as location, weather, cultural habits, and type of human works. However, since large concentrated loads called for detailed classifications and special representation in order to determine operational characteristics, studies have been performed aiming to achieve a more precise categorization for different types of loads (DANDENO et al., 1973). Hereby, a new classification following the voltage dependency of the actual loads becomes more important in the representation as the EDN gets closer to individual loads. The demand of a distribution network is classified into loads that can be represented as:

1. constant power loads,
2. constant impedance loads,
3. constant current loads, or
4. a combination of those.

Although load modelling in power systems is a well-studied topic, approached by several researches related to voltage and angular system stability, this issue has to be also taken into account on decision-making algorithms related to the steady-state operation of the grid. As discussed in Padilha-Feltrin, Quijano e Mantovani (2015), Ahmadi, MartÍ e Dommel (2015), Sabillon-Antunez et al. (2017), the effectiveness of several mathematical models in EDNs is highly dependent on the accuracy of the load representation. Dependence on the voltage magnitude and frequency is considered in the load models; mathematically, this dependence can be represented by static and dynamic load models described by the traditional ZIP model. In this regards, two static models are commonly studied for the representation of the active and reactive demanded powers

(P^D and Q^D, respectively): the polynomial load model and the exponential load model shown in (68) and (69), respectively (KORUNOVIC et al., 2012).

$$P^D = P^o\left(P^{Zo}\frac{V^2}{V^{o2}} + P^{Io}\frac{V}{V^o} + P^{Po}\right)$$
$$Q^D = Q^o\left(Q^{Zo}\frac{V^2}{V^{o2}} + Q^{Io}\frac{V}{V^o} + Q^{Po}\right) \tag{68}$$

$$P^D = P^o\left(\frac{V}{V^o}\right)^{\alpha}(1 + K_{pf}(f_r - f_r^o))$$
$$Q^D = Q^o\left(\frac{V}{V^o}\right)^{\beta}(1 + K_{qf}(f_r - f_r^o)) \tag{69}$$

Where, P^o, Q^o, and V^o, are the nominal active and reactive power and bus voltage, respectively. P^{Zo}, P^{Io} , and P^{Po}, are the active power percentage of the total load classified as constant impedance, constant current, and constant power, respectively. Likewise, Q^{Zo}, Q^{Io} , and Q^{Po}, are the reactive power percentage for constant impedance, constant current, and constant power, respectively. In the polynomial load model (68), the loads are treated as a combination of constant impedance constant current and/or constant power; hence the sum of these coefficients will represent the total load, as shown in (70). On the other hand, in the exponential load model (69) the load voltage dependency is generalized, and the demanded active and reactive powers vary according to the voltage exponents α and β. These voltage exponents depend on the type and composition of the load.

$$P^{Zo} + P^{Io} + P^{Po} = 1$$
$$Q^{Zo} + Q^{Io} + Q^{Po} = 1 \tag{70}$$

Moreover, f_r represents the frequency of the bus voltage and f_r^o represents the nominal frequency. The coefficients K_{pf} and K_{qf} are the frequency sensitivities for the active and reactive power loads, respectively. Nevertheless, for the exponential model the effects associated with frequency may be disregarded in steady-state studies, as shown in (71). Hence, with an appropriate adjustment of the constants α and β the model can be restricted to the steady-state analysis case (i.e., dependence directly on the voltage magnitude). Appropriate values for these constants may be found in previous works, such as IEEE (1995).

$$P^D = P^o\left(\frac{V}{V^o}\right)^{\alpha} \qquad (71)$$
$$Q^D = Q^o\left(\frac{V}{V^o}\right)^{\beta}$$

In some decision-making processes for EDNs, the load voltage dependency is a key aspect of the suitable representation of the network operation, e.g., volt-var control. Hence, they must be included in the LP formulations presented in (17) and (44), where the demanded active and reactive powers were considered as constant values.

Current-Based Representation - Polynomial load model: In order to include the load voltage dependency in the LP problem presented in (17), the values of the demanded powers have to be replaced by (68) in (13) and (14). Therefore, the expressions representing the functions g and h are presented in (72) and (73).

$$\begin{aligned} g =\ & \frac{P^o_{n,f} V^{re}_{n,f}}{{V^{re}_{n,f}}^2 + {V^{im}_{n,f}}^2}\left(\frac{P^{Zo}_{n,f}}{{V^o_n}^2}\left({V^{re}_{n,f}}^2 + {V^{im}_{n,f}}^2\right) + \frac{P^{Io}_{n,f}}{V^o_n}\sqrt{\left({V^{re}_{n,f}}^2 + {V^{im}_{n,f}}^2\right)} + P^{Po}_{n,f}\right) \\ & + \frac{Q^o_{n,f} V^{im}_{n,f}}{{V^{re}_{n,f}}^2 + {V^{im}_{n,f}}^2}\left(\frac{Q^{Zo}_{n,f}}{{V^o_n}^2}\left({V^{re}_{n,f}}^2 + {V^{im}_{n,f}}^2\right) + \frac{Q^{Io}_{n,f}}{V^o_n}\sqrt{\left({V^{re}_{n,f}}^2 + {V^{im}_{n,f}}^2\right)} + Q^{Po}_{n,f}\right) \\ & \forall n \in N, f \in F \end{aligned} \qquad (72)$$

$$\begin{aligned} h =\ & \frac{P^o_{n,f} V^{im}_{n,f}}{{V^{re}_{n,f}}^2 + {V^{im}_{n,f}}^2}\left(\frac{P^{Zo}_{n,f}}{{V^o_n}^2}\left({V^{re}_{n,f}}^2 + {V^{im}_{n,f}}^2\right) + \frac{P^{Io}_{n,f}}{V^o_n}\sqrt{\left({V^{re}_{n,f}}^2 + {V^{im}_{n,f}}^2\right)} + P^{Po}_{n,f}\right) \\ & - \frac{Q^o_{n,f} V^{re}_{n,f}}{{V^{re}_{n,f}}^2 + {V^{im}_{n,f}}^2}\left(\frac{Q^{Zo}_{n,f}}{{V^o_n}^2}\left({V^{re}_{n,f}}^2 + {V^{im}_{n,f}}^2\right) + \frac{Q^{Io}_{n,f}}{V^o_n}\sqrt{\left({V^{re}_{n,f}}^2 + {V^{im}_{n,f}}^2\right)} + Q^{Po}_{n,f}\right) \\ & \forall n \in N, f \in F \end{aligned} \qquad (73)$$

Current-Based Representation: Exponential load model: Likewise, to include the exponential load model in (17), (13) and (14) have to be rewritten, as shown in (74) and (75).

$$g = P^o_{n,f}\frac{V^{re}_{n,f}}{{V_o}^{\alpha_{n,f}}}\left(V^{re^2}_{n,f} + V^{im^2}_{n,f}\right)^{\frac{\alpha_{n,f}}{2}-1} + Q^o_{n,f,t}\frac{V^{im}_{n,f}}{{V_o}^{\beta_{n,f}}}\left(V^{re^2}_{n,f} + V^{im^2}_{n,f}\right)^{\frac{\beta_{n,f}}{2}-1} \qquad (74)$$
$$\forall n \in N, f \in F$$

$$h = P^{o}_{n,f} \frac{V^{im}_{n,f}}{V_{o}{}^{\alpha_{n,f}}} \left(V^{re^2}_{n,f} + V^{im^2}_{n,f} \right)^{\frac{\alpha_{n,f}}{2}-1} - Q^{o}_{n,f,t} \frac{V^{re}_{n,f}}{V_{o}{}^{\beta_{n,f}}} \left(V^{re^2}_{n,f} + V^{im^2}_{n,f} \right)^{\frac{\beta_{n,f}}{2}-1} \quad \forall n \in N, f \in F \tag{75}$$

Power-Based Representation: Polynomial load model: For the power-based linear representation shown in (44), the expressions for the demanded power (68) are directly added to the formulation; notwithstanding, the nonlinearities of these equations must be dealt with, as shown in (76) and (77).

$$P^{D}_{n,f} = P^{o}_{n,f} \left(P^{Zo}_{n} \frac{V^{sqr}_{n,f}}{V^{o}_{n}{}^{2}} + P^{Io}_{n} \frac{V^{sqr}_{n,t}}{V^{*}_{n,t} V^{o}_{n}} + P^{Po}_{n} \right) \qquad \forall n \in N, f \in F \tag{76}$$

$$Q^{D}_{n,f} = Q^{o}_{n,f} \left(Q^{Zo}_{n} \frac{V^{sqr}_{n,f}}{V^{o}_{n}{}^{2}} + Q^{Io}_{n} \frac{V^{sqr}_{n,t}}{V^{*}_{n,t} V^{o}_{n}} + Q^{Po}_{n} \right) \qquad \forall n \in N, f \in F \tag{77}$$

Hence, the complete LP formulation, considering the polynomial model for the load voltage dependency, is given by (78).

$$\min \alpha \tag{78}$$

subject to: (31)- (33), (41), (45), (46), (74), and (75)

Power-Based Representation: Exponential load model: Finally, to include the exponential load model in the power-based LP formulation, expressions (71) are added. To avoid the nonlinearities associated to these expressions, (71) is rewritten as shown in (79) and (80).

$$P^{D}_{n,f} = P^{o}_{n,f} \left(\frac{V^{sqr}_{n,f}}{V^{o}_{n}{}^{2}} \right)^{\frac{\alpha_{n,f}}{2}} \qquad \forall n \in N, f \in F \tag{79}$$

$$Q^{D}_{n,f} = Q^{o}_{n,f} \left(\frac{V^{sqr}_{n,f}}{V^{o}_{n}{}^{2}} \right)^{\frac{\beta_{n,f}}{2}} \qquad \forall n \in N, f \in F \tag{80}$$

Later, Taylor's approximation is applied to linearize (79) and (80).

$$P^{D}_{n,f} = P^{o}_{n,f}\left(\frac{V^{sqr*}_{n,f}}{V^{o\,2}_{n}}\right)^{\frac{\alpha_{n,f}}{2}} + \frac{\alpha_{n,f}}{2}\frac{P^{o}_{n,f}}{(V^{o}_{n})^{\frac{\alpha_{n,f}}{2}}} V^{sqr*\left(\frac{\alpha_{n,f}}{2}-1\right)}_{n,f}\left(V^{sqr}_{n,f} - V^{sqr*}_{n,f}\right) \quad (81)$$

$$\forall n \in N, f \in F$$

$$Q^{D}_{n,f} = Q^{o}_{n,f}\left(\frac{V^{sqr*}_{n,f}}{V^{o\,2}_{n}}\right)^{\frac{\beta_{n,f}}{2}} + \frac{\beta_{n,f}}{2}\frac{Q^{o}_{n,f}}{(V^{o}_{n})^{\frac{\beta_{n,f}}{2}}} V^{sqr*\left(\frac{\beta_{n,f}}{2}-1\right)}_{n,f}\left(V^{sqr}_{n,f} - V^{sqr*}_{n,f}\right) \quad (82)$$

$$\forall n \in N, f \in F$$

Therefore, the complete LP formulation, considering the exponential load voltage dependency model, is given by (83).

$$\min \alpha \quad (83)$$

subject to: (31)- (33), (41), (45), (46), (81), and (82)

2.7.2 Special Loads: Plug-In Electric Vehicles

A large number of EVs is expected to be integrated to the transport sector in the upcoming years, as an answer to environmental concerns related to the reduction of greenhouse gas emissions (ANGLANI; FATTORI; MULIERE, 2012). From the point of view of the customers, EVs represent an economical option in response to high fuel costs. On the other hand, for the EDN, EVs represent an additional load which need to be attended, increasing the conventional demand in several ways, depending on the charging place (CLEMENT-NYNS; HAESEN; DRIESEN, 2010). Hence, EVs represent a new load in EDN which has to be taken into account in optimization studies for the grid.

EVs recharge their batteries from the distribution network, and an uncontrolled charging of large fleets can cause overloads, voltage limit violations, and excessive energy losses (WU; ALIPRANTIS; GKRITZA, 2011). Hence, the EV charging coordination (EVCC) problem have to be tackled as part of the distribution network operation, and has received much attention in recent years, as exposed in O'Connell, Keane e Flynn (2014) and in Antunez et al. (2016b). Furthermore, the ability of EVs to inject power into the grid (also known as vehicle-to-grid (V2G) technology), providing ancillary services to the EDN, also represent a highly studied subject (AL-AWAMI; SORTOMME, 2012).

In order to include the EVCC within the EDN optimization framework, let EV be the set of EVs plugged into the grid. P_e^{EV} is the power injected/drawn by EV e, and it is equal to the sum of the maximum charging and discharging powers ($\bar{P}_e^{EV+}$ and $\bar{P}_e^{EV-}$, respectively) multiplied by the binary variables y_e and z_e, which represent the charging or discharging state, as shown in (84). Moreover, (85) ensures only one action for the EV (e.g., charging, discharging, or idle). Due to the binary nature of these variables, a MILP model is obtained as the result of their inclusion.

$$P_e^{EV} = \bar{P}_e^{EV+} y_e - \bar{P}_e^{EV-} z_e \qquad \forall e \in EV \tag{84}$$

$$y_e + z_e \leqslant 1 \qquad \forall e \in EV \tag{85}$$

On the other hand, EVs storage capacity also needs to be taken into account, i.e., the maximum energy limit ($\bar{E}_e^{EV}$) and, for V2G applications, the maximum depth of discharge (DoD) must be always fulfilled. Hence, if an EV is charged/discharged constantly at P_e^{EV} during a time interval Δt, (86) ensures that the state of charge (SOC) is always maintained between the pre-established limits.

$$\min \left(E_e^{EVi}, \bar{E}_e^{EV} DoD\right) \leqslant E_e^{EVi} + \Delta t(\bar{P}_e^{EV+} y_e \eta_e^{EV+} - \bar{P}_e^{EV-} z_e \eta_e^{EV-}) \leqslant \bar{E}_e^{EV} \qquad \forall e \in EV \tag{86}$$

Where, E_e^{EVi} is the initial SOC for EV e; while, η_e^{EV+} and η_e^{EV-} are the charging and discharging efficiencies, respectively.

The interaction of the EVs with the grid is integrated in the steady-state operation as follows.

Current-Based Representation – EV: Equations (87) and (88) represent the EV active and reactive powers in terms of the voltage operation point (V_e^*) where the EV is plugged, and the EV current (I_e^{EVre}). Considering that EVs will only exchange active power. Moreover, (89) and (90) are the extensions of (8) and (9) taking into account the EV current injection in each node.

$$P_e^{EV} = V_e^{re*} I_e^{EVre} + V_e^{im*} I_e^{EVim} \qquad \forall e \in EV \tag{87}$$

$$0 = -V_e^{re*} I_e^{EVim} + V_e^{im*} I_e^{EVre} \qquad \forall e \in EV \tag{88}$$

$$\begin{aligned} I_{m,f}^{Gre} + \sum_{km \in L} I_{km,f}^{re} - \sum_{mn \in L} I_{mn}^{re} - \left(\sum_{km \in L} B_{km,f} + \sum_{mn \in L} B_{mn,f} \right) \frac{V_{m,f}^{im}}{2} \\ = I_{m,f}^{Dre} + \sum_{e \in EV} I_e^{EVre} \gamma_{e,m,f} \qquad \forall m \in N, f \in F \end{aligned} \tag{89}$$

$$\begin{aligned} I_{m,f}^{Gim} + \sum_{km \in L} I_{km,f}^{im} - \sum_{mn \in L} I_{mn}^{im} - \left(\sum_{km \in L} B_{km,f} + \sum_{mn \in L} B_{mn,f} \right) \frac{V_{m,f}^{re}}{2} \\ = I_{m,f}^{Dim} + \sum_{e \in EV} I_e^{EVim} \gamma_{e,m,f} \qquad \forall m \in N, f \in F \end{aligned} \tag{90}$$

Where, $\gamma_{x,m,f}$ is a binary parameter that takes a value of 1 if the device x is connected at node m and phase f.

Power-Based Representation – EV: For this formulation, (91) represents the active power balance in each node, taking into account the EV active power injection/consumption.

$$\sum_{km \in L} P_{km,f} - \sum_{mn \in L} \left(P_{mn,f} + P_{mn,f}^{L} \right) + P_{m,f}^{G} = P_{m,f}^{D} + \sum_{e \in EV} P_e^{EV} \gamma_{e,m,f} \qquad \forall m \in N, f \in F \tag{91}$$

Therefore, the complete MILP formulations for an unbalanced EDN, considering EV operation is presented in (92) and (93) for the current-based and power-based formulations, respectively.

$$\min \alpha \tag{92}$$

subject to: (6)- (9), (15), (16), and (84)- (90)

$$\min \alpha \tag{93}$$

subject to: (31), (41)- (43), (84)- (86), and (91)

2.8 DISTRIBUTED GENERATION

Since the decade of 2000s, distributed generation has continuously grown among EDNs, motivated by economic, environmental, technical, and market related features (ACKERMANN; ANDERSSON; SÖDER, 2001; QIAN et al., 2008). Due to the flexibility of DG as a power source, distribution networks have been transformed from a passive network to an active network. Nowadays, DG plays an important role in the operation, structure and design of EDNs; therefore, several researches have been developed to model the integration of DG units in the network operation (BOLLEN; HASSAN, 2011; LOPES et al., 2007; RUEDA-MEDINA et al., 2013).

DG units are integrated into the EDN in places that were not originally adapted to connect them, and can create several problems for distribution networks in terms of stability and power quality; particularly, when large amounts of DG units are connected to high impedance networks. In addition, integrating renewable sources of DG, such as wind or solar power, can mean new challenges to the EDN operation. Furthermore, according to the capacity of the DG units, the EDN can become an active network, attending loads without the need of the energy purchased from the main grid. Therefore, the inclusion of the DG in the study of the operation of EDNs is imperative (ALEIXO et al., 2013).

On the other hand, DG may also offer several advantages to the EDN, i.e., improving system reliability, reducing energy losses, reducing transmission and distribution line costs, and alleviating congestion in the grid. Moreover, the installation of small-scale DG units, close to loads, may delay or avoid investments in additional transmission or distribution infrastructure. In addition, certain types of DGs also have the ability to offer ancillary services, such as reactive power support, voltage control, and frequency control (RUEDA-MEDINA et al., 2013).

Typically, in mathematical representations for DG units in steady-state studies, the models of synchronous generators (SiGs), induction generators (IGs), and doubly-fed induction generators (DFIGs) are disregarded. DG units are commonly modelled by a simple representation and coupling elements are not detailed. Hence, a simple mathematical representation is presented in (94)–(97) for the generation limits of DG units.

$$\left(P_n^{DG}\right)^2 + \left(Q_n^{DG}\right)^2 \leqslant \left(\bar{S}_n^{DG}\right)^2 \qquad \forall n \in DG \tag{94}$$

$$Q_n^{DG} \leqslant P_n^{DG} \tan(\arccos(pf_n^{DG})) \qquad \forall n \in DG \tag{95}$$

$$\underline{Q_n^{DG}} \leqslant Q_n^{DG} \leqslant \overline{Q_n^{DG}} \qquad \forall n \in DG \tag{96}$$

$$P_n^{DG} \geqslant 0 \qquad \forall n \in DG \tag{97}$$

Where, $DG \subseteq N$represents the set of nodes in which a DG unit is connected. P_n^{DG} and $Q_n^{DG}$are the active and reactive powers of DG unit n; while, pf_n^{DG} is the minimum power factor, $\underline{Q}_n^{DG}$ and $\bar{Q}_n^{DG}$are the minimum and maximum reactive power limits, and, S_n^{DG} is the maximum apparent power. Therefore, (94) shows the nonlinear representation for the apparent power limit, and it is approximated in (98) via a piecewise linearization technique. Constraints (95) and (96) limit the reactive power in terms of the power factor and the maximum and minimum reactive power limits, respectively. Finally, (97) ensures non-negativity for the active power of the DG unit.

$$f\left(P_n^{DG}, \overline{P_n^{DG}}, \Lambda\right) + f\left(Q_n^{DG}, \overline{Q_n^{DG}}, \Lambda\right) \leqslant (\bar{S}_n^{DG})^2 \qquad \forall n \in DG \tag{98}$$

On the other hand, an improved and realistic model for DG units, considering the capability curves (see Fig. 5) for SiGs and DFIGs is presented in Rueda-Medina et al. (2013). These types of generators are widely used in DG applications, e.g., wind turbines, biomass-based CHP generation systems, and small hydroelectric plants.

Figure 5 – Capability curves: (a) DFIG and (b) SiG.

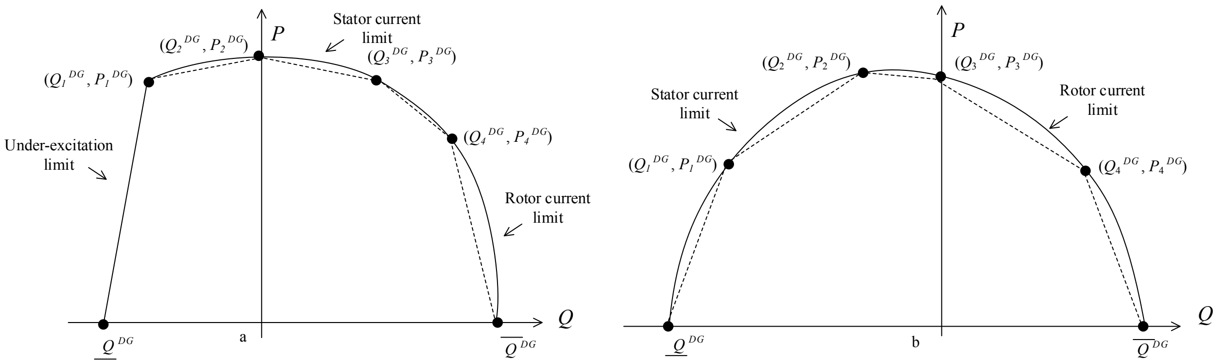

Source: Adapted (RUEDA-MEDINA et al., 2013).

Fig. 5 defines the points $(Q_{1,n}^{DG}, P_{1,n}^{DG})$, $(Q_{2,n}^{DG}, P_{2,n}^{DG})$, $(Q_{3,n}^{DG}, P_{3,n}^{DG})$, and $(Q_{4,n}^{DG}, P_{4,n}^{DG})$, which are used to obtain linear expressions for the DG operation constraints, as shown in (99)- (102). Table 2 shows how these points were obtained for each type of generator.

Table 2 – Linearization points for the linearization of DG capability curves

	SiG	DFIG
$(Q_{1,n}^{DG}, P_{1,n}^{DG})$	the intersection between the under-excitation and armature current limits	half of the arc of the armature current limit between points $(\underline{Q}_n^{DG}, 0)$ and $(Q_{2,n}^{DG}, P_{2,n}^{DG})$
$(Q_{2,n}^{DG}, P_{2,n}^{DG})$	the intersection between the armature current limit and the P axis	the intersection between the armature current and field current limits,
$(Q_{3,n}^{DG}, P_{3,n}^{DG})$	half of the arc of the armature current limit between points $(Q_{2,n}^{DG}, P_{2,n}^{DG})$ and $(Q_{4,n}^{DG}, P_{4,n}^{DG})$	the intersection between the field current limit and the P axis
$(Q_{4,n}^{DG}, P_{4,n}^{DG})$	the intersection between the armature current and field current limits	the half of the arc of the field current limit between points $(Q_{3,n}^{DG}, P_{3,n}^{DG})$ and $(\bar{Q}_n^{DG}, 0)$

Source: Adapted (RUEDA-MEDINA et al., 2013).

$$P_n^{DG} \leqslant \frac{P_{1,n}^{DG}}{Q_{1,n}^{DG} - \underline{Q}_n^{DG}}(Q_n^{DG} - \underline{Q}_n^{DG}) \qquad \forall n \in DG \tag{99}$$

$$P_n^{DG} \leqslant \frac{P_{2,n}^{DG} - P_{1,n}^{DG}}{Q_{2,n}^{DG} - Q_{1,n}^{DG}}(Q_n^{DG} - Q_{2,n}^{DG}) + P_{2,n}^{DG} \qquad \forall n \in DG \tag{100}$$

$$P_n^{DG} \leqslant \frac{P_{3,n}^{DG} - P_{2,n}^{DG}}{Q_{3,n}^{DG} - Q_{2,n}^{DG}}(Q_n^{DG} - Q_{3,n}^{DG}) + P_{3,n}^{DG} \qquad \forall n \in DG \tag{101}$$

$$P_n^{DG} \leqslant \frac{P_{4,n}^{DG}}{Q_{4,n}^{DG} - \bar{Q}_n^{DG}}(Q_n^{DG} - \bar{Q}_n^{DG}) \qquad \forall n \in DG \tag{102}$$

Moreover, the power injection of the DG units connected in the system is integrated in the EDN steady-state formulations as follows.

Current-Based Representation – DG Units: Assuming three-phase DG units, (103) and (104) represent the DG unit active and reactive powers in terms of the voltage operation point and their currents ($I_{n,f}^{DG}$). Finally, the current injection due to DG units is included in the current balance for each node, as shown in (105) and (106).

$$P_n^{DG}/3 = V_{n,f}^{re*} I_{n,f}^{DGre} + V_{n,f}^{im*} I_{n,f}^{DGim} \qquad \forall n \in DG, f \in F \tag{103}$$

$$Q_n^{DG}/3 = -V_{n,f}^{re*} I_{n,f}^{DGim} + V_{n,f}^{im*} I_{n,f}^{DGre} \qquad \forall n \in DG, f \in F \tag{104}$$

$$I_{m,f}^{Gre} + I_{m,f}^{DGre} + \sum_{km \in L} I_{km,f}^{re} - \sum_{mn \in L} I_{mn}^{re} - \left(\sum_{km \in L} B_{km,f} + \sum_{mn \in L} B_{mn,f}\right)\frac{V_{m,f}^{im}}{2} = I_{m,f}^{Dre} \tag{105}$$
$$\forall m \in N, f \in F$$

$$I_{m,f}^{Gim} + I_{m,f}^{DGim} + \sum_{km \in L} I_{km,f}^{im} - \sum_{mn \in L} I_{mn}^{im} - \left(\sum_{km \in L} B_{km,f} + \sum_{mn \in L} B_{mn,f} \right) \frac{V_{m,f}^{re}}{2} = I_{m,f}^{Dim} \quad (106)$$

$$\forall m \in N, f \in F$$

Power-Based Representation – DG Units: For this formulation, active and reactive powers are included in the power balance as shown in (107) and (108).

$$\sum_{km \in L} P_{km,f} - \sum_{mn \in L} \left(P_{mn,f} + P_{mn,f}^{L} \right) + P_{m,f}^{G} + P_{m}^{DG}/3 = P_{m,f}^{D} \qquad \forall m \in N, f \in F \quad (107)$$

$$\sum_{km \in L} Q_{km,f} - \sum_{mn \in L} \left(Q_{mn,f} + Q_{mn,f}^{L} \right) + Q_{m,f}^{G} + Q_{m}^{DG}/3 = Q_{m,f}^{D} \qquad \forall m \in N, f \in F \quad (108)$$

Therefore, the complete LP formulations for an unbalanced EDN, considering DG units is presented in (109) and (110) for the current-based and power-based formulations, respectively.

$$\min \alpha \quad (109)$$

subject to: (6)- (9), (15), (16), (95)- (98), and (103)- (106)

$$\min \alpha \quad (110)$$

subject to: : (31), (41)- (43), (95)- (98), (107), and (108)

2.8.1 Renewable DG

Different from the dispatchable DG, in which the EDN operator controls the active and reactive powers injection for each DG unit, renewable generation depends on availability of renewable resources (e.g., wind speed and solar irradiance). Nowadays, renewable DG has taken an important role in the decentralization of energy production (ATWA et al., 2010). Due to difficulties related to DG forecasting when it operates from renewable energy sources, additional considerations must be taken into account to properly include this type of DG into a distribution network optimization framework. Moreover, with the increase in penetration of these technologies, issues related to voltage profiles, energy losses, restoration actions, and network reinforcements have to be addressed.

In this regard, (111) represents an additional constraint for renewable DG units, and models an active power curtailment. This technique is used in order to avoid undesired levels of power injection from renewable sources which can lead to voltage rises and high energy losses (TONKOSKI; LOPES; EL-FOULY, 2011; WECKX; GONZALEZ; DRIESEN, 2014).

$$\hat{P}_n^{DG} = P_n^{DG} + \tilde{P}_n^{DG} \qquad \forall n \in DG \tag{111}$$

Where, $\hat{P}_n^{DG}$ and $\tilde{P}_n^{DG}$are the maximum available power and the power curtailment for DG unit n. Under this optimization scheme, $\hat{P}_n^{DG}$ will depend on the availability related to the renewable energy source (e.g., wind speed and solar irradiance); hence, multi-scenario approaches are mainly used to tackle this problems.

2.9 ENERGY STORAGE DEVICES

ESSs have been foregrounded as an answer to conciliate time-difference between excessive generation and peak demand. In recent years, energy storage devices prices have declined, which in turn, raised the usage of these technologies in the EDNs. For electric distribution, battery-based ESSs (BESS) are the most common type of storage. This is because other storage technologies such as super capacitors and flywheels are characterized by their high energy cost and are primarily applied on high power, short duration applications. Hence, due to the growth in the utilization of BESS and their constant interaction with renewable DG and EVs, their inclusion in the distribution network steady-state operation must be addressed (ELNOZAHY; ABDEL-GALIL; SALAMA, 2015; ROSS et al., 2010; SABILLON-ANTUNEZ et al., 2017).

2.9.1 BESS Operation

The BESS power drawn or injected from/to the grid must be taken into account in the steady-state operation of the system. Thus, let SD be the set of BESSs plugged into the grid. P_u^{SD} is the power injected/drawn by BESS u, and it is equal to the sum of two non-negative variables that represent the ESS charging and discharging powers (P_u^{SD+} and P_u^{SD-}, respectively), as shown in (112). Moreover, (113) and (114) limit the variables P_u^{SD+} and P_u^{SD-}, in terms of the BESS maximum charging/discharging power ($\bar{P}_u^{SD}$) and the binary variables w_u and x_u. Equation (115) ensures only one action for the BESS (e.g., charging, discharging, or idle). Due to the integer nature of these variables, once they are included in the distribution network optimization framework, we obtain a MILP problem.

$$P_u^{SD} = P_u^{SD+} - P_u^{SD-} \qquad \forall u \in SD \tag{112}$$

$$0 \leqslant P_u^{SD+} \leqslant \bar{P}_u^{SD} w_u \qquad \forall u \in SD \tag{113}$$

$$0 \leqslant P_u^{SD-} \leqslant \bar{P}_u^{SD} x_u \qquad \forall u \in SD \tag{114}$$

$$w_u + x_u \leqslant 1 \qquad \forall u \in SD \tag{115}$$

On the other hand, BESS have physical constraints regarding their storage capacity, i.e., the maximum energy limit ($\bar{E}_u^{SD}$) and the maximum DoD must be always fulfilled. Hence, if the P_u^{SD} is maintained during a time interval Δt, (116) keeps the BESS energy level between the pre-established limits.

$$\bar{E}_u^{SD} DoD \leqslant E_u^{SDi} + \Delta t(P_u^{SD+}\eta_u^{+} - P_u^{SD-}\eta_u^{-}) \leqslant \bar{E}_u^{SD} \qquad \forall u \in SD \tag{116}$$

Where, E_u^{SDi} is the initial SOC for BESS u; while, η_u^{+} and η_u^{-} are the charging and discharging efficiencies, respectively.

The interaction of the BESSs with the grid is integrated in the steady-state operation as follows.

Current-Based Representation – BESS: Initially, in (117) and (118) the active and reactive powers injected or consumed by the BESS are expressed in terms of the voltage operation point (V_u^{*}) where the BESS is connected and the BESS current (I_u^{SDre}). Considering that BESSs will only inject/drawn active power. Moreover, (119) and (120) are the extensions of (8) and (9) taking into account the BESS current injection in each node.

$$P_u^{SD} = V_u^{re*} I_u^{SDre} + V_u^{im*} I_u^{SDim} \qquad \forall u \in SD \tag{117}$$

$$0 = -V_u^{re*} I_u^{SDim} + V_u^{im*} I_u^{SDre} \qquad \forall u \in SD \tag{118}$$

$$\begin{aligned} I_{m,f}^{Gre} + \sum_{km \in L} I_{km,f}^{re} - \sum_{mn \in L} I_{mn}^{re} - \left(\sum_{km \in L} B_{km,f} + \sum_{mn \in L} B_{mn,f} \right) \frac{V_{m,f}^{im}}{2} \\ = I_{m,f}^{Dre} + \sum_{u \in SD} I_u^{SDre} \gamma_{u,m,f} \qquad \forall m \in N, f \in F \end{aligned} \tag{119}$$

$$\begin{aligned} I_{m,f}^{Gim} + \sum_{km \in L} I_{km,f}^{im} - \sum_{mn \in L} I_{mn}^{im} - \left(\sum_{km \in L} B_{km,f} + \sum_{mn \in L} B_{mn,f} \right) \frac{V_{m,f}^{re}}{2} \\ = I_{m,f}^{Dim} + \sum_{u \in SD} I_u^{SDim} \gamma_{u,m,f} \qquad \forall m \in N, f \in F \end{aligned} \tag{120}$$

Where, $\gamma_{x,m,f}$ is a binary parameter that takes a value of 1 if the device x is connected at node m and phase f.

Power-Based Representation – BESS: For this formulation, (121) represents the active power balance in each node, taking into account the BESS active power injection/consumption.

$$\begin{aligned} \sum_{km \in L} P_{km,f} - \sum_{mn \in L} \left(P_{mn,f} + P_{mn,f}^{L} \right) + P_{m,f}^{G} = P_{m,f}^{D} + \sum_{u \in SD} P_u^{SD} \gamma_{u,m,f} \\ \forall m \in N, f \in F \end{aligned} \tag{121}$$

Therefore, the complete MILP formulations for an unbalanced EDN, considering BESS is presented in (122) and (123) for the current-based and power-based formulations, respectively.

$$\min \alpha \tag{122}$$

subject to: (6)- (9), (15), (16), and (112)- (120)

$$\min \alpha \tag{123}$$

subject to: (31), (41)- (43), (112)- (116), and (121)

2.10 VOLTAGE AND REACTIVE POWER CONTROL DEVICES

Voltage optimization and reactive power control have been widely used in power systems as tools to improve energy efficiency and quality (AHMADI; MARTÍ; DOMMEL, 2015; PADILHA-FELTRIN; QUIJANO; MANTOVANI, 2015). In EDNs, the management of voltage magnitudes variations together with the reactive power flows is known as volt-var control (VVC). The main objective of the VVC is to determine control actions for the devices related to voltage management and reactive power flow management. The classical devices controlled within a VVC scheme are on-load tap changers (OLTCs), voltage regulators (VRs), and switchable capacitor banks (CBs). Hence, the optimization of the VVC will pursue a proper distribution network operation, while maximizing or minimizing an objective imposed by the distribution network operator, e.g., power loss reduction, minimization of voltage deviation, or maximization of energy efficiency.

In this framework the mathematical modeling for the optimization of the VVC problem is presented. A solution for the VVC problem will provide the number of enabled/disabled modules in every CB, and the tap position for the OLTCs and VRs. Hence, the mathematical representation for the switchable CBs, OLTCs, and VRs, are shown for both LP formulations. Due to the integer nature of the variables that model the operation of the VVC devices, the obtained formulations correspond to a MILP problem.

2.10.1 Capacitor Banks

The inclusion of switchable CBs in the EDN operation will represent an injection of reactive power that will depend on the number of CB modules enabled. Thus, let $CB \subseteq N$ be the set of nodes where a three-phase CB is installed. B_n is an integer variable that represents the number of modules enabled from the CB connected at node n; $\bar{B}_n$ is the maximum number of CB modules; Q_n^{cb} is the reactive power delivered; and Q_n^{esp} is the reactive power capacity of each module. Equation (124) represents the reactive power injected by the modules of the switchable CBs, while the maximum number of operating modules for each BC is modeled by (125).

$$Q_n^{cb} = B_n Q_n^{esp} \qquad \forall n \in CB \tag{124}$$

$$0 \leqslant B_n \leqslant \bar{B}_n \qquad \forall n \in CB \tag{125}$$

Furthermore, in a multi-period optimization where the CB operations permitted along the entire time period must be limited, (126) must be taken into account.

$$\sum_{t \in T} |B_{n,t} - B_{n,t-1}| \leqslant \Delta^{cb} \qquad \forall n \in CB \tag{126}$$

Where, T is the set of time intervals;$B_{n,t}$ is the number of modules enabled from the CB connected at node n in time t; and Δ^{cb} is the maximum number of operations allowable over the time period.

The reactive power injection Q_n^{cb} is included in the steady-state operation of the distribution network as follows.

Current-Based Representation – Capacitor Banks: The active and reactive power of the switchable CBs are represented by (127) and (128), considering that the value for the active power injection of every CB will always be equal to zero. Moreover, the current balances in each node are updated to include the injection due to the CB reactive power , as shown in (129) and (130).

$$0 = V_{n,f}^{re*} I_{n,f}^{cbre} + V_{n,f}^{im*} I_{n,f}^{cbim} \qquad \forall n \in CB, f \in F \tag{127}$$

$$\frac{Q_n^{cb}}{3} = -V_{n,f}^{re*} I_{n,f}^{cbim} + V_{n,f}^{im*} I_{n,f}^{cbre} \qquad \forall n \in CB, f \in F \tag{128}$$

$$I_{m,f}^{Gre} + \sum_{km \in L} I_{km,f}^{re} - \sum_{mn \in L} I_{mn}^{re} - \left(\sum_{km \in L} B_{km,f} + \sum_{mn \in L} B_{mn,f} \right) \frac{V_{m,f}^{im}}{2} = I_{m,f}^{Dre} - I_{n,f}^{cbre} \quad \forall n \in N, f \in F \tag{129}$$

$$I_{m,f}^{Gim} + \sum_{km \in L} I_{km,f}^{im} - \sum_{mn \in L} I_{mn}^{im} - \left(\sum_{km \in L} B_{km,f} + \sum_{mn \in L} B_{mn,f} \right) \frac{V_{m,f}^{re}}{2} = I_{m,f}^{Dim} - I_{n,f}^{cbim} \quad \forall n \in N, f \in F \tag{130}$$

Where, $I_{n,f}^{cbre}$ and $I_{n,f}^{cbre}$ are the real and imaginary parts of the current injected in phase f, by the CB connected and node n.

Power-Based Representation – Capacitor Banks: For this formulation, the $Q^{cb}$is included in the reactive power balance as shown in (131).

$$\sum_{km \in L} Q_{km,f} - \sum_{mn \in L} \left(Q_{mn,f} + Q_{mn,f}^{L} \right) + Q_{m,f}^{G} = Q_{m,f}^{D} - Q_m^{cb} \qquad \forall n \in N, f \in F \tag{131}$$

2.10.2 On-load Tap Changers and Voltage Regulators

OLTCs and VRs are the devices in charge of controlling the voltage magnitudes in the EDN, within a VVC environment. These devices adjust their input voltage through tap changing, and their operation can be represented under the same mathematical formulation. Thus, let $RT \subseteq L$ be the set of circuits where a VR is installed. $tp_{mn,f}$ is the integer variable that defines the tap position for the VR installed in circuit mn, in phase f; while, $Tp_{mn,f}$ is the maximum number of taps; and $\%R_{mn}$ is the regulation percentage.

Independent of the steady-state formulation adopted, (132) represents the minimum and maximum limits of the tap position. Analogue to CB, the number of tap changes permitted along the entire time period must be limited in a multi-period optimization; hence, under such scenario (133) must be taken into account. Where, Δ^{vr} represents the maximum number of tap changes allowed.

$$-Tp_{mn} \leqslant tp_{mn,f} \leqslant Tp_{mn} \qquad \forall mn \in RT, f \in F \tag{132}$$

$$\sum_{t \in T} |tp_{mn,f,t} - tp_{mn,f,t-1}| \leqslant \Delta^{vr} \qquad \forall mn \in RT, f \in F \tag{133}$$

Current-Based Representation – OLTCs and VRs: In this formulation, (134) and (135) represent the real and imaginary regulated voltage; while, (136) and (137) represent the real and imaginary regulated current on each VR.

$$V^{re}_{n,f} = (1 + \%R_{mn} tp_{mn,f}/Tp_{mn}) V^{re}_{m,f} \qquad \forall mn \in RT, f \in F \tag{134}$$

$$V^{im}_{n,f} = (1 + \%R_{mn} tp_{mn,f}/Tp_{mn}) V^{im}_{m,f} \qquad \forall mn \in RT, f \in F \tag{135}$$

$$I^{re}_{km,f} = (1 + \%R_{mn} tp_{mn,f}/Tp_{mn}) I^{re}_{mn,f} \qquad \forall mn \in RT, f \in F \tag{136}$$

$$I^{im}_{km,f} = (1 + \%R_{mn} tp_{mn,f}/Tp_{mn}) I^{im}_{mn,f} \qquad \forall mn \in RT, f \in F \tag{137}$$

Equations (134)- (137) represent the operation of VRs and OLTCs in terms of the real and imaginary voltages and currents of the EDN. Nevertheless, the nonlinearities presented have to be addressed, i.e., the product of the decision variables $tp_{mn,f}$ and, $V_{m,f}$ or $I_{mn,f}$ on the real and imaginary components. In this regard, the integer number of steps is represented as a set of binary variables $bt_{mn,f}$ and the products $tp_{mn,f}V_{m,f}$, $tp_{mn,f}I_{mn,f}$ are substituted by auxiliary variables $V^c_{mn,f,k}$ and $I^c_{mn,f,k}$, respectively.

A linear extension for (134)- (137) is presented in (138)- (151), where (138) and (139) represent the calculation of the regulated voltage, and, (140) and (141) the calculation of the regulated current. Constraint (142) associates the set of binary variables with the tap integer variable. Equations (143)- (144), and (145)- (146), define the auxiliary variables $V^c_{mn,f,k}$ and $I^c_{mn,f,k}$, respectively; while, (147)- (148), and (149)- (150) describe their limits. Finally, (151) represents the sequencing of the binary variable $bt_{mn,f}$.

$$V^{re}_{n,f} = (1 - \%R_{mn})V^{re}_{m,f} + \sum_{k=1}^{2Tp_{mn}} \frac{\%R_{mn}}{Tp_{mn}} V^{c(re)}_{mn,f,k} \qquad \forall mn \in RT, f \in F \tag{138}$$

$$V^{im}_{n,f} = (1 - \%R_{mn})V^{im}_{m,f} + \sum_{k=1}^{2Tp_{mn}} \frac{\%R_{mn}}{Tp_{mn}} V^{c(im)}_{mn,f,k} \qquad \forall mn \in RT, f \in F \tag{139}$$

$$I^{re}_{km,f} = (1 - \%R_{mn})I^{re}_{mn,f} + \sum_{k=1}^{2Tp_{mn}} \frac{\%R_{mn}}{Tp_{mn}} I^{c(re)}_{mn,f,k} \qquad \forall mn \in RT, f \in F \tag{140}$$

$$I^{im}_{km,f} = (1 - \%R_{mn})I^{im}_{mn,f} + \sum_{k=1}^{2Tp_{mn}} \frac{\%R_{mn}}{Tp_{mn}} I^{c(im)}_{mn,f,k} \qquad \forall mn \in RT, f \in F \tag{141}$$

$$\sum_{k=1}^{2Tp_{mn}} bt_{mn,f,k} - Tp_{mn} = tp_{mn,f} \qquad \forall mn \in RT, f \in F \tag{142}$$

$$|V^{re}_{m,f} - V^{c(re)}_{mn,f,k}| \leq \bar{V}(1 - bt_{mn,f,k}) \qquad \forall mn \in RT, f \in F, k = 1...2Tp_{mn} \tag{143}$$

$$|V^{im}_{m,f} - V^{c(im)}_{mn,f,k}| \leqslant \bar{V}(1 - bt_{mn,f,k}) \qquad \forall mn \in RT, f \in F, k = 1...2Tp_{mn} \tag{144}$$

$$|V^{c(re)}_{mn,f,k}| \leqslant \bar{V} bt_{mn,f,k} \qquad \forall mn \in RT, f \in F, k = 1...2Tp_{mn} \tag{145}$$

$$|V^{c(im)}_{mn,f,k}| \leqslant \bar{V} bt_{mn,f,k} \qquad \forall mn \in RT, f \in F, k = 1...2Tp_{mn} \tag{146}$$

$$|I^{re}_{mn,f} - I^{c(re)}_{mn,f,k}| \leqslant \bar{I}_{mn}(1 - bt_{mn,f,k}) \qquad \forall mn \in RT, f \in F, k = 1...2Tp_{mn} \tag{147}$$

$$|I^{im}_{mn,f} - I^{c(im)}_{mn,f,k}| \leqslant \bar{I}_{mn}(1 - bt_{mn,f,k}) \qquad \forall mn \in RT, f \in F, k = 1...2Tp_{mn} \tag{148}$$

$$|I^{c(re)}_{mn,f,k}| \leqslant \bar{I}_{mn} bt_{mn,f,k} \qquad \forall mn \in RT, f \in F, k = 1...2Tp_{mn} \tag{149}$$

$$|I^{c(im)}_{mn,f,k}| \leqslant \bar{I}_{mn} bt_{mn,f,k} \qquad \forall mn \in RT, f \in F, k = 1...2Tp_{mn} \tag{150}$$

$$bt_{mn,f,k} \leqslant bt_{mn,f,k-1} \qquad \forall mn \in RT, f \in F, k = 1...2Tp_{mn} \tag{151}$$

Power-Based Representation – OLTCs and VRs: For the power-based formulation, $V^{sqr}_{m,f}$ is altered by the square of the regulation ratio, which is expressed in terms of the regulation percentage, the tap integer value, and the maximum tap, as shown in (152).

$$V^{sqr}_{n,f} = \left(1 + \%R_{mn} \frac{tp_{mn,f}}{Tp_{mn}}\right)^2 V^{sqr}_{m,f} \qquad \forall mn \in RT, f \in F \tag{152}$$

In order to cope with the nonlinearities observed in (152), $tp^2_{mn,f}$ is represented as a set of binary variables $\forall mn \in RT, f \in F$, and the product $tp^2_{n,f} V^{sqr}_{m,f}$ is represented using the auxiliary variables $V^c_{mn,f}$, as shown in set (153)- (157).

$$V^{sqr}_{n,f} = \sum_{k=1}^{2Tp_{mn}} \left[\frac{\%R_{mn}}{Tp_{mn}} \left(\frac{(2k-1)\%R_{mn}}{Tp_{mn}} + 2(1 - \%R_{mn})\right) V^c_{mn,f,k}\right] + V^{sqr}_{m,f}(1 - \%R_{mn})^2 \qquad \forall mn \in RT, f \in F \tag{153}$$

$$\underline{V}^2(1 - bt_{mn,f,k}) \leqslant V^{sqr}_{m,f} - V^c_{mn,f,k} \qquad \forall mn \in RT, f \in F, k = 1...2Tp_{mn} \tag{154}$$

$$V^{sqr}_{m,f} - V^c_{mn,f,k} \leqslant \bar{V}^2(1 - bt_{mn,f,k}) \qquad \forall mn \in RT, f \in F, k = 1...2Tp_{mn} \tag{155}$$

$$\underline{V}^2 bt_{mn,f,k} \leqslant V^c_{mn,f,k} \leqslant \bar{V}^2 bt_{mn,f,k} \qquad \forall mn \in RT, f \in F, k = 1...2Tp_{mn} \tag{156}$$

$$bt_{mn,f,k} \leqslant bt_{mn,f,k-1} \qquad \forall mn \in RT, f \in F, k = 1...2Tp_{mn} \tag{157}$$

Therefore, the complete MILP formulations for VVC optimization considering operational limits, are presented in (158) and (159), for the current-based and power-based representations, respectively.

$$\min \alpha \tag{158}$$

subject to: (6)- (9), (15), (16), (52), (53), (57), (61)- (63), (124), (125), (127)- (130), (132), and (138)- (151)

$$\min \alpha \tag{159}$$

subject to: (31), (41)- (43), (54), (58), (61), (64), (65), (124), (125), (131), (132), and (153)- (157)

2.11 PIECEWISE LINEARIZATION TECHNIQUE

The piecewise linearization is a technique in which a nonlinear function is approximated using a set of piecewise linear functions (FRANCO et al., 2013). Widely used in engineering, this technique is often employed to cope with quadratic nonlinearities, helping to reach LP models. Typically, a function f is defined in order to calculate the square value of a variable σ, represented as $\sigma^+ + \sigma^-$ and limited by the interval $[0, \bar{\sigma}]$. This type of function has a general structure, as follows:

$$f(\sigma, \bar{\sigma}, \Lambda) = \sum_{\lambda=1}^{\Lambda} \phi_{\sigma,\lambda} \Delta_{\sigma,\lambda} \tag{160}$$

$$\sigma = \sigma^+ - \sigma^- \tag{161}$$

$$\sigma^+ + \sigma^- = \sum_{\lambda=1}^{\Lambda} \Delta_{\sigma,\lambda} \tag{162}$$

$$0 \leqslant \Delta_{\sigma,\lambda} \leqslant \bar{\sigma}/\Lambda \qquad \forall \lambda \in \Lambda \tag{163}$$

$$\phi_{\sigma,\lambda} = (2\lambda - 1)\bar{\sigma}/\Lambda \qquad \forall \lambda \in \Lambda \tag{164}$$

The parameter $\phi_{\sigma,\lambda}$ is calculated to compute the contribution of $\Delta_{\sigma,\lambda}$ in each step of the discretization. The parameter $\bar{\sigma}$ represents the maximum value of σ, while Λ is the number of discretizations used in the linearization.

It is important to remark that this approach is limited to maximizing strictly concave functions or minimizing convex functions. If the application of this technique under different conditions is desired, the inclusion of binary variables and additional constraints is mandatory.

2.12 COMPARATIVE OVERVIEW AND DISCUSSION

The formulations presented, efficiently model the steady-state operation of unbalanced EDNs; constituting a mathematical framework that can be used by planners and operators as a tool inside optimization methods and algorithms, aiming to optimize specific goals. Although both formulations target the same objective, the planner/operator can choose the one that better accommodates and fits the problem that he is aiming to tackle. In order to make this decision, the following considerations must be addressed and well-thought:

1. Although both formulations show high accuracy determining the steady-state operation point, the current-based model slightly outperforms the power-based.
2. Due to its representation in terms of the real and imaginary parts of voltages and currents, modeling operational limits within the current-based formulation requires a high number of constraints. This fact conveys to higher computational burden, which can slow down the solution process especially in large-scale test systems.
3. In optimization methods or algorithms applied over non-stressed test systems, where operational limits are not a concern to the optimizer (e.g., demand response or market-based optimizations), the current-based formulation may highlight as a better option.

4. As mentioned, both formulations can handle optimizations algorithms taking into account smart grid devices plugged into the network. Nevertheless, the mathematical representation of the considered smart grid devices can sway the formulation choice; e.g., in a volt-var approach, the power-based formulation will be recommended, as the volt-var devices influence directly over the voltage magnitude and reactive power flows.

5. Finally, the load behavior is also an important feature to take into account as it impacts directly in the operation point estimation. Both LP formulations rely on the accuracy of the estimated operation point. In this regard, in little observable distribution networks, estimating voltages will be an easier task to the planner/operator than estimating power flows along the grid. Hence, the current-based formulation will suit better to this application.

It is important to remark that every optimization problem targeted in EDN will bring specific considerations that have to be analyzed to make the best choice.

2.13 CHAPTER CONCLUSIONS

This chapter has presented two mathematical formulations for the steady-state operation of EDN that consider the unbalance of three-phase networks. Mathematical representations for the operational limits and several smart-grid-related devices (e.g., electric vehicles, energy storage systems, voltage regulators, and capacitor banks) were also presented. Besides, distributed generation units were included in the formulations. Finally, the load voltage dependency, which is an important feature in voltage and reactive power control algorithms, was modeled in both representations.

The performance of these representations was compared with the simulation tool OpenDSS; and the results showed that both representations offer a good accuracy. These formulations constitute a mathematical framework for optimization analysis of the EDN operation, which makes it possible to formalize decision-making processes (i.e., control algorithms and strategies for the network operation). Objectives related to technical and/or economic aspects can be pursued within the framework.

The EDN was modeled using sets of nonlinear constraints. Nevertheless, linear programming (LP) representations were later reached, aiming to avoid the complexity related to the solution of nonlinear programming problems. Nonlinearities were coped with using linearization and approximation techniques, which were applied to achieve an LP model for each approach. Both formulations are equivalent, and the selection of either will depend on the complexity of the problem to be solved. It is important to recall that several linearization techniques increase the number of variables and constraints; hence, the complexity of the problem increase when solved via classical optimization.

Part II

Smart Grid Operation Optimization

3 ELECTRIC VEHICLES CONSIDERING V2G TECHNOLOGY

In this chapter, a new methodology based on a mixed integer linear programming formulation is proposed to solve the optimal charging coordination of electric vehicles (EVs) in unbalanced electrical distribution networks (EDNs) considering vehicle-to-grid (V2G) technology. The steady-state operation of the EDN is represented using the real and imaginary parts of voltages and currents at nodes and circuits respectively. Distributed generation (DG) and the imbalance of the system circuits and loads are taken into account. The developed method defines an optimal charging schedule for the EVs. This charging schedule considers the EVs' arrival and departure times and their arrival state of charge, along with the energy contribution of EVs equipped with V2G technology. The presented formulation was tested in a 123-nodes distribution system. The charging schedule obtained was compared in terms of V2G and DG scenarios, demonstrating the efficiency of the proposed method.

3.1 INTRODUCTION

In recent years, energy and transport sectors have been experiencing revolutionary changes due to environmental concerns and desires for energy independence. The transport sector is becoming part of the electrification movement. As such, the use of EV will increase over the coming years (ANGLANI; FATTORI; MULIERE, 2012; BEVIS et al., 2009). Instead of fossil fuel energy, EVs use batteries to store the energy needed for transportation. Reducing the dependency on fossil fuel, these batteries are charged on an EDN. If the charging of EVs is not controlled, the EDN can experience overloads, voltage limit violations, and an excessive increase in power losses (LIN et al., 2010; WU; ALIPRANTIS; GKRITZA, 2011). Given the increasing presence of EVs in the EDN, these issues must be anticipated. To counteract the problem associated with a high load of EVs linked to the system, a charging schedule must be set to coordinate the recharging of EV batteries. The communication infrastructure of forthcoming smart grids will become an essential part of controlling EV recharging in EDNs (SOJOUDI; LOW, 2011).

The EV charging coordination (EVCC) problem seeks an optimal charging schedule for the recharging of EV batteries in a specific time period. In addition to throttling the battery charge, the optimal charging schedule must maximize the energy charged to the EV batteries and minimize power losses. Also, an economical operation for the EDN must be defined, while satisfying operational constraints.

Various works have approached the EVCC problem in EDNs (SOJOUDI; LOW, 2011; TRIPPE; MASSIER; HAMACHER, 2013; WU; ALIPRANTIS; GKRITZA, 2011). Charging costs are optimized in Trippe, Massier e Hamacher (2013) by using a mixed integer linear programming (MILP) formulation in which battery charging profiles are detailed. Mobility demands and maximum power limits are considered, but the impact of the EV load on the grid is disregarded.

Real-time solutions for EVCC are presented in O'Connell, Keane e Flynn (2014), Shaaban et al. (2014), and Deilami et al. (2011). A multi-period optimization for EV charging in EDNs is proposed on O'Connell, Keane e Flynn (2014). This optimization aims to minimize the cost of charging EVs, while disregarding the energy cost of the loads on the EDN. A nonlinear programming model is proposed and solved using a nonlinear programming function of MATLAB. In Shaaban et al. (2014), the goal is to optimally charge the EVs and minimize system operating costs without violating the power system constraints. A prediction unit that forecasts the EV power demand is proposed to ensure the feasibility of the charging process. A two-stage optimization process is presented to ensure effective charging coordination. In Deilami et al. (2011), an algorithm based on sensitivities is proposed for the real-time coordination of EV charging considering the random arrivals and departures of EVs, voltage profile, and power generation limits, in order to minimize the total energy cost.

In Karfopoulos e Hatziargyriou (2013), Unda et al. (2014), and Papadopoulos et al. (2013), EV charging management models with operational frameworks based on multi-agent system (MAS) technology are proposed. A distributed price-based control method that considers owners' preferences is developed in Karfopoulos e Hatziargyriou (2013). In Unda et al. (2014), a charging control method developed over a three-layer architecture MAS is presented. The optimal EV charging schedule at the beginning of each charging period is obtained by solving an optimization problem, which considers individual EV needs. The charging schedules are later validated to ensure the technical viability of the solution. In Papadopoulos et al. (2013), important features are added to the approach presented in Unda et al. (2014). The control method presented in Papadopoulos et al. (2013) is also based on a three-layer MAS. This formulation presents not only an optimal charging scheme for normal operation but also an emergency planning method employed when normal conditions are restored after a technical limit breach. However, the EVs are disconnected to restore the proper performance of the EDN (i.e., thermal or voltage limits are already unfulfilled) and not to avoid technical limit violations.

As EVs are gaining relevance in EDNs, the idea of power flowing in both directions is taking hold. The ability of EVs to inject power into the grid is called vehicle-to-grid (V2G) technology. V2G can be defined as the purveyance of energy and ancillary services from an EV to the grid (AL-AWAMI; SORTOMME, 2012). Either at home or in a parking lot, EVs with V2G technology (EV-V2Gs) can provide power to the grid, increasing the stability and reliability of the EDN and reducing EDN costs (KEMPTON; TOMIC, 2005). Studies of battery sizing together with economic assessments of V2G availability have proved how profitable this technology may become (LIU et al., 2012; ROY; BREUCKER; DRIESEN, 2011).

Different approaches to taking advantage of V2G technology have been proposed in the specialized literature. In Han, Han e Sezaki (2010), an aggregator for V2G frequency regulation is developed. This approach establishes that any vehicle that is idle and under aggregator control is a potential provider of a regulation service, considering its available power capacity. The objective is to optimize the aggregator's revenue, while fulfilling the energy requirements of the EV owner. An estimation algorithm for V2G real-time capacity is presented in Kumar et al. (2014). This paper proposes a dynamic scheduling algorithm for EV charging in high-rise residential buildings, office buildings, and commercial buildings. Furthermore, the capacity of an EV fleet to supply V2G power to a building during peak hours is demonstrated, and renewable energy resources are taken into account. The EV-V2Gs were shown to be effective for load peak shaving, but the impact on the EV battery's lifetime was not assessed.

Recent works such as Kumar et al. (2014) and He, Venkatesh e Guan (2012) have foregrounded the importance of the dynamic scheduling on EV charging. In the latter work, the issues arising in the EDN due to uncontrolled EV charging processes are remarked. Nevertheless, the EV charging scheduling alone does not account for EV owners' behavior patterns or unforeseen changes in EV features. Dynamic scheduling is, therefore, crucial for attending EV owners' needs because scheduling may involve the random arrivals and departures of EVs and varying values for the initial charge of the EV batteries. These are the most important EV characteristics addressed by the EVCC problem, and the correct inclusion of these features ensures the better performance of the presented solution method.

A step-by-step methodology based on a MILP formulation is proposed in this work to solve the optimal charging coordination of EVs in unbalanced EDNs considering V2G technology. The steady-state operation of the EDN is represented using the real and imaginary parts of voltages and currents at nodes and circuits, respectively. Linearization techniques were applied to the formulation in order to obtain a MILP model. The imbalance of the system circuits and loads are taken into account. In addition, the proposed formulation considers distributed generation (DG). The developed method defines an optimal charging schedule for the EVs considering the EVs' arrival and departure times and their arrival state of charge, along with the energy contribution of EVs equipped with V2G technology. The model was written in mathematical modeling language AMPL and solved using the commercial solver CPLEX. The classical optimization techniques used to solve the MILP formulation guarantee the optimal solution to the problem. The presented formulation was tested in a 123-node distribution system. The charging schedules obtained for different EV load scenarios evaluated on the EDN prove the robustness of the methodology. This work's main contributions are as follows:

- A new methodology for dynamically controlling the EVCC problem considering V2G technology in unbalanced distribution systems. The methodology is based on an MILP formulation that offers the optimal solution to the problem;
- A step-by-step methodology that considers the randomness of EVs' arrivals and departures times and initial state of charge, as well as different battery sizes and forecast uncertainties;
- A methodology that enhances the EDN operation by including unforeseen EV loads at any time interval. This approach not only solves the EVCC problem, but also optimizes the operation of the EDN, reducing the overall energy costs, while satisfying operational constraints such as voltage and thermal limits.

3.2 METHODOLOGY

The presented methodology solves the EVCC problem finding an optimal schedule for the energy exchange between EV batteries and the grid; moreover, an economic operation for the EDN is defined and operational constraints are satisfied. The optimal charging schedule must minimize the energy cost, avoiding curtailment on the EV batteries and reducing power losses in the EDN. As V2G technology on EVs is taken into account, the solution must provide an optimal schedule that determines when the EV batteries must be charged and when the EV-V2Gs must inject energy into the grid. The complexity of the charging schedule increases, as it is responsible for throttling the battery charge and for allowing the grid to use the vehicles' battery stored energy. In this work, the following considerations are assumed:

- At departure, the vehicles should be completely charged.
- The initial state of charge (SOC) of every vehicle is known when the vehicle is plugged into the grid.
- The batteries can be controlled in each time interval into which the time period is divided.

- The EV-V2Gs can be controlled in order to inject power into the grid according to their available energy.
- The EV-V2Gs owners permit the EDN operator to utilize the energy stored in their vehicles.

Operational constraints such as voltage limits, active and reactive power generation limits, and maximum currents limits, must be satisfied by the model as the charging schedule is being optimized. When being plugged in, the EV's SOC is read, and the EV user may provide a departure time; otherwise, it will be assumed that the vehicle will remain plugged in until a probable time interval has lapsed, as determined by an EV record of departure.

The model is solved in every time interval updating the actual number of connected EVs to be charged. Fig 6 shows how the model is solved for each time interval defining the next step to be implemented by the EDN operator. The red boxes in Fig 6 indicate how the binary nature of variables $y_{n,t}$ and $z_{n,t}$, associated with the charging and discharging of the EVs, is considered only for the next $k-$intervals (defined by the EDN operator); in the remaining time intervals, the binary nature of those variables is disregarded.

Figure 6 – Solution Cycle.

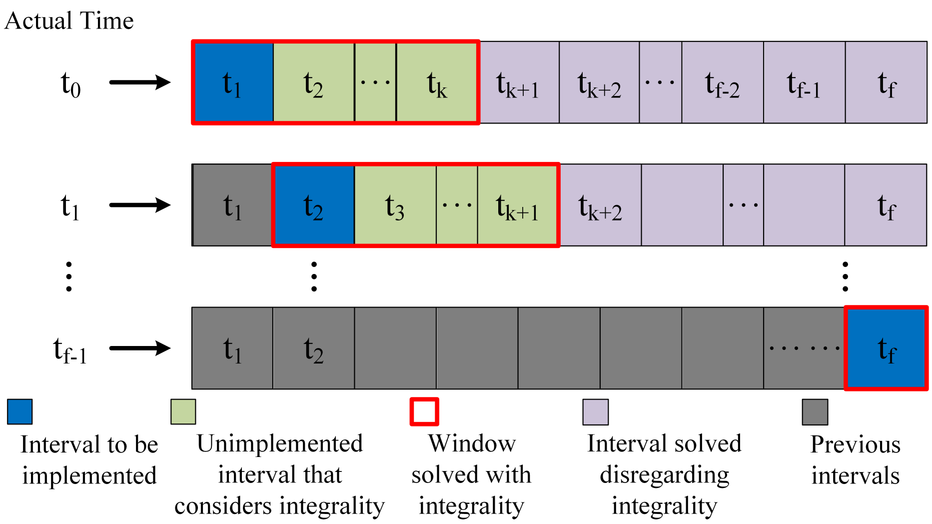

Source: Created by the author.

The EVs' charging schedule will be generated between arrival and departure, ideally dispatching a fully charged battery for every vehicle. Energy curtailment on any EV at departure will incur a penalty. With the model being solved in every time interval, the charging schedule is to be constructed step-by-step, with previous $y_{n,t}$ and $z_{n,t}$ values given from preceding solutions and only the immediate interval's $y_{n,t}$ and $z_{n,t}$ values fixed. When defining the charging schedule, the later connection of EVs is taken into account in order to avoid overloads in the system when added to the EVs already connected.

Therefore, the proposed model includes expected arrival times in the solution. Possible plugs, estimated arrival times, and SOCs are used to get more accurate charging schedules for initial solutions. Later on in the process, when the EVs are actually plugged in, the information can be updated with the real parameters. In cases where the possible arrival time is reached and the EV has not arrived, a different estimation may be used, or the EV may be disregarded altogether. Several techniques can be applied to EVs in order to obtain the estimated parameters for initial SOCs, arrival times and departure times, such as those in Melo, Carreno e Padilha-Feltrin (2014), Qian et al. (2011), and Lojowska et al. (2012). The mathematical model takes into account these parameters when building a charging schedule for every vehicle between their arrival and departure times.

3.3 MATHEMATICAL PROGRAMMING MODEL FOR THE EVCC PROBLEM

A mixed integer nonlinear programming (MINLP) model is presented in (165)–(187) to solve the EVCC problem considering EVs and EV-V2Gs. The EVCC problem is later modeled as a mixed-integer linear programming (MILP) problem. This will improve the solution's robustness and permit the utilization of classical optimization techniques and commercial software, which will guarantee the optimal solution to the problem. In order to obtain a MILP for the EVCC problem, linearization techniques are applied to the MINLP nonlinear expressions.

The proposed formulations consider the sets Ξ, F, L, N, and T to represent electric vehicles, phases, circuits, nodes, and time intervals, respectively. Furthermore, $V^{re/im}_{n,f,t}$ are the real/imaginary parts of the voltage at node n, phase f and time interval t, while $I^{Gre/im}_{n,f,t}$ and $I^{Dre/im}_{n,f,t}$ are the real/imaginary parts of the generated and demanded currents. $P^{G/D}_{n,f,t}$ and $Q^{G/D}_{n,f,t}$ are the generated/demanded active and reactive powers. In addition, $I^{re/im}_{mn,f,t}$ represents the real/imaginary parts of the current through the circuit connecting nodes m and n, while $B_{mn,f}$ is its shunt susceptance for phase f. The real/imaginary parts of the currents corresponding to the EV u are defined as $I^{EVre/im}_{u,t}$, respectively; while $\widehat{V}^{re/im}_{u,t}$ is the real/imaginary part of the voltage at the node and phase associated with electric vehicle u in time t. Finally, $R_{mn,f,h}$ and $X_{mn,f,h}$ are the resistance and reactance for circuit mn between phases f and h.

The circuits and the conventional loads are considered using a three-phase representation, as the EDN is modeled as an unbalanced system. The steady state operation of an unbalanced EDN is indicated by the set of equations (166)–(178), based on the model presented in Franco, Rider e Romero (2015), which considers the presence of DG. In this work, active and reactive power injections of DGs are taken into account and the loads are modeled as a constant power type. EVs may arrive and leave in any time interval within the charging period. If no departure time is specified the model will schedule a fully charged battery by the EV's probable departure time interval. In effect, before its departure time, a vehicle may have any charge level between its initial SOC and its $\overline{E}_u^{EV}$. For EV-V2Gs, this energy level may be lower than its initial SOC but not greater than the maximum depth of discharge (DoD), maintaining at least a minimum energy level $\left(\bar{E}_u^{EV}\xi\right)$.

The time period is divided into several time intervals ordered in the set T; the time interval that begins at a specific time t is associated with the t element from set T. The time duration for every time interval is represented by Δ_t. The proposed model is solved at the beginning of each time interval, constructing a step-by-step solution over the entire time period, and updating the number of EVs connected and their associated data.

The objective function of the EVCC problem represented by (165) aims to minimize the cost of the energy provided by the substation and the distributed generators (the first and second terms, respectively) and to reduce the EV's energy curtailment if the EVs can not be completely charged (third term).

$$\min \sum_{f\in F}\sum_{t\in T}\alpha^G_{S,t}\Delta_t\left(V^{re}_{S,f,t}I^{Gre}_{S,f,t}+V^{im}_{S,f,t}I^{Gim}_{S,f,t}\right)+\sum_{n\in N}\sum_{t\in T}\alpha^G_{n,t}\Delta_t P^G_{n,t}+\sum_{u\in\Xi}\beta E^{SH}_u \tag{165}$$

Subject to:

$$I^{Gre}_{m,f,t}+\sum_{km\in L}I^{re}_{km,f,t}-\sum_{mn\in L}I^{re}_{mn,t}-\left(\sum_{km\in L}B_{km,f}+\sum_{mn\in L}B_{mn,f}\right)\frac{V^{im}_{m,f,t}}{2} = I^{Dre}_{m,f,t}+\sum_{u\in\Xi}I^{EVre}_{u,t}\gamma(u,m,f) \tag{166}$$

$$I^{Gim}_{m,f,t}+\sum_{km\in L}I^{im}_{km,f,t}-\sum_{mn\in L}I^{im}_{mn,t}-\left(\sum_{km\in L}B_{km,f}+\sum_{mn\in L}B_{mn,f}\right)\frac{V^{re}_{m,f,t}}{2} = I^{Dim}_{m,f,t}+\sum_{u\in\Xi}I^{EVim}_{u,t}\gamma(u,m,f) \tag{167}$$

$$P^D_{m,f,t}=V^{re}_{m,f,t}I^{Dre}_{m,f,t}+V^{im}_{m,f,t}I^{Dim}_{m,f,t} \tag{168}$$

$$Q^D_{m,f,t}=-V^{re}_{m,f,t}I^{Dim}_{m,f,t}+V^{im}_{m,f,t}I^{Dre}_{m,f,t}, \tag{169}$$

$$\forall m\in N, f\in F, t\in T$$

$$V^{re}_{m,f,t}-V^{re}_{n,f,t}=\sum_{h\in F}(R_{mn,f,h}I^{re}_{mn,h,t}-X_{mn,f,h}I^{im}_{mn,h,t}) \tag{170}$$

$$V^{im}_{m,f,t}-V^{im}_{n,f,t}=\sum_{h\in F}(X_{mn,f,h}I^{re}_{mn,h,t}+R_{mn,f,h}I^{im}_{mn,h,t}) \tag{171}$$

$$\forall mn\in L, f\in F, t\in T$$

$$0 \leq P_{n,t}^{G} \leq \overline{P}_{n}^{G} \tag{172}$$
$$\underline{Q}_{n}^{G} \leq Q_{n,t}^{G} \leq \overline{Q}_{n}^{G} \tag{173}$$
$$|Q_{n,t}^{G}| \leq P_{n,t}^{G} \tan(\arccos(\phi_n)) \tag{174}$$
$$\frac{P_{n,t}^{G}}{3} = V_{n,f,t}^{re} I_{n,f,t}^{Gre} + V_{n,f,t}^{im} I_{n,f,t}^{Gim} \tag{175}$$
$$\frac{Q_{n,t}^{G}}{3} = -V_{n,f,t}^{re} I_{n,f,t}^{Gim} + V_{n,f,t}^{im} I_{n,f,t}^{Gre} \tag{176}$$
$$\underline{V}^2 \leq {V_{n,f,t}^{re}}^2 + {V_{n,f,t}^{im}}^2 \leq \overline{V}^2 \tag{177}$$
$$\forall n \in N, f \in F, t \in T$$

$$0 \leq {I_{mn,f,t}^{re}}^2 + {I_{mn,f,t}^{im}}^2 \leq {\overline{I}_{mn}}^2 \tag{178}$$
$$\forall mn \in L, f \in F, t \in T$$

$$P_{u,t}^{EV} = V_{u,t}^{re} I_{u,t}^{EVre} + V_{u,t}^{im} I_{u,t}^{EVim} \tag{179}$$
$$0 = -V_{u,t}^{re} I_{u,t}^{EVim} + V_{u,t}^{im} I_{u,t}^{EVre} \tag{180}$$
$$\bar{E}_{u}^{EV} = E_{u,T}^{EV} + E_{u}^{SH} \tag{181}$$
$$P_{u,t}^{EV} = \bar{P}_{u}^{CH} y_{u,t} - \bar{P}_{u}^{DC} z_{u,t} \tag{182}$$
$$E_{u,t}^{EV} = E_{u}^{ini} + \sum_{k \in T, k \leq t} \Delta_k P_{u,k}^{EV} \tag{183}$$
$$\min\left(E_{u}^{ini}, \bar{E}_{u}^{EV} \xi\right) \leq E_{u,t}^{EV} \leq \bar{E}_{u}^{EV} \tag{184}$$
$$y_{u,t} + z_{u,t} \leq 1 \tag{185}$$
$$z_{u,t} \in \{0,1\} \tag{186}$$
$$y_{u,t} \in \{0,1\} \tag{187}$$
$$\forall u \in \Xi, t \in T$$

Also considering that:

$\alpha_{n,t}^{G}$ is the energy cost at node n in time t;

β is the electric vehicle energy curtailment cost;

$\gamma(u, m, f)$ is the function that indicates whether electric vehicle u is connected at node m and phase f;

Δ_t is the duration of the time t;

ϕ_n is the minimum power factor for the operation of the distributed generator at node n;

θ is the vector of reference phase angles;

θ_1/θ_2 is the maximum negative/positive deviation of the phase angle from the reference angle for each phase;

ξ is the minimum percentage of energy for electric vehicles;

$\overline{E}_u^{EV}$ is the energy capacity of electric vehicle u;

E_u^{ini} is the initial charge state of electric vehicle u;

$\overline{P}_u^{CH}$ is the maximum power consumption of electric vehicle u;

$\overline{P}_u^{DC}$ is the maximum power injection of electric vehicle u;

$\boldsymbol{S}$ is the substation node;

T_f is the last time interval of the time period;

$\overline{V}, \underline{V}$ is the maximum and minimum voltage magnitude limits;

$X_{mn,f,h}$ is the reactance of circuit mn between phases f and h;

$\delta_{mn,f,t,\lambda}$ is the value of the λth block of the piecewise linearization for the current of circuitmn for phase$f$ in time t ;

τ_u is the time interval at which charge and discharge cycles are separated for electric vehicle u;

$\dot{\tau}_u$ is the auxiliary variable used for the calculation of τ_u;

$E_{u,t}^{EV}$ is the energy of electric vehicle at node u at the end of time t;

$E_{u,T}^{EV}$ is the energy of electric vehicle at node u at the end of the time period;

E_u^{SH} is the energy curtailment of electric vehicle u at the end of the time period;

$I_{mn,f,t}^{sqr}$ is the square of the current in circuit mn for phase f in time t; and

$P_{u,t}^{EV}$ is the active power consumption of electric vehicle u in time t.

Equations (166) and (167) represent the balance of the real and imaginary parts of the circuit currents at each node, respectively. The term $\gamma(u, m, f)$ is a binary function that takes a value of 1 if the EV u is connected at node m and at phase f. Equations

(168) and (169) define the load currents. The relationship between power, voltage, and current for the loads may also be written as shown in (188) and (189).

$$I^{Dre}_{n,f,t} = \frac{P^{D}_{n,f,t}V^{re}_{n,f,t} + Q^{D}_{n,f,t}V^{im}_{n,f,t}}{{V^{re}_{n,f,t}}^2 + {V^{im}_{n,f,t}}^2} \tag{188}$$

$$I^{Dim}_{n,f,t} = \frac{P^{D}_{n,f,t}V^{im}_{n,f,t} - Q^{D}_{n,f,t}V^{re}_{n,f,t}}{{V^{re}_{n,f,t}}^2 + {V^{im}_{n,f,t}}^2} \qquad \forall n \in N, f \in F, t \in T \tag{189}$$

If the right part of equations (188) and (189), which are nonlinear functions of the voltage's real and imaginary parts, are represented by $g(P^D_{n,f,t}, Q^D_{n,f,t}, V^{re}_{n,f,t}, V^{im}_{n,f,t})$ and $h(P^D_{n,f,t}, Q^D_{n,f,t}, V^{re}_{n,f,t}, V^{im}_{n,f,t})$, respectively, and taking advantage of the relatively small and limited variation range of the voltage magnitude in an EDN, these equations can be linearized around an estimated operation point $(V^{re^*}_{n,f,t}, V^{im^*}_{n,f,t})$, as shown in (190) and (191).

$$I^{Dre}_{n,f,t} = g^* + \frac{\partial g}{\partial V^{re}}\bigg|^{*}(V^{re}_{n,f,t} - V^{re^*}_{n,f,t}) + \frac{\partial g}{\partial V^{im}}\bigg|^{*}(V^{im}_{n,f,t} - V^{im^*}_{n,f,t}) \tag{190}$$

$$I^{Dim}_{n,f,t} = h^* + \frac{\partial h}{\partial V^{re}}\bigg|^{*}(V^{re}_{n,f,t} - V^{re^*}_{n,f,t}) + \frac{\partial h}{\partial V^{im}}\bigg|^{*}(V^{im}_{n,f,t} - V^{im^*}_{n,f,t}) \qquad \forall n \in N, f \in F, t \in T \tag{191}$$

Linear equations (190) and (191) can be used to approximate the currents demanded by the loads previously represented by the nonlinear expressions (168) and (169). The quality of the estimated operation point will define the approximation error. Historical data and the knowledge of the EDN operator are used to estimate the operation point. Equations (170) and (171) are the result of applying Kirchhoff's Voltage Law to each independent loop in the EDN. Constraints (172)–(174) define the operation limits of the DGs and (175)–(176) represent their active and reactive powers. The nonlinearity of the DGs active and reactive powers is approximated using an estimated operation point $(V^{re^*}_{n,f,t}, V^{im^*}_{n,f,t})$ as shown in (192)–(193).

$$\frac{P^G_{n,t}}{3} = V^{re^*}_{n,f,t} I^{Gre}_{n,f,t} + V^{im^*}_{n,f,t} I^{Gim}_{n,f,t} \tag{192}$$

$$\frac{Q^G_{n,t}}{3} = -V^{re^*}_{n,f,t} I^{Gim}_{n,f,t} + V^{im^*}_{n,f,t} I^{Gre}_{n,f,t}, \qquad \forall n \in N, f \in F, t \in T \tag{193}$$

The limits for the voltage magnitude in each circuit are stated in (177). The phase angle variation around the reference voltage for each phase in the EDN is small. Because of this fact, (177) can be modeled by defining the boundaries of the feasible region of the voltage, considering operation limits. If θ_1 and θ_2 are the maximum negative and maximum positive deviations of the phase angle around the reference ($\theta = [0°, +120°, -120°]$) for each phase, the constraints (194), (195), (196), (197), and (198) limit the voltage magnitudes between $[\underline{V}, \overline{V}]$ and the phase angles $[\theta_f - \theta_1, \theta_f + \theta_2]$. Constraints (194), (195), (196), (197), and (198) are related with lines L_1, L_2, L_3, L_4 and L_5, respectively,

Figure 7 – Constraints for Voltage Limits (phase A).

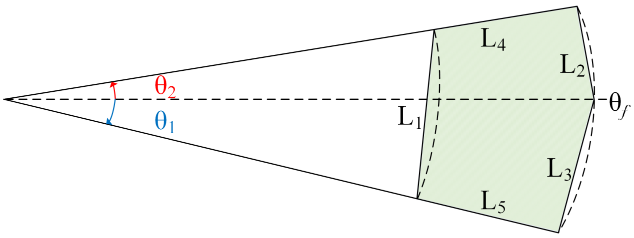

Source: Created by the author.

as shown in Fig. 2.

$$V^{im}_{n,f,t} \leq \frac{\sin(\theta_f+\theta_2)-\sin(\theta_f-\theta_1)}{\cos(\theta_f+\theta_2)-\cos(\theta_f-\theta_1)}\left[V^{re}_{n,f,t}-\underline{V}\cos(\theta_f+\theta_2)\right]+\underline{V}\sin(\theta_f+\theta_2) \tag{194}$$

$$V^{im}_{n,f,t} \leq \frac{\sin(\theta_f+\theta_2)-\sin\theta_f}{\cos(\theta_f+\theta_2)-\cos\theta_f}\left[V^{re}_{n,f,t}-\overline{V}\cos\theta_f\right]+\overline{V}\sin\theta_f \tag{195}$$

$$V^{im}_{n,f,t} \geq \frac{\sin(\theta_f-\theta_1)-\sin\theta_f}{\cos(\theta_f-\theta_1)-\cos\theta_f}\left[V^{re}_{n,f,t}-\overline{V}\cos\theta_f\right]+\overline{V}\sin\theta_f \tag{196}$$

$$V^{im}_{n,f,t} \leq V^{re}_{n,f,t}\tan(\theta_f+\theta_2) \tag{197}$$

$$V^{im}_{n,f,t} \geq V^{re}_{n,f,t}\tan(\theta_f-\theta_1) \qquad \forall n \in N, f=A, t \in T \tag{198}$$

The limits for current capacity in each circuit are stated in (178). As shown in 2.11, (178) is linearized using (199)–(206). The terms $\sum_{\lambda=1}^{\overline{\lambda}} \sigma_{mn,\lambda}\delta^{re}_{mn,f,t,\lambda}$ and $\sum_{\lambda=1}^{\overline{\lambda}} \sigma_{mn,\lambda}\delta^{im}_{mn,f,t,\lambda}$ are the linear approximations of ${I^{re}_{mn,f,t}}^2$ and ${I^{im}_{mn,f,t}}^2$, respectively. $\sigma_{mn,\lambda}$ and $\overline{\delta}_{mn}$ are constant parameters, as defined by (207) and (208).

$$I^{sqr}_{mn,f,t} = \sum_{\lambda=1}^{\overline{\lambda}} \sigma_{mn,\lambda}\delta^{re}_{mn,f,t,\lambda} + \sum_{\lambda=1}^{\overline{\lambda}} \sigma_{mn,\lambda}\delta^{im}_{mn,f,t,\lambda} \tag{199}$$

$$I^{re}_{mn,f,t} = I^{re+}_{mn,f,t} - I^{re-}_{mn,f,t} \tag{200}$$

$$I^{im}_{mn,f,t} = I^{im+}_{mn,f,t} - I^{im-}_{mn,f,t} \tag{201}$$

$$I^{re+}_{mn,f,t}+I^{re-}_{mn,f,t}=\sum_{\lambda=1}^{\overline{\lambda}} \delta^{re}_{mn,f,t,\lambda} \tag{202}$$

$$I^{im+}_{mn,f,t}+I^{im-}_{mn,f,t}=\sum_{\lambda=1}^{\overline{\lambda}} \delta^{im}_{mn,f,t,\lambda} \tag{203}$$

$$0 \leq \delta^{re}_{mn,f,t,\lambda} \leq \overline{\delta}_{mn} \tag{204}$$

$$0 \leq \delta^{im}_{mn,f,t,\lambda} \leq \overline{\delta}_{mn} \tag{205}$$

$$I^{re+}_{mn,f,t}, I^{re-}_{mn,f,t}, I^{im+}_{mn,f,t}, I^{im-}_{mn,f,t} \geq 0 \tag{206}$$

$$\sigma_{mn,\lambda} = (2\lambda-1)\overline{\delta}_{mn} \tag{207}$$

$$\overline{\delta}_{mn} = \frac{\overline{I}_{mn}}{\overline{\lambda}} \qquad \forall mn \in L, f \in F, t \in T, \lambda=1\ldots\overline{\lambda} \tag{208}$$

Along with the estimated operation point, the number of discretization blocks $\overline{\lambda}$ must be adjusted in order to enhance the quality of the linear approximations. The

EVs' active and reactive demanded powers are specified in (179) and (180). Similar to (175)–(176), (179)–(180) are approximated using $(V^{re^*}_{u,t}, V^{im^*}_{u,t})$; (209)–(210) show these approximations.

$$P^{EV}_{u,t} = V^{re^*}_{u,t} I^{EVre}_{u,t} + V^{im^*}_{u,t} I^{EVim}_{u,t} \tag{209}$$

$$0 = -V^{re^*}_{u,t} I^{EVim}_{u,t} + V^{im^*}_{u,t} I^{EVre}_{u,t} \qquad \forall u \in \Xi, t \in T \tag{210}$$

Equation (181) establishes the energy balance between the EV's storage capacity, charged energy, and energy curtailment. The demanded power for each vehicle in each time interval is specified by (182). Equation (183) represents the energy stored in every EV in each time interval. The energy limits of an EV are defined by (184), which ensures that the maximum energy level is not violated for all EVs. Furthermore, the grid will not take more than the available energy from the EV-V2G batteries, complying with a security level that limits the minimum energy level for each EV battery. The binary variables $y_{n,t}$ and $z_{u,t}$ define the EV's charging state, influencing the demanded power directly. Equation (185) limits the direction of the power flow in each time interval for every EV. The set of EV charging state variables has a binary nature, as detailed in (186) and (187). These two variables, model the energy transference between an EV battery and the grid. $y_{n,t}$ has a value of 1 if the battery is charging at its maximum power $\overline{P}^{CH}_n$ and a value of 0 if the battery is not charging; $z_{n,t}$ has a value of 1 if the battery is injecting energy into the grid at its maximum capacity $\overline{P}^{DC}_n$ and a value of 0 otherwise. In this way, the EVCC problem is modeled as a MINLP in (165)–(187), the complete MILP model for the EVCC problem is modeled by:

$$\min (165)$$

Subject to: (166)–(167), (170)–(174), (181)–(187), (190)–(206), (209)–(210)

$$0 \leq I^{sqr}_{mn,f,t} \leq \overline{I}_{mn}^{\,2} \qquad \forall mn \in L, f \in F, t \in T \tag{211}$$

A linear relaxation of the MILP model, where the binary nature of the decision variables is temporarily ignored, is initially solved in order to obtain a more accurate estimated operation point. To extend the lifetime of the EV batteries, equations are included to separate the charging and discharging cycles of EV-V2Gs. Constraints (212)–(216) prevent alternation between charging and discharging cycles, thereby, disallowing the commencement of a discharging cycle once the charging cycle has begun. In addition, these equations use the auxiliary variables $\dot{\tau}_{u,t}$ and τ_u to find the optimal time interval to switch from discharging to charging for every EV.

$$ty_{u,t} \geq \dot{\tau}_{u,t} \tag{212}$$

$$tz_{u,t} \leq \tau_u \tag{213}$$

$$1 \leq \tau_u \leq T_f \tag{214}$$

$$\dot{\tau}_{u,t} \leq T_f y_{u,t} \tag{215}$$

$$\tau_u - \dot{\tau}_{u,t} \leq T_f \left(1 - y_{u,t}\right) \qquad \forall u \in V2G, t \in T \tag{216}$$

3.4 TESTS AND RESULTS

3.4.1 Case Study I

The proposed model was tested in a 123-node distribution system with nominal voltage of 4.16kV based on (IEEE/PES, 2014). The maximum and minimum voltage magnitude limits were 1.00pu and 0.90pu, respectively. The voltage magnitude at the substation was fixed at 1.0pu. The energy capacity of the EV batteries was 50kWh for Tesla EVs and 20kWh for Nissan Leafs (TESLA-MOTORS, 2014), (NISSAN, 2014). The charging maximum power was 10kW and 4kW, and for EV-V2Gs the discharging maximum power was 5kW and 2kW, respectively. The parameter $\overline{I}_{mn}$ was 500A for all feeders. The time period was set for 18:00h to 08:00h, divided into half-hour time intervals; β was 10 US$/kWh. The parameters θ_1 and θ_2 were set to 5° and 3°, respectively, and λ was set at 10. The full day hourly energy cost and load variation percentage are presented in Table 3. The considered time period is the bolded area on Table 3 and it is assumed that any vehicle can arrive and depart during this period.

Table 3 – Hourly energy cost and load variation

hour	energy cost $/kWh	% of peak load	hour	energy cost $/kWh	% of peak load
08:00	0.038	46	**20:00**	**0.075**	**91**
09:00	0.048	55	**21:00**	**0.077**	**87**
10:00	0.055	63	**22:00**	**0.07**	**75**
11:00	0.059	70	**23:00**	**0.06**	**65**
12:00	0.058	75	**00:00**	**0.048**	**55**
13:00	0.057	83	**01:00**	**0.036**	**40**
14:00	0.058	88	**02:00**	**0.034**	**37**
15:00	0.062	90	**03:00**	**0.03**	**35**
16:00	0.063	95	**04:00**	**0.028**	**33**
17:00	0.064	100	**05:00**	**0.027**	**33**
18:00	**0.066**	**100**	**06:00**	**0.027**	**41**
19:00	**0.07**	**93**	**07:00**	**0.029**	**44**

Source: Created by the author.

Phases A, B, and C of the EDN were charged with 40.7%, 26.2%, and 33.1% of the total demand, respectively. The conventional demands of the system were 1420 kVA, 915 kVA and 1155 kVA, connected to phases A, B and C, respectively.

Table 4 – Case description

Case	EV	EV V2G	DG	Forecast error (%)	EV Balance A/B/C (%)	Tesla:Leaf Ratio
Dumb Charge	240	160	x	x	33.25/33.25/33.5	10:0
I	240	160	x	x	33.25/33.25/33.5	10:0
II	240	160	x	x	28/35/37	10:0
III	240	160	✓	x	33.25/33.25/33.5	10:0
IV	400	x	x	x	33.25/33.25/33.5	10:0
V	240	160	x	10	33.25/33.25/33.5	10:0
VI	240	160	x	x	33.25/33.25/33.5	9:1
VII	180	120	x	x	33.25/33.25/33.5	10:0
VIII	120	80	x	x	33.25/33.25/33.5	10:0

Source: Created by the author.

Table 5 – Summary of the test

Case	O.F (US$)	Total E_u^{SH} (kWh)	cases Energy from V2G (kWh)	Number of Used EV-V2Gs	Energy from DG (kWh)
Dumb Charge	2564.81	0	0	0	0
I	1921.85	0	1825	124	0
II	1921.92	0	1825	124	0
III	1606.50	0	1837.5	128	11200
IV	1996.47	0	0	0	0
V	1921.33	0	1840	128	0
VI	1903.69	0	1716.5	128	0
VII	1846.40	0	1360	96	0
VIII	1765.92	0	990	68	0
I	2037.75	0	977.5	105	0

Source: Created by the author.

Tests were initially carried out for eight different cases. Table 4 presents the different cases tested in the 123-node system and their specific features. For all cases, the k-number of time periods, which considers the binary nature of the charging variables, was set at 3. Table 4 also shows the dumb charge operation for Case I. In this instance, the EDN had the same settings as in Case I, except that the EV recharge was done without any charging coordination. This meant that the EV batteries started an uninterrupted charging process as soon as they were plugged into the system.

In Case III, the EDN had two DGs connected at nodes 56 and 104, with energy cost $\alpha_{n,t}^{G}$ equal to 0.04 US$/kWh. The maximum active powers were 1200kW and 400kW, respectively. The minimum and maximum reactive powers were equal to -300kVAr and 300kVAr and -100kVAr and 100kVAr, respectively. Finally, the minimum power factor for the operation of both DGs was 0.90. As described in section III, the model takes into account the later connection of EVs. In the initial time intervals, the estimated arrivals and initial SOCs of expected EVs are included to avoid overloads in the system. Case V studied a scenario in which 10% of the forecasts for arrivals and initial SOCs were not correct. This test was carried to identify the performance of the proposed methodology when there is unexpected power demand. Cases VII and VIII have been included to demonstrate the performance of the formulation under different levels of EV penetration in the EDN.

For Cases I–VIII, the arrival and departure time intervals were generated based on the two chi-squared probability functions with 8 and 4 degrees of freedom, respectively, as shown in Fig. 8. Moreover, the initial SOC of the EVs was generated using the normal probability function displayed in Fig. 9. The mean value and the standard deviation of the SOC probability function were set at 15 and 10, respectively. All of the values were maintained within the red limits shown in both figures.

Figure 8 – Arrival and Departure Distribution Function Probability.

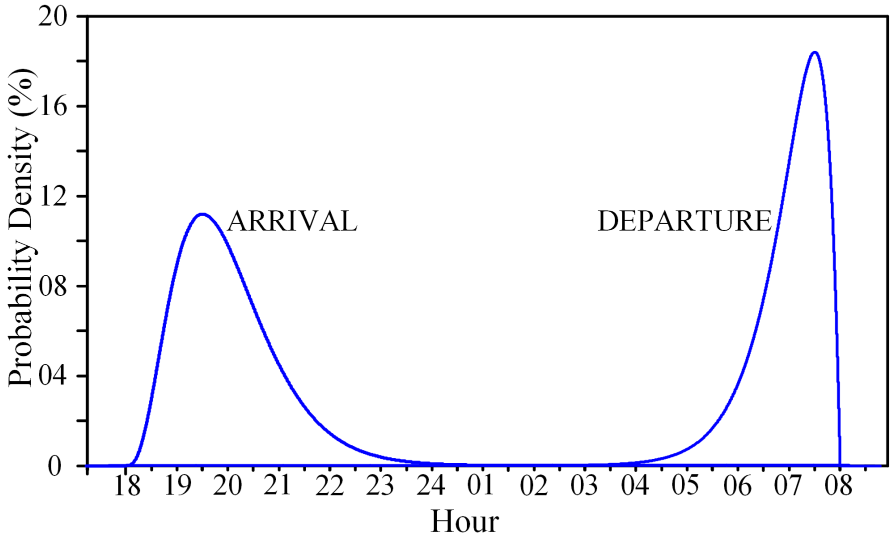

Source: Created by the author.

Figure 9 – Initial SOC Distribution Function Probability.

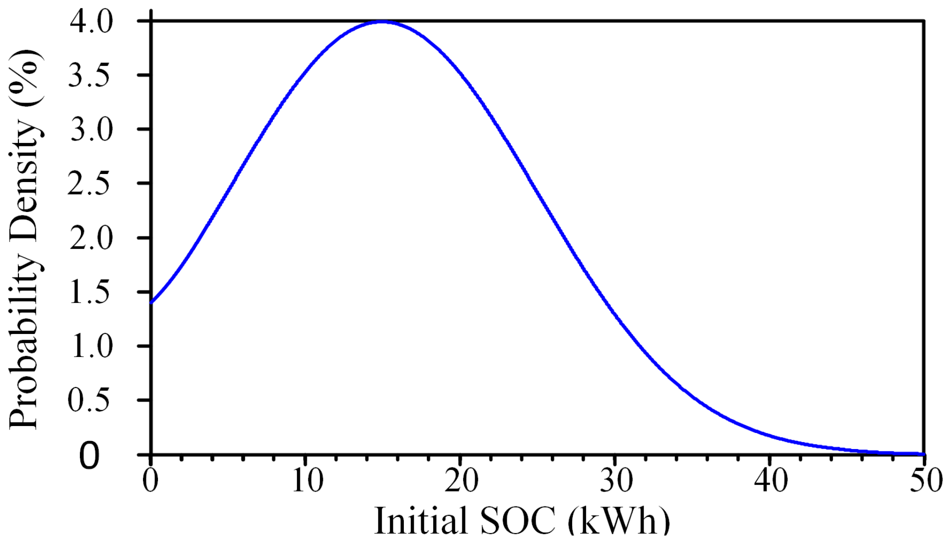

Source: Created by the author.

The model was implemented in AMPL (FOURER; GAY; KERNIGHAN, 2003) and solved with CPLEX (ILOG INC., 2009) using a computer with an Intel $i7$ 4770

Figure 10 – Dumb Case Simulation Results.

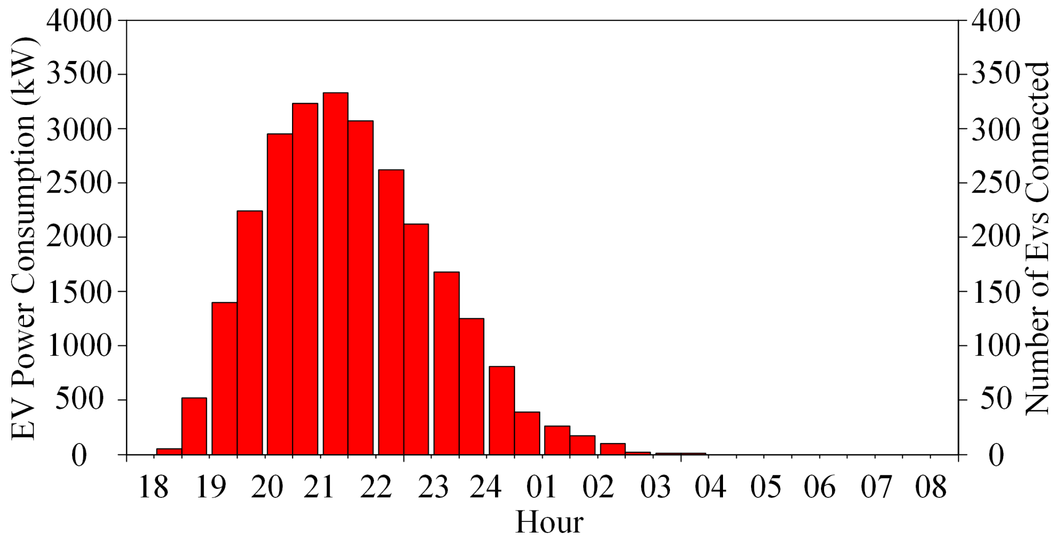

Source: Created by the author.

processor. The time limit for the solution process in each time interval was 180s.

Table 5 shows a summary of the results from the test cases. For all of the tests, the resultant EV charging schedule presented no energy curtailment, which means that all of the EVs were completely charged at the time of departure. In Figs. 10–19 the power related to the grid and EV-battery energy exchange are shown for each case. The power related to the charging of EVs is shown in red, while the power related to the discharging of EV-V2Gs is shown in blue. Following convention, the EV charging power and the EV-V2G discharging power are given in positive and negative values, respectively.

Fig. 10 presents the EV power for the dumb charge case. As explained, no coordination was applied to the EV batteries at recharge, and all vehicles were continuously charged upon being plugged into the grid. The peak load for this case was between 21:00 and 22:00, that is, the time when most vehicles had arrived and were already plugged in. As shown in Table 5, this case presented the highest objective function due to the fact that the EV recharge peak load corresponded with the time intervals when energy prices were the highest.

Figs. 11 and 12 show the solutions for Cases I and II. For Case I the EVs were balanced on the EDN phases, while for Case II the EV imbalance shown in Table 4 was considered. Table 5 shows a very small difference between the objective functions of these two cases, evidencing the flexibility of the model when there is an imbalance in the EVs connected.

The total active power demand for the dumb charge case and Case I are shown in Figs. 13 and 14, respectively. As the EVCC is included, the load peak is reduced and reallocated to the low-cost energy time intervals. Figs. 15 and 24 depict the overload on the EDN due to the uncoordinated connection of EVs; the voltage and current magnitudes

Figure 11 – Case I Simulation Results.

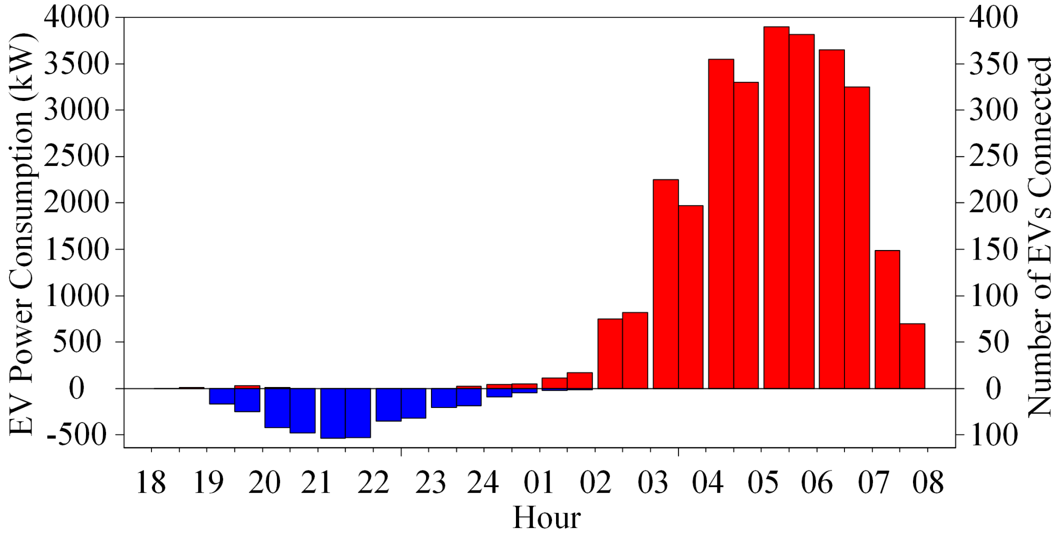

Source: Created by the author.

Figure 12 – Case II Simulation

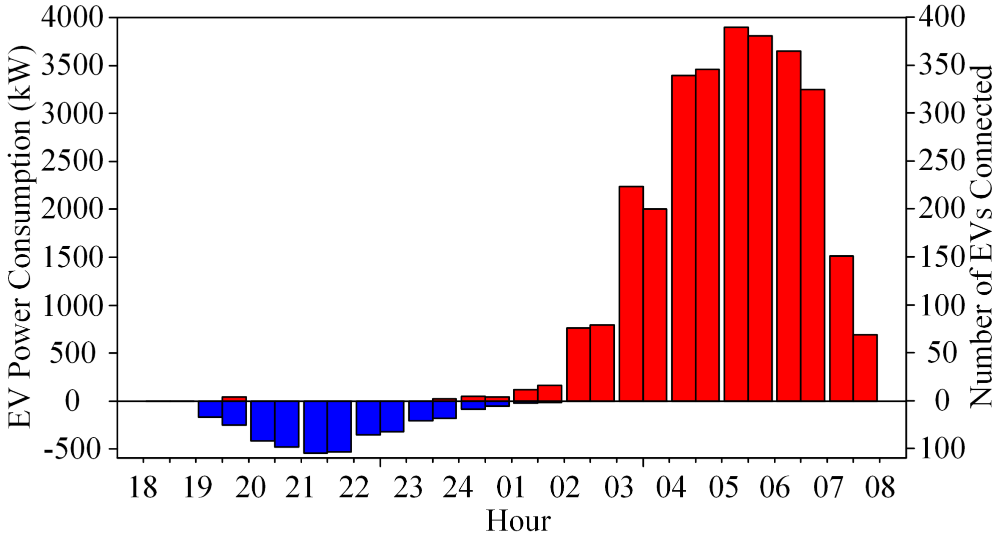

Source: Created by the author.

outstrip their statutory limits. Hence, the coordination of EV recharging in the EDN is beneficial not only for load peak reduction, but also for maintaining the operation of the EDN within the stipulated voltage and thermal limits.

The inclusion of DGs was studied in Case III. This case presented the lowest objective function because of the utilization of the low cost energy from the DGs. Due to the alleviation that DGs offer to the EDN, Fig. 16 shows how more EVs were able to be charged during high energy cost time intervals with a substantial reduction to the objective function. Fig. 17 shows the power exchange for Case IV, where the V2G technology was disregarded for all vehicles. The objective function for this case rose by 4% when compared to Case I, evidencing the improvement offered by V2G technology. Similar to all the presented cases with controlled EV recharge, the EV peak load of Case

Figure 13 – Dumb Charge Total Active Power Demand.

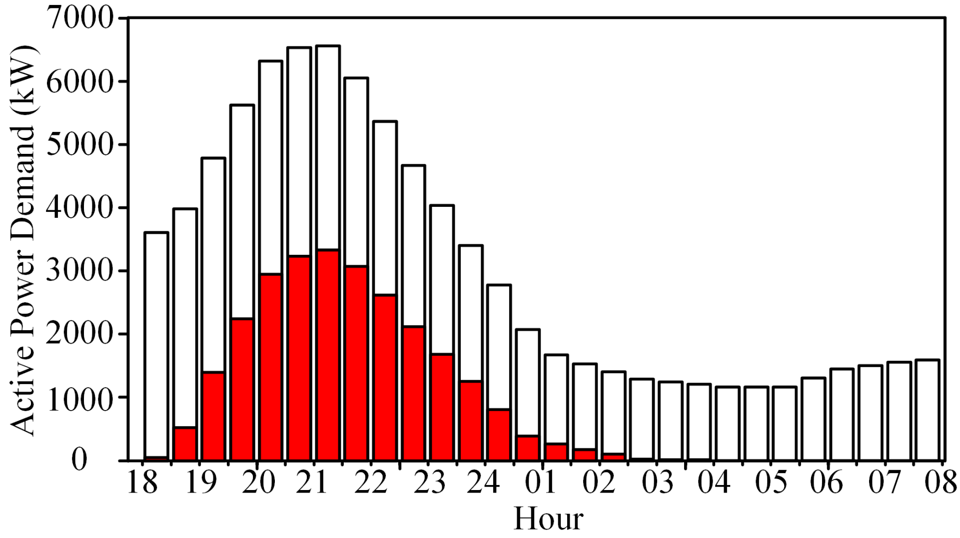

Source: Created by the author.

Figure 14 – Case I Total Active Power

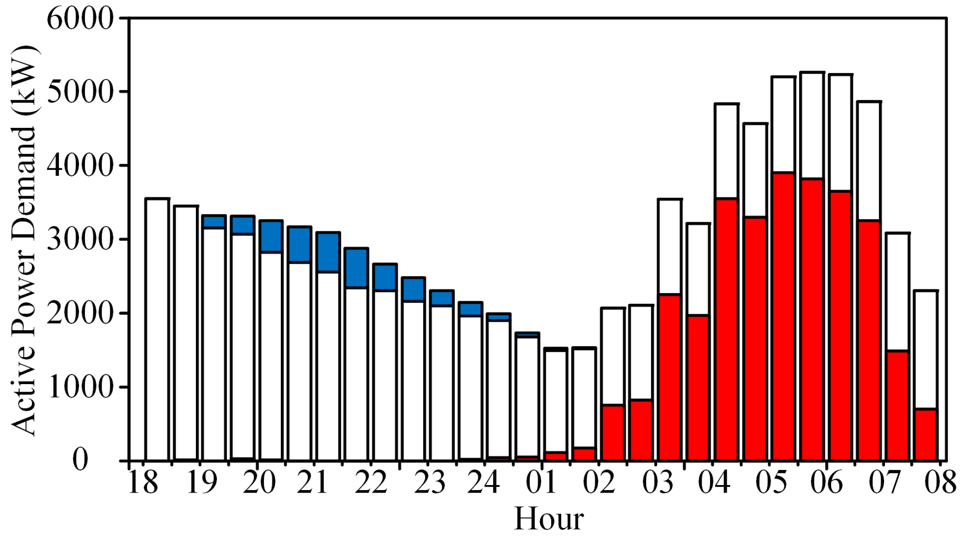

Source: Created by the author.

IV was between 05:00 and 06:00; yet, in the best charging schedule found for this case, no EVs were charged before midnight.

As shown in Table 5, Case V included a 10% forecast error. This means that 10% of the EVs had a mistaken forecast in terms of the time of arrival and initial SOC. In the initial time intervals when most of the EVs have not yet arrived, the methodology finds charging schedules using data from false forecasts. These schedules may not fit the EVs' actual plugging periods and energy requirements. Unexpected late arrivals and low initial SOCs may create overloads on the EDN or force energy curtailments on the EV batteries. Even under these conditions, the methodology found a charging schedule with null energy curtailment and with a minimal difference in terms of the objective function. These results demonstrate the adaptability of the methodology when unforeseen changes

Figure 15 – Maximum Current Magnitudes (Dumb Charge vs Case I)

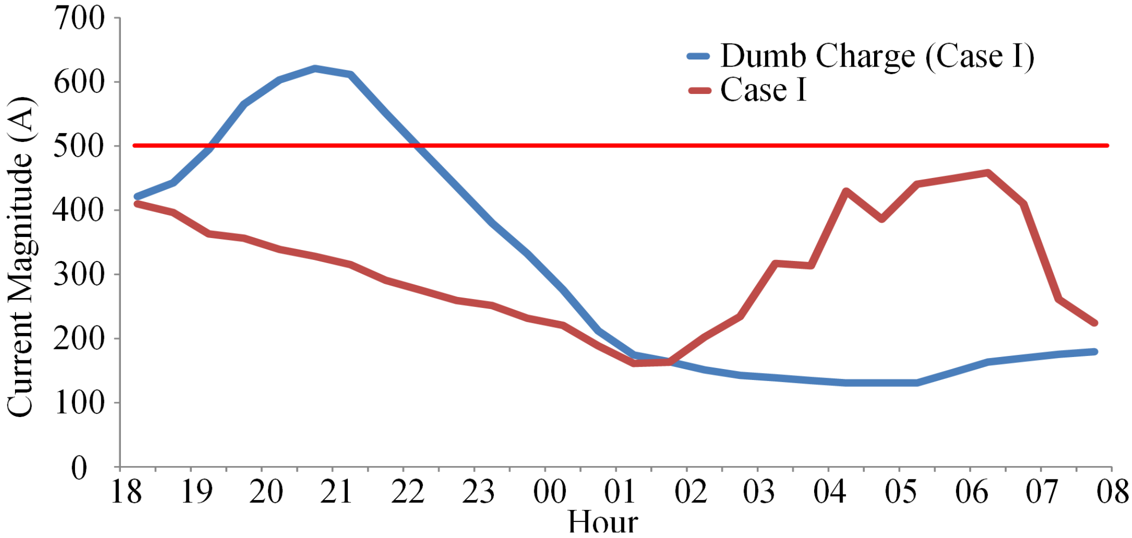

Source: Created by the author.

Figure 16 – Case III Simulation

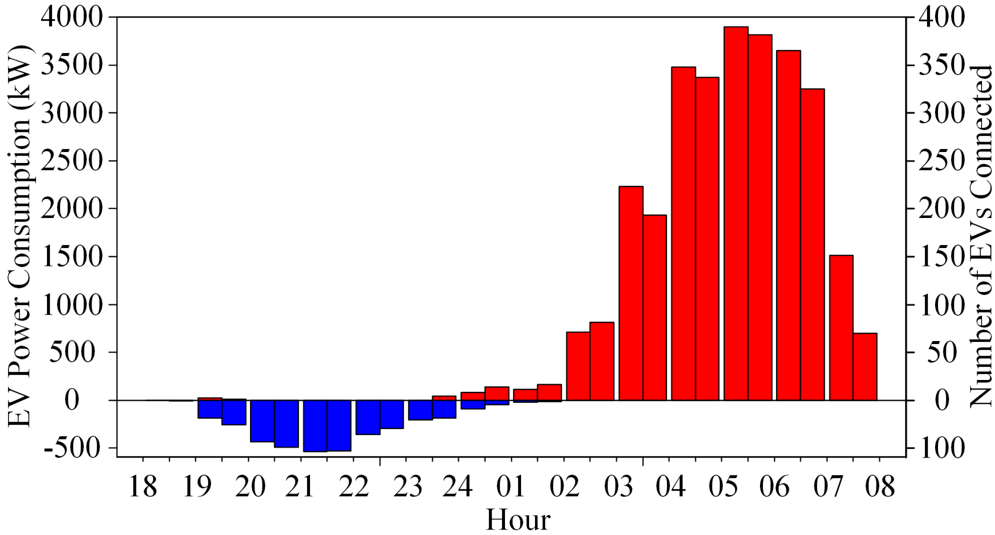

Source: Created by the author.

occur in the EVs' arrivals or SOCs. Case VI tested the proposed method with different types of batteries connected to the grid. 10% of the EVs that were plugged in were Nissan Leafs with the aforementioned specifications. The solution found presented no energy curtailment and a US\$603.91 improvement in the O.F. compared to uncontrolled EV charging under Case VI conditions; however, the objective function value cannot be compared with previous cases because the EV energy demand of Case VI was less, since smaller batteries were connected to the grid. Finally, Cases VII and VIII were tested in order to demonstrate the efficiency of the methodology with different EV penetration. Both charging schedules were developed with no energy curtailment for the EVs.

For Case IX, the values of the initial SOC were obtained by applying the formulation presented in Melo, Carreno e Padilha-Feltrin (2014) to a mid-sized city in

Figure 17 – Case IV Simulation Results.

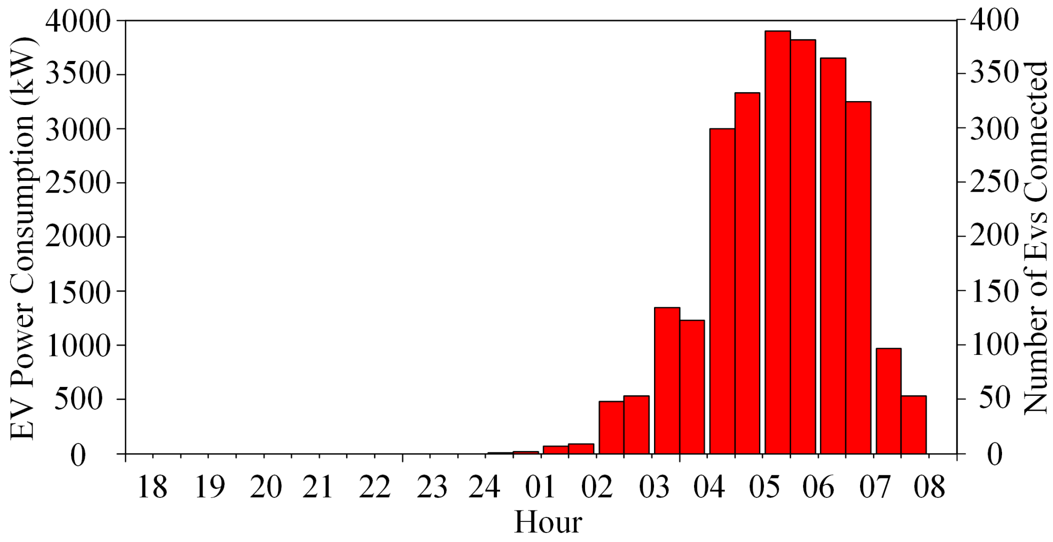

Source: Created by the author.

Figure 18 – Case V Simulation

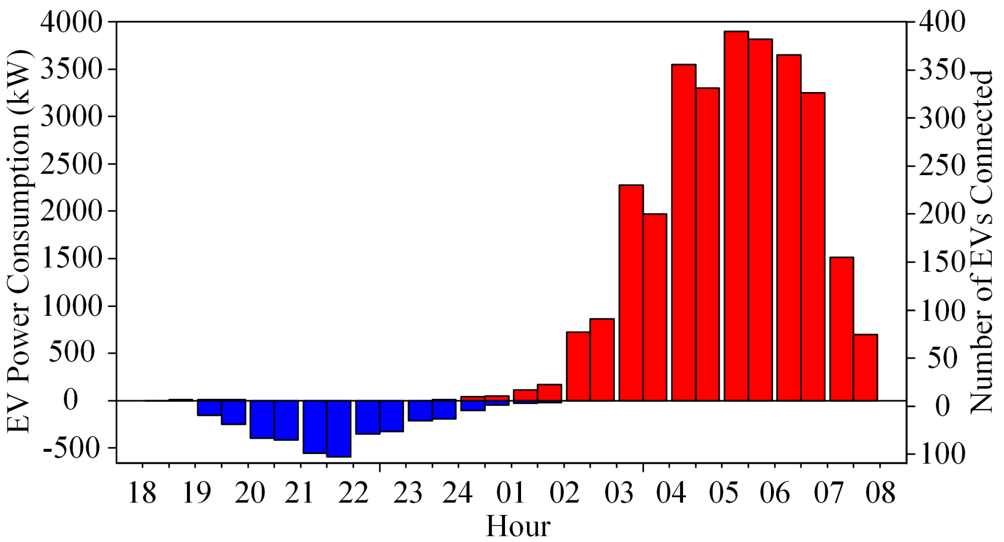

Source: Created by the author.

Brazil. Fig. 23 shows the probability distribution function obtained from this data. The mean and standard deviation calculated for the sample were 10.78kWh and 5.90kWh, respectively. The initial SOC profile obtained was lower than that one used in the previous cases. As expected and as shown in Table 5, the energy demand of the complete EV fleet is higher than in Case I, which is directly reflected in an increase in the O.F. For this case, the methodology found a solution that also presents no energy curtailment on the EV batteries.

The minimum voltage in the EDN for each time interval is shown in Fig 24 for all test cases. For the dumb charge scenario, the EDN did not satisfy operational constraints, as the voltage magnitude dropped below the acceptable limit between 20:00 and 22:00. This fact demonstrate the significance of the burden added to the grid by the EVs and

Figure 19 – Case VI Simulation Results.

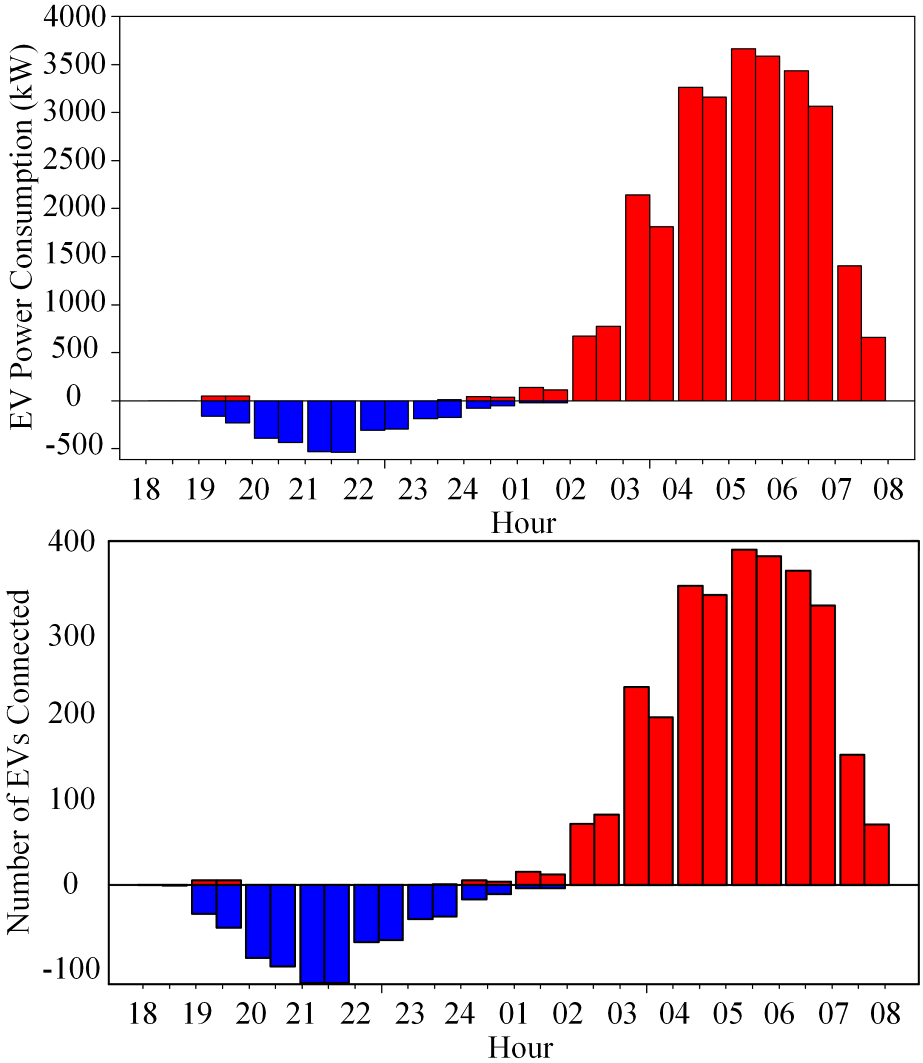

Source: Created by the author.

proves the importance of a coordinated EV recharging schedule. For all cases including V2G technology, the EV-V2G energy available for the grid was used during earlier time intervals due to their high energy cost. At the same time, the charging process for most EVs occurred during the final time intervals when the EDN had low energy costs. The charging process was completed between arrival and departure times, and all presented cases generated schedules ensuring that the EVs left with a fully charged battery at the end of the charging period.

Comparing Case I and Case IV, as shown in Table 5, the objective function was reduced by 3.74% when the V2G property of the EVs was considered. At the end of the time period, the economic improvement for the EDN was US$74.62. In Case I, 100% of the EV-V2Gs with energy available that were connected to the grid were employed; in more than 98% of the cases, all the available energy was drawn from the EV-V2Gs.

The EV-V2G owners should be compensated for the energy delivered to the grid,

Figure 20 – Case VII Simulation Results.

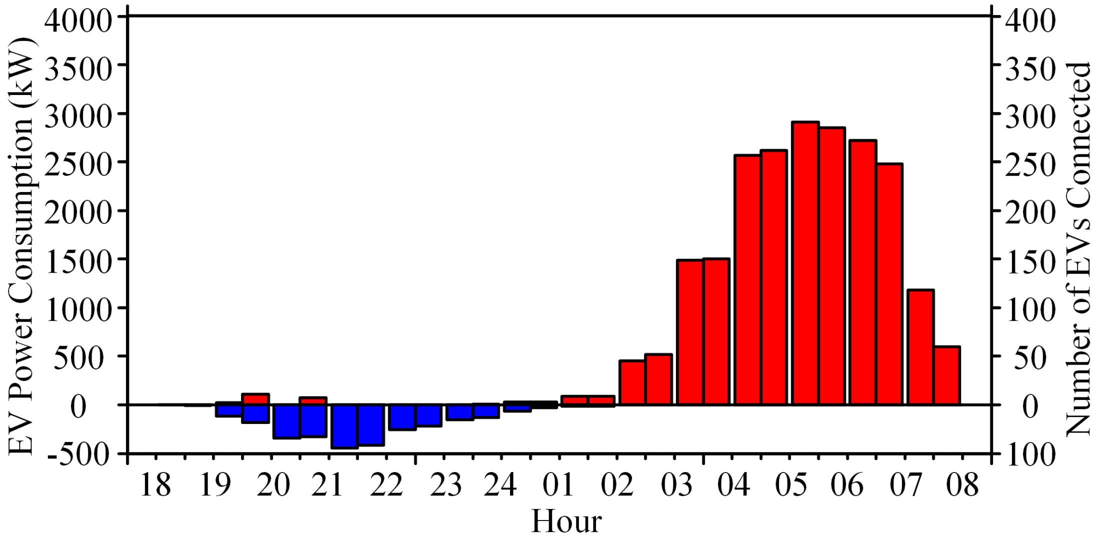

Source: Created by the author.

Figure 21 – Case VIII Simulation

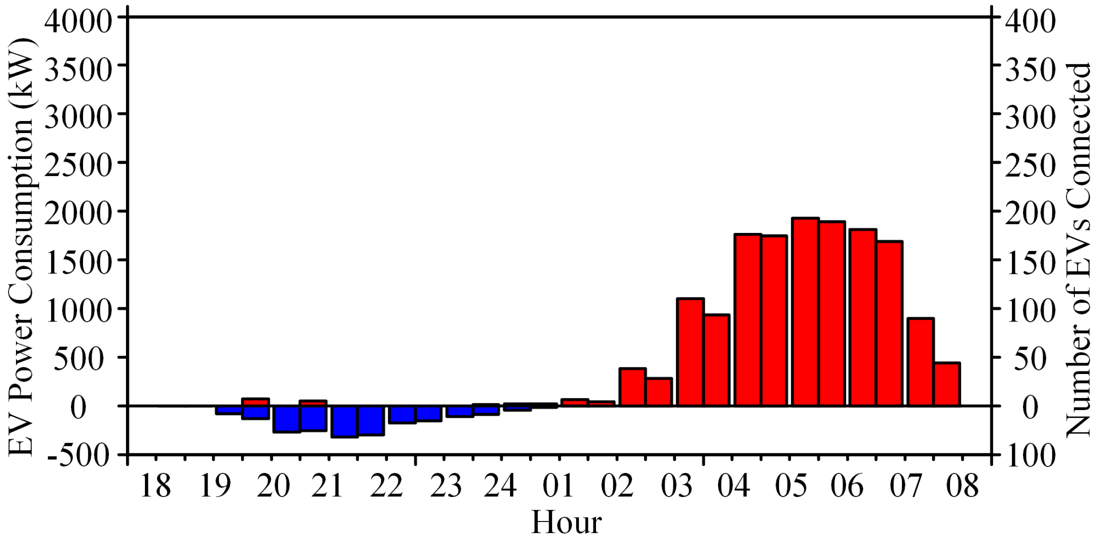

Source: Created by the author.

as this energy is used during high energy cost time intervals and supplied back during low energy cost time intervals. This compensation corresponds to the additional energy consumed by the EV-V2G to recharge the battery up to its initial value. At the same time, the maximum number of feasible charge cycles of an EV battery is directly influenced by the DoD. Therefore, the lifetime of an EV battery is reduced as the discharge depth is increased for each cycle. The following calculation can be used to estimate the minimum compensation for EV-V2G owners with respect to anticipated EV battery replacement.

As they plug into the system, the average DoD of the EV-V2Gs used by the grid in Case I is 60%; later, once the grid has taken the energy from the V2G function, the average DoD of the EV-V2G reaches 90%. In (LIU et al., 2012) is presented a characteristic curve of charge cycles influenced by the DoD of the battery. The number of charge cycles for

Figure 22 – Case IX Simulation Results.

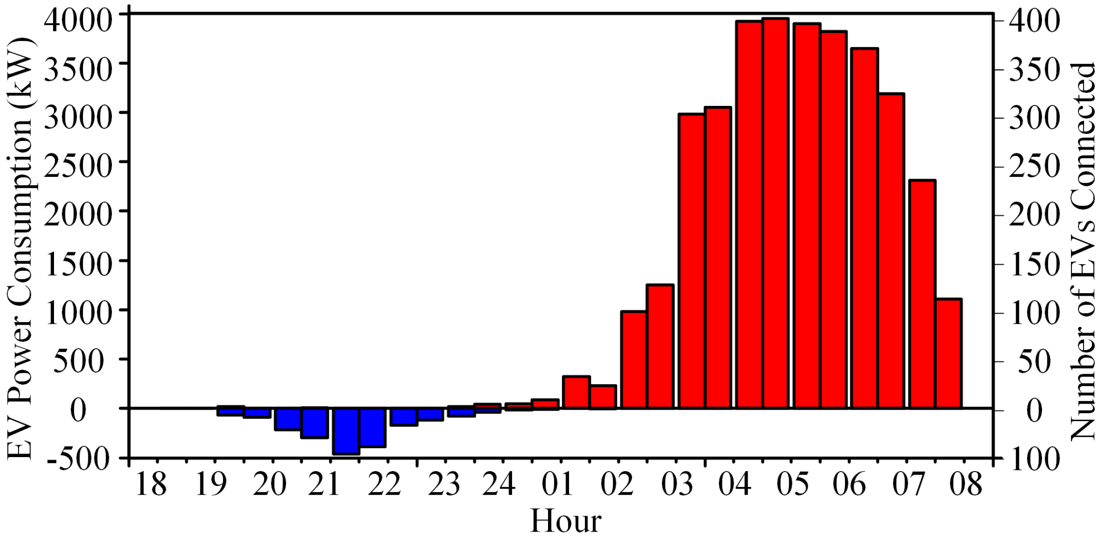

Source: Created by the author.

Figure 23 – Initial SOC Distribution Function Probability Case

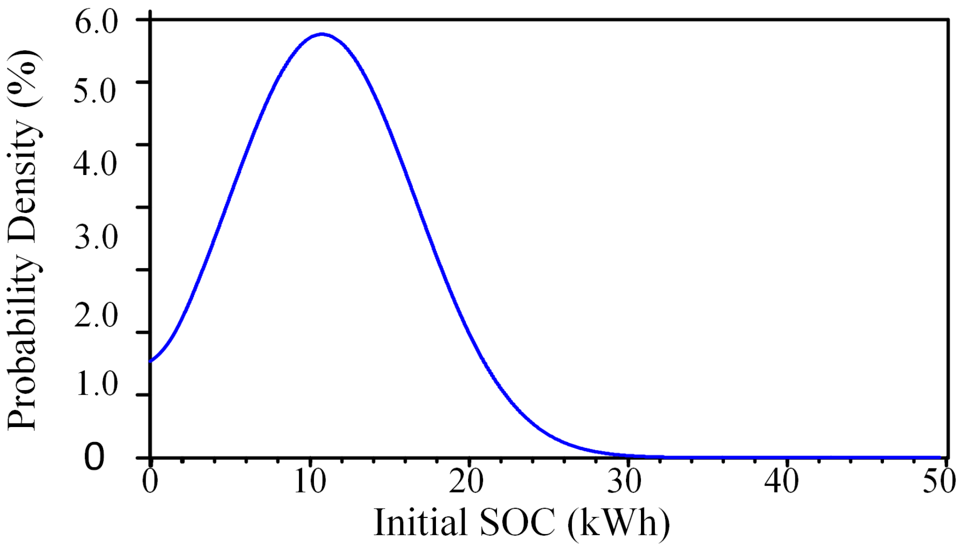

Source: Created by the author.

the EV batteries drops from 4,357 to 2,497. In other words, the expected lifetime of the EV battery is shortened from 12 years (4,357 cycles) to 7 years (2,497 cycles).Therefore, EV-V2G owners must be reimbursed for the deterioration of their EV batteries in order for them to allow their EVs to provide the V2G service.

Assuming a battery replacement cost of US$300 per kWh of storage capacity (NYKVIST; NILSSON, 2015), the 50kWh Tesla model used in this work will have a battery cost of US$15,000. The annualized value for an EV battery replacement increases from US$2,201.40 for a 12-year lifetime, disabling V2G, to US$3,081.10 for a 7-year lifetime, enabling V2G. Over a 1-year period, the estimated battery replacement cost to be reimbursed to each EV-V2G owner would be US$879.70.

Figure 24 – Minimum Voltage Magnitudes.

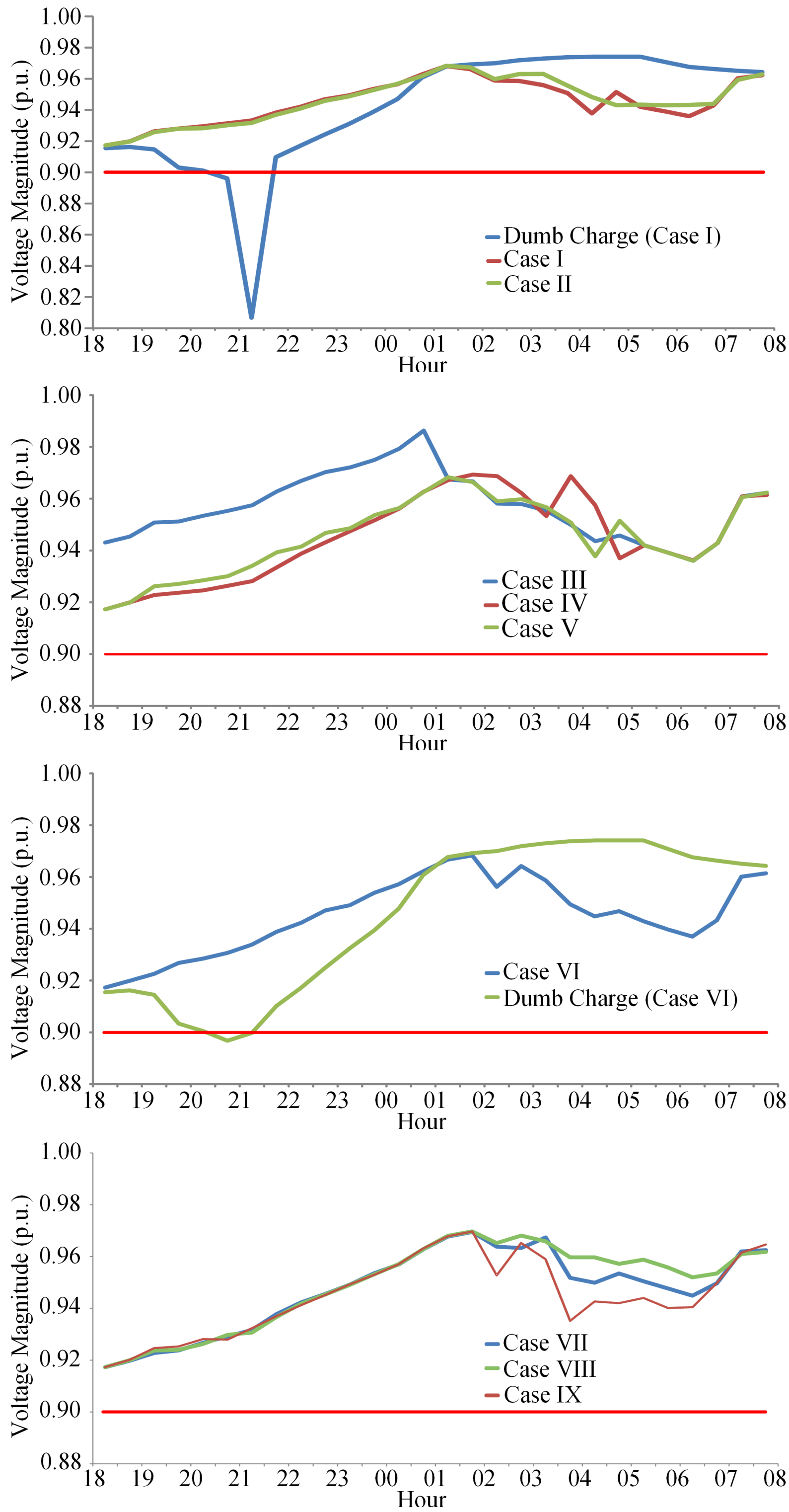

Source: Created by the author.

The proposed charging coordination approach can be incorporated into a simple market scheme in which an aggregator synchronizes the charge and discharge operations of multiple EVs, similar to the proposals in Unda et al. (2014) and Han, Han e Sezaki (2010). In such a scheme, EV-V2G owners may be remunerated for different services provided by their vehicles. The aggregator ensures that EVs provide a practical service to the EDN through the utilization of V2G technology. In addition, the aggregator must elaborate and sign bilateral contracts with the EV owners and the EDN. The aggregator receives payments from the EDN due to, among others, V2G energy delivery, energy quality improvements, and avoidance of technical limit violations. On the other hand, the aggregator make payments to the EV owners due to the energy delivered from V2G, battery depreciation, and available power capacity, among others.

Assuming that the benefit obtained from using V2G technology is equally divided among the EV-V2G owners annually, each owner would receive an amount of US$219,65. This amount is 25% of the battery replacement amount due to the utilization of V2G. Hence, it may be assumed that for the simulated case and from an EV owner's point of view, it is not economically appealing to allow the use of the V2G service. Nevertheless, it is important to note, that this only considers the economic enhancement of the EDN operation as related to energy costs. Meanwhile, important features that are highly affected by V2G enabling are disregarded, such as voltage and frequency regulation, voltage and current profile improvements, technical limit violation avoidance and power capacity availability. Considering these features and with the decreasing trend of battery prices, V2G utilization may become appealing to EV owners over the short term. In light of this, the presented charging control methodology is increasingly important.

3.4.2 Case Study II

The proposed model was tested in a 34-node distribution system with nominal voltage of 13.8kV (IEEE/PES,). The maximum and minimum voltage magnitude limits were 1.00pu and 0.90pu respectively. The voltage magnitude at the substation was fixed at 1.0pu. The energy capacity of the EV batteries was 50kWh with a charging maximum power of 10kW (TESLA-MOTORS,). For EV-V2Gs the discharging maximum power was 5kW.

The parameter $\overline{I}_{mn}$ was 200A for all feeders. The time period was stipulated from 18:00h to 08:00h, and the time intervals had a duration of one quarter hour, while β was 10 US$/kWh.

The conventional demand of the system is 418.2 kVA, 441.6 kVA, and 396.8 kVA, connected in phases A, B, and C respectively. So, phases A, B, and C are charged with 33.3%, 35.1%, and 31.6% of the total demand, respectively.

Tests were carried out for three different cases. In Table 6 the different cases tested on the 34-node system and their specific features are shown. In the cases marked with DG (✓), the EDN had two distributed generators connected at nodes 10 and 22, with energy costs $\alpha^{G}_{n,t}$ equal to 0.04 US$/kWh, maximum active power of 500kW, and minimum and maximum reactive power equal to -100kVAr and 100kVAr. The minimum power factor for the operation of the distributed generators was 0.90.

The model was implemented in AMPL (FOURER; GAY; KERNIGHAN, 2003) and solved with CPLEX (ILOG INC., 2009) using a computer with an Intel $i7$ 4770 processor. The time limit for the solution process was 100s.

Table 7 shows a summary of the results from the test cases. For all of the tests, the resultant EV charging schedule presents no energy curtailment, which means that all of the EVs were completely charged at departure.

Table 6 – Case description

Case	EV	EV-V2G	DG
Base	x	x	x
I	100	x	x
II	60	40	x
III	60	40	✓

Source: Created by the author.

Table 7 – Summary of the test cases

Case	F.O	Total E^{SH}_{u} (kWh)	Energy from V2G (kWh)	Number of Used EV-V2Gs	Energy from DG (kWh)
Base	568.37	0	0	0	0
I	671.67	0	0	0	0
II	647.25	0	621.25	28	0
III	467.43	0	486.25	32	6064.25

Source: Created by the author.

The power related to the grid and EV-battery energy exchange are shown in Figs. 25–27 for all cases. The power related to the charging of EVs is shown in red, while the power related to the discharging of EV-V2Gs is shown in blue. For convention, the EV charging power and the EV-V2G discharging power are positive and negative values respectively. The minimum voltage is shown in Fig 28 for all test cases. The operation of the system without EVs is illustrated with a black dotted line.

All cases present the lowest voltage around 6 a.m., tallying with the charging power peak for EVs. This fact demonstrate how significant is the burden added to the grid by the EVs and proves the importance of a coordinated schedule for their recharge.

The objective function was reduced by 3.6% from Case I to Case II, showing that V2G technology on EVs improves the operation of the system and makes it possible to reduce the energy cost. The best objective function was achieved when DG was

Figure 25 – Case I Simulation Results.

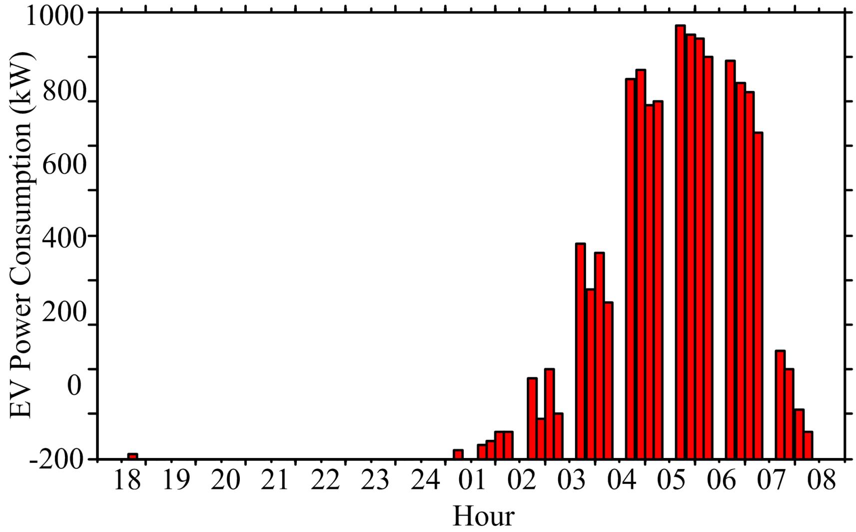

Source: Created by the author.

Figure 26 – Case II Simulation

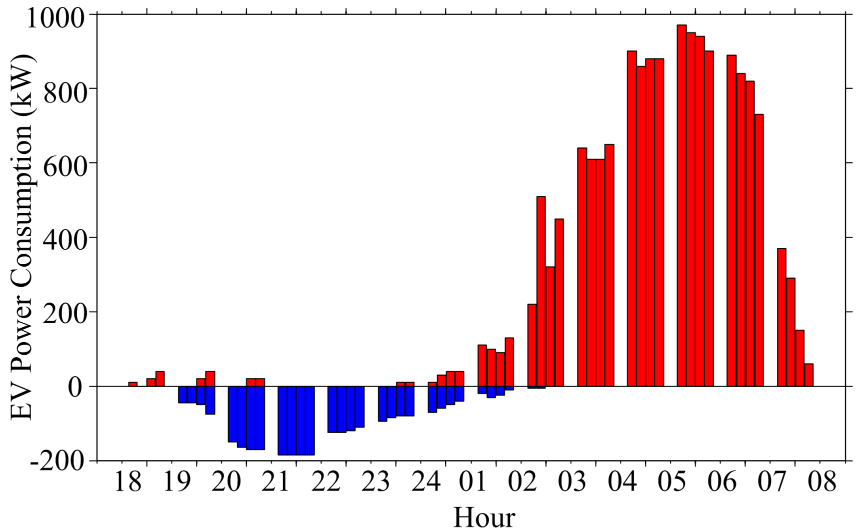

Source: Created by the author.

included because the EDN had the flexibility to operate using the power of the distributed generators, which has a lower energy cost in comparison to the energy cost at the substation.

The charging process is done between arrival and departure times and all schedules granted that the EVs leave with a fully charged battery at the end of the charging period, as presented in Table 7. Furthermore, operational constraints like voltage and currents limits were satisfied in all cases.

The proposed optimization model aims to minimize the energy cost of the EV charging. Because the final hours of the time period have a lower cost, the EVs are mostly charged on the last time intervals. In the same way, being the first hours the ones with

Figure 27 – Case III Simulation Results.

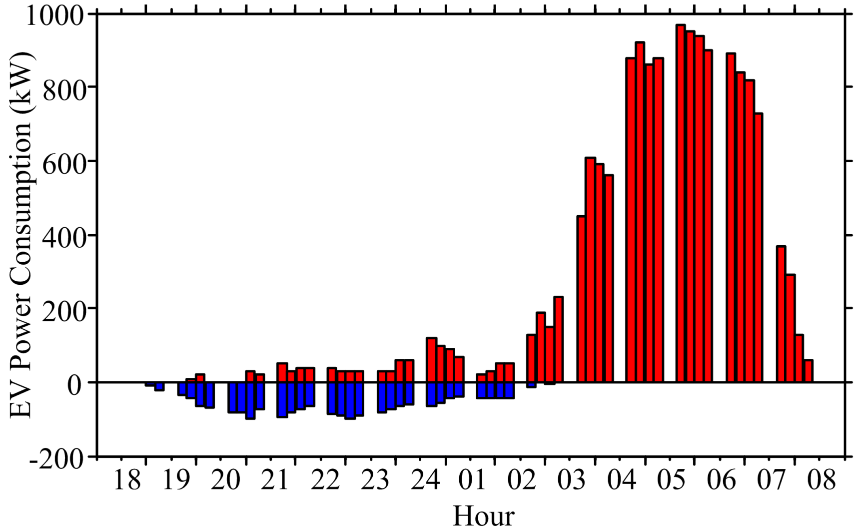

Source: Created by the author.

higher energy costs, the EV-V2Gs energy available for the grid is used in earlier time intervals.

Fig. 26 presents a reduction on the power delivered by the EV-V2Gs when compared with Fig. 27 due to the alleviation that DG provides to the system.

Figure 28 – Minimum Voltage Magnitudes.

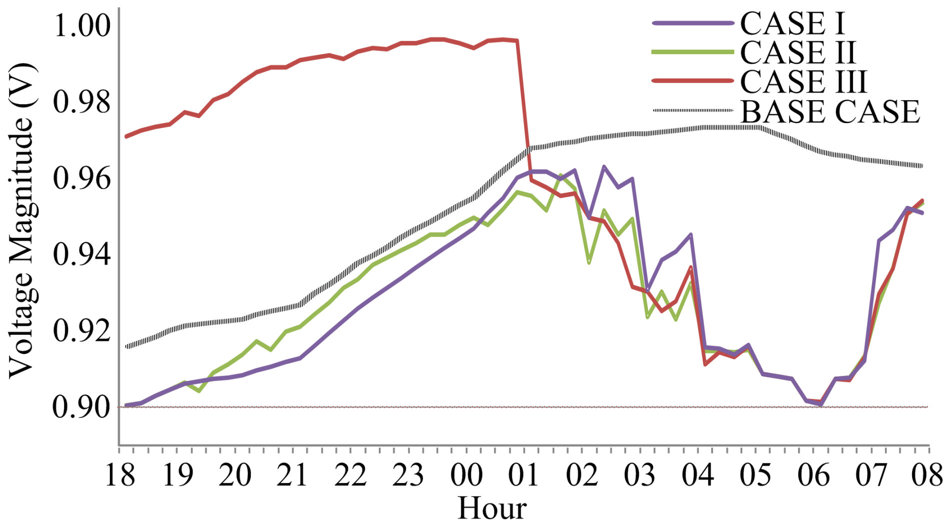

Source: Created by the author.

3.5 CHAPTER CONCLUSIONS

A step-by-step methodology based on a mixed integer linear programming formulation was presented to solve the optimal charging coordination of EV in unbalanced EDN considering vehicle-to-grid (V2G) technology. The proposed method can be used to define optimal charging schedules in order to avoid operational concerns associated with uncontrolled EV recharging.

The methodology was proven to efficiently handle EV load imbalance; randomness in EVs' arrival and departure times, and initial state of charge; different battery sizes; and forecast uncertainties. For every scenario, the methodology found charging schedules with no EV energy curtailment. In addition, the charging schedules satisfied operational constraints, taking into account the imbalance of the system circuits and loads; they also achieved a better economical operation of the EDN.

These results show the methodology to be very useful, as it defines each step to be implemented and gives a broad view of the state of the EDN throughout the whole time period. The methodology also offers great adaptability for incorporating new loads, e.g. EV plugs for recharge. Also, from the tests carried out, it can be concluded that the utilization of V2G in EDN is economically unsound, because the impact on the battery lifetime outstrips the economical improvement shown by this technology.

4 VVC AND ESS OPERATION TO IMPROVE THE EVCC

In this chapter, a new approach is presented to solve the electric vehicle charging coordination (EVCC) problem considering Volt-VAr control, energy storage systems (ESSs) operation and dispatchable distributed generation (DG) available in three-phase unbalanced electrical distribution networks (EDNs). Dynamic scheduling for the EVCC is proposed through a step-by-step methodology, which solves a mixed integer linear programming (MILP) problem for the whole time period. The objective is to minimize the total cost of energy purchased from the substation and DG units, the cost of energy curtailment on electric vehicles, the cost of energy injected from the ESSs and the cost of energy curtailment on the ESSs. The Volt-VAr control considers the management of on-load tap changers, voltage regulators, and switchable capacitors installed along the grid. Furthermore, the formulation takes into account the voltage dependency of the loads, while the steady-state operation of the unbalanced distribution systems is modeled using linear constraints. The proposed model was tested in a 178-node three phase unbalanced EDN considering a one-day time period.

4.1 INTRODUCTION

Increasing energy efficiency and reducing energy costs through a Volt VAr control (VVC) in electrical distribution networks (EDNs) has received plenty of attention in recent years (AHMADI; MARTÍ; DOMMEL, 2015; BISERICA et al., 2012; PADILHA-FELTRIN; QUIJANO; MANTOVANI, 2015; SCHNEIDER; WEAVER, 2014). The VVC problem finds a control scheme for the proper operation of the devices in the EDN that manage variations in voltage magnitudes and reactive power flows. These devices include among others, voltage regulators (VRs), capacitor banks (CBs) and on-load tap changers (OLTCs) (CIVANLAR; GRAINGER, 1985; BARAN; HSU, 1999; BOROZAN; BARAN; NOVOSEL, 2001; ROYTELMAN; WEE; LUGTU, 1995).

Recently, several VVC methodologies have been presented in the specialized literature. In Biserica et al. (2012), it is proposed a centralized function for VVC, in which, a state estimation based on pseudo-measurements using neural networks is used as input for the VVC. A multi-objective optimization for the VVC was presented in Padilha-Feltrin, Quijano e Mantovani (2015). In this work, a strategy was formulated based on an hourly load forecast for the next day, taking into account the active power demand reduction and the voltage magnitude deviation. Finally, a deterministic framework based on a mixed-integer quadratically constrained programming problem capable of optimally controlling the Volt-VAr problem was formulated in Ahmadi, MartÍ e Dommel (2015). Finally, an evaluation scheme for the VVC, based on energy consumption reduction and reactive power flow optimization was presented in Schneider e Weaver (2014), this method could be used over VVC optimization approaches (e.g., (BISERICA et al., 2012; PADILHA-FELTRIN; QUIJANO; MANTOVANI, 2015)) in order to prove effectiveness.

In recent years, energy storage systems (ESSs) have emerged as a solution to even out the power mismatch between renewable power generators and consumption. The ESSs store the surplus of power for use during time periods of low power generation. Nevertheless, the performance of ESSs has also proven advantageous in improving the economic and technical operation of the EDN (ATZENI et al., 2013; MACEDO et al., 2015; SCHAINKER, 2004). Reference Schainker (2004) discussed how the proper functioning of the ESSs in the EDN can improve the economic use of the existing generation, transmission and distribution infrastructure. A mixed-integer second-order cone programming model was presented in Macedo et al. (2015) to solve the optimal operation problem of ESSs in a radial EDN. The presented approach was tested in two single-phase systems and no dynamic control was presented for ESS charging. In Atzeni et al. (2013), a demand-side management approach was proposed through a day-ahead optimization process for ESSs and distributed generation (DG). This formulation only considered end users, disregarding the economic and operational constraints.

Lately, the number of electric vehicles (EVs) connected to EDNs has received more attention. Because the EVs use the energy from the grid to charge their batteries, a high penetration of EVs can cause the EDN to work outside of acceptable operational limits (LIN et al., 2010). The development of EV charging schedules to prevent issues such as overloads and voltage limit violations is essential (HE; VENKATESH; GUAN, 2012). Several works have approached the EV charging coordination (EVCC) problem (DAS et al., 2014; DEILAMI et al., 2011; HE; VENKATESH; GUAN, 2012; O'CONNELL; KEANE; FLYNN, 2014).

In He, Venkatesh e Guan (2012), an EVCC problem approach was presented. The formulation could properly handle large populations and the random arrival of EVs, but the impact of the EVs on the grid was not considered. A mathematical model for EV integration into the grid was presented in Das et al. (2014). An economical evaluation was assessed in order to find the optimal energy cost that would benefit both EV owners and the EDN operator. In O'Connell, Keane e Flynn (2014), a multi-period optimization for EV charging in EDNs was presented. The optimization aimed at minimizing the cost of charging EVs. An algorithm based on sensitivities was proposed for the real-time EVCC in

Deilami et al. (2011), considering the random arrivals/departures of EVs, voltage profiles, and power generation limits in order to minimize the total energy cost.

The presented approach overcomes the shortcomings of previous studies, which solved the VVC and the EVCC separately, by engaging both problems in a more global control optimization of the EDN. Furthermore, the advantages offered by ESSs and dispatchable DG units are also considered in this formulation. While VVC devices and ESSs improve the operation of the EDN, the formulation seeks to avoid violations of operational limits and reduce the overall costs in the grid. In addition, the EVCC tries to optimally charge the EVs plugged into the EDN, while avoiding the issues that a high EV penetration may cause.

This work proposes an approach that simultaneously uses the VVC (management of OLTCs, VRs, and CBs), ESS operation, and dispatchable DG units to improve the EVCC in a three-phase unbalanced EDN. Different from the single phase equivalent, the three-phase unbalance representation allows the inclusion of the mutual coupling effects in the circuits, reaching a more realistic representation. Moreover, in order to develop a thorough analysis and a more accurate economic improvement, the load's voltage dependency is also taken into account.

In order to integrate the described devices and achieve the aforementioned objectives, a mixed-integer nonlinear programming (MINLP) formulation is found. Linearization techniques are later used to obtain a mixed-integer linear programming (MILP) model that can be solved using commercial software, guaranteeing the optimal solution to the problem. A step-by-step methodology that offers a broad view of the EDN's behavior in future periods is used to solve a 24h time period. The proposed formulation was tested in an EDN with 34 medium-voltage nodes and 144 low-voltage nodes. The results demonstrate the efficiency and robustness of the methodology. This work's main contributions are as follows:

- A step-by-step methodology that solves the EVCC problem and finds the optimal operation of the EDN, throughout a centralized coordination, taking into account the benefits and flexibility brought to the grid by VVC devices, ESSs, and dispatchable DG units.
- A multi–period MILP formulation to solve the EVCC problem together with VVC, ESS operation and dispatchable DG units in a three-phase unbalanced EDN, considering a voltage dependent load model.

4.2 PROBLEM FORMULATION AND SOLUTION TECHNIQUE

This section describes the EVCC problem as well as the advantages and all technical concerns related to the VVC and the ESS operation. Besides, the step-by-step methodology proposed to solve the EVCC taking into account VVC, ESS operation, and dispatchable DG units in a three-phase unbalanced EDS considering a voltage dependent load model, will be presented.

4.2.1 EVCC, VVC and ESS scheduling

EVCC

The EVCC problem aims to find an optimal schedule for the battery charging of the EVs connected into the EDN in a specific time period. This charging scheduling not only has to satisfy the EV owner needs, but also has to avoid technical limit violations due to excessive EV load connected into the grid. An improvement in the EVCC can lead to: An economic betterment in the operation of the system, i.e., reduction in energy losses; an amelioration in the fulfillment of technical limits; a cost reduction in the EV recharge; or a reduction in the energy curtailment of the EVs at departure.

For the solution of the EVCC problem, the following considerations are assumed:

- The initial SOC of every vehicle is known when the vehicle is plugged into the grid;
- the batteries can be controlled in each time interval into which the time period is divided; and
- the EV user may provide a departure time when the vehicle is plugged; otherwise, it will be assumed that the vehicle will remain plugged in until a probable time interval determined by the historical of departure of the EV.

VVC

The VVC is defined as a control strategy to manage the voltage magnitudes and the reactive power flow throughout the EDN. This management consists in periodic adjustments over devices that inject reactive power into the grid in order to improve the voltage drop and devices that directly control voltage magnitude (BARAN; HSU, 1999). In general, VVC devices in an EDN consist in OLTCs, VRs, and switchable/fixed CBs. Therefore, an optimized VVC scheme will provide a set of values for all VVC devices (i.e., the tap step position for voltage magnitude adjustment and reactive power compensation) under all loading conditions, which in turn, will reduce the reactive power flowing throughout the EDN, hence the ohmic losses, and will maintain the voltage magnitudes within permissible limits.

In order to properly control the adjustment over VVC devices, control actions might be performed autonomous operation. This operation can follow a local decision–making based on local measurements of the EDN, i.e., each device is controlled independently; however, each action will affect the EDN operation and the performance of other devices. Thus, an integrated coordination of all VVC devices, based on remote measurements on the EDN and the operator knowledge, is necessary in order to obtain an optimal EDN operation through VVC. Therefore, for an optimal integrated VVC it is necessary a centralized coordination, a communication infrastructure, and a decision-making algorithm to optimize the VVC problem (RAHIMI; MARINELLI; SILVESTRO, 2012).

Furthermore, energy loss reduction, keeping voltage magnitudes on the EDN inside acceptable limits, has been the classical approach when solving the VVC problem. In recent works, the VVC is used not only to increase the EDN efficiency considering the classical approach, but also, to adjust the voltage profile in order to manage the load consumption in the EDN, since a reduction in the voltage magnitude within permissible levels can represent a decrease in the power consumption (PADILHA-FELTRIN; QUIJANO; MANTOVANI, 2015).

Using the classical approach, several works have shown the improvements brought to the EDN operation by an optimized VVC. Therefore, considering the effects of special loads in the EDN operation, the VVC can be a useful tool to improve the solution of the new challenges emerging in the EDN operation. Hence, an optimized dynamic coordination of the grid can be obtained with the inclusion of the VVC, which allows a more flexible adjustment in the EDN in order to avoid voltage limits violation in the presence of special loads such as EVs.

ESS operation

As mentioned, along with the EVs the proposed methodology must define an optimal charging agenda for the ESSs. Nevertheless, for the ESSs, complexity of the charging schedule increases as it is responsible for throttling the battery charge and for allowing the EDN to use the stored energy. Therefore, the formulation must determine the optimal schedule to charge and discharge the ESSs at each time interval. For the ESSs it is assumed:

- the ESSs cannot be discharged beyond their specified Depth of Discharge (DoD);
- the ESSs can be controlled through communication devices in order to define the charging state at each time step; and
- for each ESS, a goal is defined for the SOC at the end of the time period (e.g. same as the initial SOC); this goal is used to represent the utilization of the ESSs after

the considered time period (e.g. 1 day ahead).

4.2.2 Voltage Dependent Load Model

The demand of an EDN is classified into loads that can be represented as: a) constant power loads, b) constant impedance loads, c) constant current loads, or d) a combination of these. In a VVC framework for EDNs, the load's voltage dependency is a key aspect of the suitable representation of the network operation. As discussed in Padilha-Feltrin, Quijano e Mantovani (2015), Ahmadi, MartÍ e Dommel (2015), and Dabic et al. (2010), VVC models are highly dependent on the accuracy of the load representation. Dependence on the voltage magnitude and frequency is considered in the load models; mathematically, this dependence can be represented by static and dynamic load models described by the traditional ZIP model. For this analysis, two static models are commonly studied: the polynomial load model and the exponential load model (KORUNOVIC et al., 2012). The exponential expression of the load's sensitivity to the voltage and frequency variation is represented by (217) and (218).

$$P^D = P^o \left(\frac{V}{V_o}\right)^{\alpha} (1 + K_{pf}(f_r - f_r^o)) \tag{217}$$

$$Q^D = Q^o \left(\frac{V}{V_o}\right)^{\beta} (1 + K_{qf}(f_r - f_r^o)) \tag{218}$$

Where, f_r represents the frequency of the bus voltage and f_r^o represents the nominal frequency. The coefficients K_{pf} and K_{qf} are the frequency sensitivities for the active and reactive power loads, respectively. In this work, the effects associated with frequency are disregarded. Furthermore, with an appropriate adjustment of the constants α and β the model can be restricted to the steady-state analysis case (i.e., dependence directly on the voltage magnitude). Appropriate values for these constants may be found in previous works, such as IEEE (1995).

4.2.3 Methodology

The proposed methodology defines the status of the control devices (VRs, and CBs) as well as the charging status of the EVs in the network by solving an optimization problem. The operation of the EDS is modeled considering a given horizon (e.g. one-day), which is divided in time intervals. The time duration for every time interval is represented by Δ_t. The set T orders time intervals into which the time period is divided.

As shown in Fig. 29, the proposed MILP model is solved at the beginning of each time interval considering the actual number of connected EVs; besides, a forecast for the parameters related to possible EV plugs, such as estimated arrival times and initial state of charge (SOCs), is also taken into account. A dynamic scheduling (rolling multi-period optimization for the EVCC) is performed determining at each time interval

Figure 29 – Step-by-step methodology flowchart.

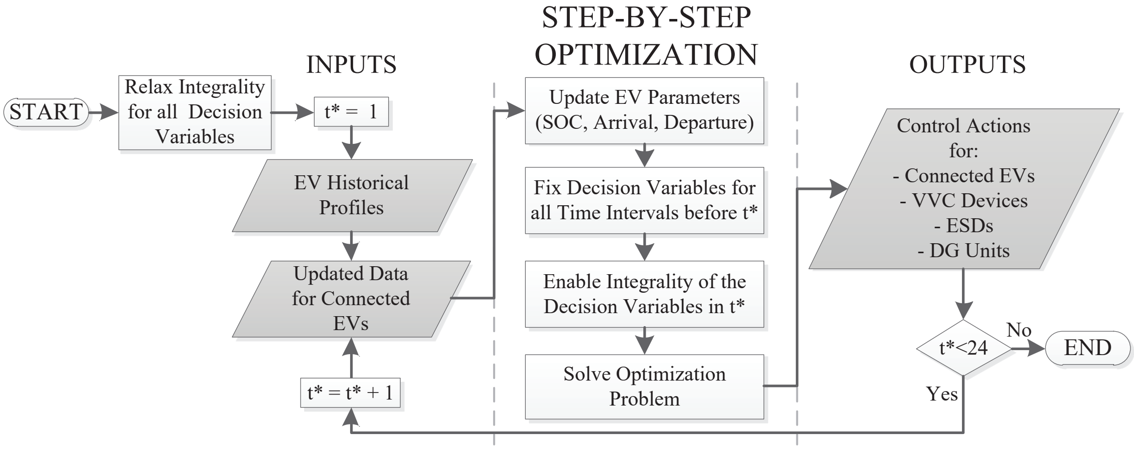

Source: Created by the author.

the optimal charging agenda of the EVs plugged and to be plugged into the grid. This dynamic scheduling is a part of the step-by-step methodology proposed, which will also determine at each time interval the control scheme for VVC devices, DG units and ESSs on the remaining time period. When a forecasted EV is actually plugged in, the parameters are updated. Nevertheless, if an EV does not arrive during the estimated time interval, a different estimation may be used or the EV may be disregarded altogether. It should be noted, that the EVs may arrive and depart during any time interval of the time period. Therefore, the EV's charging agenda will be generated between arrival and departure, ideally dispatching a fully charged battery for every vehicle. Different techniques may be applied to estimate the arrivals, departures, and initial SOCs of the EVs, as presented in Melo, Carreno e Padilha-Feltrin (2014), Qian et al. (2011), and Lojowska et al. (2012).

Operational constraints such as voltage limits, active and reactive power generation limits, and maximum current limits, are taken into account in the model. This way, a step-by-step solution is constructed over the entire time period. The solution at each time interval will determine the charging state for the EVs and ESSs, the energy delivered by the DG units, the number of modules operating in each CB, and the tap position for each phase of every VR. The nature of the control variables associated with each device is binary, which makes the VCC problem hard to solve. In order to reduce the computational complexity, only the control variables for the current time interval are treated as binary variables, i.e., control variables for the remaining time intervals are relaxed. This strategy makes it possible to solve the EVCC problem with reduced computational effort, obtaining the solution for the current time interval using updated information. An important upside of this methodology is that it offers a broad view of the state of the EDN throughout the whole time period.

4.2.4 Mixed-Integer Nonlinear Programming Model for EVCC

A mixed integer nonlinear programming (MINLP) model is presented in (219)–(254) for the proposed EVCC problem. The solution found by the formulation must define: the power delivered by each dispatchable DG unit ($P^G_{n,t}$), the number of modules connected in each CB ($B_{n,t}$), the tap position for each VR ($tp_{mn,f,t}$), the charging schedule for each EV ($y_{n,t}$), and the charging and discharging schedule for each ESS (P^{SD+}_u and P^{SD-}_u, respectively).

The proposed formulations consider the sets Ξ, CB, DG, F, L, N, SD, T, and VR to represent electric vehicles, capacitor banks, distributed generation units, phases, circuits, nodes, energy storage devices, time intervals, and voltage regulators, respectively. Furthermore, $V^{re/im}_{n,f,t}$ are the real/imaginary parts of the voltage at node n, phase f and time interval t, while $I^{Gre/im}_{n,f,t}$ and $I^{Dre/im}_{n,f,t}$ are the real/imaginary parts of the generated and demanded currents. $P^{G/D}_{n,f,t}$ and $Q^{G/D}_{n,f,t}$ are the generated/demanded active and reactive powers. In addition, $I^{re/im}_{mn,f,t}$ represents the real/imaginary parts of the current through the circuit connecting nodes m and n, while $B_{mn,f}$ is its the shunt susceptance for phase f. The real/imaginary parts of the currents corresponding to CB n, ESS, u and EV e are defined as $I^{CBre/im}_{n,t}$, $I^{SDre/im}_{u,t}$, and $I^{EVre/im}_{e,t}$, respectively; while $\widehat{V}^{re/im}_{u,t}$ is the real/imaginary part of the voltage at the node and phase associated with device u in time t. Finally, $R_{mn,f,h}$ and $X_{mn,f,h}$ are the resistance and reactance for circuit mn between phases f and h.

Objective Function (OF)

Represented by (219), the OF aims to minimize the cost of the energy provided by the substation (SE) (first term), the DG energy cost (second term), the cost of the energy curtailment on EVs (third term), and the cost of the energy injected from the ESSs to the grid (fourth term), and to penalize the deviation from the defined goals for the SOC of the ESSs (fifth term).

$$\min \sum_{f\in F}\sum_{t\in T}\zeta^G_{SE,t}\Delta_t\left(V^{re}_{SE,f,t}I^{Gre}_{SE,f,t}+V^{im}_{SE,f,t}I^{Gim}_{SE,f,t}\right)+\sum_{n\in N}\sum_{t\in T}\zeta^G_{n,t}\Delta_t P^G_{n,t}+\sum_{e\in\Xi}\zeta^{EV}_c E^{EVc}_e+$$
$$\sum_{u\in SD}\sum_{t\in T}\zeta^{SD}\Delta_t P^{SD-}_{n,t}+\sum_{u\in SD}\zeta^{SD}_c E^{SDc}_u \tag{219}$$

Where:

$\zeta^G_{n,t}$ is the energy cost at node n at time t;

$\zeta^{EV}_c, \zeta^{SD}_c$ are the EV and ESS energy curtailment costs;

ζ^{SD} is the unit cost for the active power taken from the ESS;

$\boldsymbol{S}$ is the substation node;

E_e^{EVc} is the energy curtailment on EV e at the end of the time period; and

E_u^{SDc} is the energy curtailment on ESS u at the end of the time period

Steady-State Operation Point

The equations (220)–(229) model the steady-state operation of a three-phase unbalanced EDN considering the presence of DG units, CBs, VRs, ESSs, and EVs.

$$I_{n,f,t}^{Gre} + \sum_{n \in CB} I_{n,d}^{cbre} + \sum_{km \in L \cup VR} I_{km,f,t}^{re} - \sum_{mn \in L} I_{mn,t}^{re} - (\sum_{km \in L} B_{km,f}^{sh} + \sum_{mn \in L} B_{mn,f}^{sh}) \frac{V_{m,f,t}^{im}}{2} = I_{m,f,t}^{Dre} + \sum_{e \in \Xi} I_{e,t}^{EVre} \gamma(e,m,f) + \sum_{u \in SD} I_{u,t}^{SDre} \gamma(u,m,f) \tag{220}$$

$$I_{n,f,t}^{Gim} + \sum_{n \in CB} I_{n,d}^{cbim} + \sum_{km \in L \cup VR} I_{km,f,t}^{im} - \sum_{mn \in L} I_{mn,t}^{im} - (\sum_{km \in L} B_{km,f}^{sh} + \sum_{mn \in L} B_{mn,f}^{sh}) \frac{V_{m,f,t}^{re}}{2} = I_{m,f,t}^{Dim} + \sum_{e \in \Xi} I_{e,t}^{EVim} \gamma(e,m,f) + \sum_{u \in SD} I_{u,t}^{SDim} \gamma(u,m,f) \tag{221}$$

$$I_{n,f,t}^{Dre} = (P_{n,f,t}^{D} V_{n,f,t}^{re} + Q_{n,f,t}^{D} V_{n,f,t}^{im}) / V_{n,f,t}^{re^2} + V_{n,f,t}^{im^2} \tag{222}$$

$$I_{n,f,t}^{Dim} = (P_{n,f,t}^{D} V_{n,f,t}^{im} - Q_{n,f,t}^{D} V_{n,f,t}^{re}) / V_{n,f,t}^{re^2} + V_{n,f,t}^{im^2} \tag{223}$$

$$P_{n,f,t}^{D} = P_{n,f,t}^{o} (\sqrt{V_{n,f,t}^{re^2} + V_{n,f,t}^{im^2}} / V_o)^{\alpha_{n,f}} \tag{224}$$

$$Q_{n,f,t}^{D} = Q_{n,f,t}^{o} (\sqrt{V_{n,f,t}^{re^2} + V_{n,f,t}^{im^2}} / V_o)^{\beta_{n,f}} \tag{225}$$

$$V_{m,f,t}^{re} - V_{n,f,t}^{re} = \sum_{h \in F} (R_{mn,f,h} I_{mn,h,t}^{re} - X_{mn,f,h} I_{mn,h,t}^{im}) \tag{226}$$

$$V_{m,f,t}^{im} - V_{n,f,t}^{im} = \sum_{h \in F} (X_{mn,f,h} I_{mn,h,t}^{re} + R_{mn,f,h} I_{mn,h,t}^{im}) \tag{227}$$

$$\underline{V}^2 \leq {V_{n,f,t}^{re}}^2 + {V_{n,f,t}^{im}}^2 \leq \overline{V}^2 \tag{228}$$

$$0 \leq {I_{mn,f,t}^{re}}^2 + {I_{mn,f,t}^{im}}^2 \leq {\overline{I}_{mn}}^2 \tag{229}$$

$$\forall mn \in L, \forall n \in N, f \in F, t \in T$$

Also considering that $\alpha_{n,f}$, $\beta_{n,f}$ are the load voltage dependence parameters of the active and reactive power at node n, phase$f$; $\gamma\,(u,m,f)$ is the function that indicates whether device u is connected at node m and phase f; $P_{n,f,t}^{o}, Q_{n,f,t}^{o}$ are the nominal active and reactive power demand at node n, phase$f$, time t; and Q_n^{esp} is the CB module reactive power capacity at node n.

The balance of the currents at each node is represented by (220) and (221). Moreover, γ is a binary function that takes a value of 1 if the EV e or ESS u are connected at node m and at phase f. The load currents shown in (222) and (223) define the relationship between voltage, current and the active and reactive powers demanded by the loads. Moreover, (224) and (225) are the exponential representation of the load's voltage dependency. Equations (226) and (227) are the result of applying Kirchhoff's

Voltage Law to each independent loop of the EDN. Finally, the limits for the voltage magnitude and current capacity in each circuit are stated in (228) and (229), respectively.

DG Constraints

The operation limits of the DG units are defined by (230)–(232), while the active and reactive power injections are represented by (233)–(234), respectively. Considering ϕ_n as the minimum power factor for the operation of the DG at node n.

$$0 \leq P^G_{n,t} \leq \overline{P}^G_n \tag{230}$$
$$\underline{Q}^G_n \leq Q^G_{n,t} \leq \overline{Q}^G_n \tag{231}$$
$$|Q^G_{n,t}| \leq P^G_{n,t} \tan(\arccos(\phi_n)) \tag{232}$$
$$P^G_{n,t}/3 = V^{re}_{n,f,t} I^{Gre}_{n,f,t} + V^{im}_{n,f,t} I^{Gim}_{n,f,t} \tag{233}$$
$$Q^G_{n,t}/3 = -V^{re}_{n,f,t} I^{Gim}_{n,f,t} + V^{im}_{n,f,t} I^{Gre}_{n,f,t}, \qquad \forall n \in N|_{n \exists DG}, f \in F, t \in T \tag{234}$$

CBs Constraints

Similar to the DG units, the active and reactive power of the switchable CBs are represented by (235) and (236). The value for the active power injection of every CB will always be equal to zero. Equation (237) represents the number of capacitor modules connected to the grid for each bank, while the allowable limit of modules is modeled by (238). Finally, as the lifetime of switchable CBs are significantly impacted by the amount of operations, (239) limits the maximum number of operations permitted over the entire time period.

$$0 = V^{re}_{n,f,t} I^{cbre}_{n,f,t} + V^{im}_{n,f,t} I^{cbim}_{n,f,t} \tag{235}$$
$$Q^{cb}_{n,t}/3 = -V^{re}_{n,f,t} I^{cbim}_{n,f,t} + V^{im}_{n,f,t} I^{cbre}_{n,f,t} \tag{236}$$
$$Q^{cb}_{n,t} = B_{n,t} Q^{esp}_n \tag{237}$$
$$0 \leq B_{n,t} \leq \overline{B}_n \tag{238}$$
$$\sum_{t \in T} |B_{n,t} - B_{n,t-1}| \leq \Delta^{cb} \qquad \forall n \in N|_{n \exists CB}, f \in F, t \in T \tag{239}$$

Where, $\overline{B}_n$ is the maximum number of CB modules at node n, Δ^{cb} is the maximum number of operations allowable over the time period for the CBs, and $Q^{cb}_{n,t}$is the reactive power delivered by a CB at node n, time t.

VR and OLTC Constraints

The mathematical model of a VR or a OLTC is shown in (240)–(243). In this model, (240) represents the real part of the regulated voltage and (241) represents the real part of the regulated current on each VR/OLTC. Expression (242) represents the minimum and maximum limits of the tap position represented by the integer variable $tp_{mn,f,d}$. Analogue to (239), (243) limits the maximum number of operations allowable for a VR/OLTC over the time period in order to avoid an excessive wear and tear of the devices. Expressions similar to (240) and (241) were implemented to describe the imaginary component for both the regulated voltage and current.

$$V^{re}_{n,f,t} = (1 + \%R_{mn} tp_{mn,f,t}/Tp_{mn}) V^{re}_{m,f,t} \tag{240}$$

$$I^{re}_{km,f,t} = (1 + \%R_{mn} tp_{mn,f,t}/Tp_{mn}) I^{re}_{mn,f,t} \tag{241}$$

$$-Tp_{mn} \leq tp_{mn,f,t} \leq Tp_{mn} \tag{242}$$

$$\sum_{t \in T} |tp_{mn,f,t} - tp_{mn,f,t-1}| \leq \Delta^{vr} \qquad \forall mn \in L|_{mn \exists VR}, f \in F, t \in T \tag{243}$$

For the set of VR consider, Δ^{vr} is the maximum number of operations allowable over the time period for the VRs; $\%R_{mn}$ is the regulation percentage of the VR in circuit mn; Tp_{mn} is the maximum number of steps of the VR in circuit mn; $bt_{mn,f,t,k}$ is the binary variable that describes the tap position of the VR in circuit mn, phase f, time t, position k; $I^{c(re)}_{mn,f,t,k}$ is the real part of the VR current calculation auxiliary variable in circuit mn, phase f, time t, position k; $tp_{mn,f,t}$ is the integer variable for the number of steps of the VR in circuit mn, phase f, time t; and $V^{c(re)}_{mn,f,t,k}$ is the real part of the VR voltage calculation auxiliary variable in circuit mn, phase f, time t, position k; $I^{im*}_{mn,f,t}$, $I^{re*}_{mn,f,t}$ are the imaginary and real part of the estimated current of the VR in circuit mn, phase f, time t.

ESS Constraints

For the ESSs, (244) and (245) represent the active and reactive power exchange between each ESS and the grid. In (246), the energy balance in an ESS is written in terms of the energy that must be charged, the charging power in each time interval and the defined goal for the SOC at the end of the charging period. Equation (247) defines the energy stored in each SD at every interval and (248) limits the ESS's energy level ensuring that it does not exceed the battery's maximum capacity or the pre-established DoD. Finally, (249) defines the limits for the charging and discharging active powers for each ESS.

$$(P_{u,t}^{SD+} - P_{u,t}^{SD-})/3 = V_{u,t}^{re} I_{u,t}^{SDre} + V_{u,t}^{im} I_{u,t}^{SDim} \tag{244}$$

$$0 = -V_{u,t}^{re} I_{u,t}^{SDim} + V_{u,t}^{im} I_{u,t}^{SDre} \tag{245}$$

$$E_u^{SD_f} = E_{u,T}^{SD} + E_u^{SDc} \tag{246}$$

$$E_{u,t}^{SD} = E_u^{SDi} + \sum_{k \in T, k \leq t} \Delta_k (P_{u,t}^{SD+} \eta_u^+ - P_{u,t}^{SD-}/\eta_u^-) \tag{247}$$

$$\min(E_u^{SDi}, \overline{E}_u^{SD} DoD) \leq E_{u,t}^{SD} \leq \overline{E}_u^{SD} \tag{248}$$

$$0 \leq P_{u,t}^{SD+}, P_{u,t}^{SD-} \leq \overline{P}_u^{SD} \qquad \forall u \in SD, t \in T \tag{249}$$

Where, η_u^+, η_u^- are the charging and discharging efficiencies of the charging station for ESS u; $\overline{E}_e^{EV}, \overline{E}_u^{SD}$ are the energy capacity of EV e and ESS u; $E_u^{SD_f}$ is the goal for the state of charge of ESS u at the end of the time period; E_u^{SDi} is the initial state of charge of ESS u; $\overline{P}_u^{SD}$ is the maximum charging/discharging active power of ESS u; $E_{u,T}^{SD}$ is the energy of ESS u at the end of the time period; and $P_{u,t}^{SD+}$, $P_{u,t}^{SD-}$ are the charging and discharging power of the ESS u, time t.

EV Constraints

The active and reactive powers of the EVs are presented in (250) and (251), respectively. The instant power in (252) is represented in terms of the maximum charging power and the binary control variable $y_{n,t}$. Constraint (253) determines the energy curtailment on each EV, as (254) determines the energy of each EV at departure. The variable $y_{n,t}$ has a value of 1 if the EV battery is charging at its maximum power $\overline{P}_e^{EVch}$ and a value of 0 otherwise.

$$P_{e,t}^{EV} = V_{e,t}^{re} I_{e,t}^{EVre} + V_{e,t}^{im} I_{e,t}^{EVim} \tag{250}$$

$$0 = -V_{e,t}^{re} I_{e,t}^{EVim} + V_{e,t}^{im} I_{e,t}^{EVre} \tag{251}$$

$$P_{e,t}^{EV} = \overline{P}_e^{EVch} y_{e,t} \tag{252}$$

$$\overline{E}_e^{EV} = E_e^{EV} + E_e^{EVc} \tag{253}$$

$$E_e^{EV} = E_e^{ini} + \sum_{t \in T} \Delta_t P_{e,t}^{EV} \eta_e \qquad \forall e \in \Xi, t \in T \tag{254}$$

Where, η_e is the charging efficiency of the charging station for EV e; E_e^{ini} is the initial state of charge of EV e; $\overline{P}_e^{EVch}$ is the maximum power consumption of EV e; E_e^{EV} is the energy of EV e at the end of the time period; and $P_{e,t}^{EV}$ is the EV e active power consumption, time t.

4.2.5 Mixed-Integer Linear Programming Model for EVCC

To enhance the robustness of the solution and to enable the utilization of classic optimization methods and commercial solvers, linearization techniques are applied to the nonlinear expressions in (219)–(254) in order to obtain a MILP formulation.

Linearization for Nonlinear Constraints of the Steady-State Operation Point

Constraints (222)–(225), (228), and (229), are nonlinear expressions. Equations (222)–(225) are rewritten as shown in (255) and (256). Constraints (257) and (258) show the first-order linearization for (255) and (256) around an estimated operation point $(V^{re^*}_{n,f,t}, V^{im^*}_{n,f,t})$. Furthermore, (228) and (229) are linearized as presented in Franco, Rider e Romero (2015).

$$g(V^{re}_{n,f,t},V^{im}_{n,f,t}) = P^o_{n,f,t}\frac{V^{re}_{n,f,t}}{V_o^{\alpha_{n,f}}}\left(V^{re^2}_{n,f,t}+V^{im^2}_{n,f,t}\right)^{\frac{\alpha_{n,f}}{2}-1} + Q^o_{n,f,t}\frac{V^{im}_{n,f,t}}{V_o^{\beta_{n,f}}}\left(V^{re^2}_{n,f,t}+V^{im^2}_{n,f,t}\right)^{\frac{\beta_{n,f}}{2}-1} \quad (255)$$

$$h(V^{re}_{n,f,t},V^{im}_{n,f,t}) = P^o_{n,f,t}\frac{V^{im}_{n,f,t}}{V_o^{\alpha_{n,f}}}\left(V^{re^2}_{n,f,t}+V^{im^2}_{n,f,t}\right)^{\frac{\alpha_{n,f}}{2}-1} - Q^o_{n,f,t}\frac{V^{re}_{n,f,t}}{V_o^{\beta_{n,f}}}\left(V^{re^2}_{n,f,t}+V^{im^2}_{n,f,t}\right)^{\frac{\beta_{n,f}}{2}-1} \quad (256)$$

$$I^{Dre}_{n,f,t} = g^* + \left.\frac{\partial g}{\partial V^{re}}\right|^*(V^{re}_{n,f,t} - V^{re^*}_{n,f,t}) + \left.\frac{\partial g}{\partial V^{im}}\right|^*(V^{im}_{n,f,t} - V^{im^*}_{n,f,t}) \quad (257)$$

$$I^{Dim}_{n,f,t} = h^* + \left.\frac{\partial h}{\partial V^{re}}\right|^*(V^{re}_{n,f,t} - V^{re^*}_{n,f,t}) + \left.\frac{\partial h}{\partial V^{im}}\right|^*(V^{im}_{n,f,t} - V^{im^*}_{n,f,t}) \qquad \forall n \in N, f \in F, t \in T \quad (258)$$

Linearization of DG, CBs, ESSs and EVs Nonlinear Constraints

The nonlinear expressions of the DG, CBs, ESSs and EVs (constraints (233), (234), (235), (236), (244), (245), (250) and (251)) are approximated using an estimated operation point $(V^{re^*}_{n,f,t}, V^{im^*}_{n,f,t})$ as shown in Franco, Rider e Romero (2015). The quality of the estimated operation point will define the approximation error. Historical data and the EDN operator knowledge, nominal values for the voltage magnitudes, or a linear relaxation of the MILP model initially solved (in which the binary nature of the decision variables is temporarily ignored), could be used to estimate the operation point.

Linearization of VR/OLTC Nonlinear Constraints

In the expressions (240) and (241), the product of the decision variables $tp_{mn,f,t}$ and, $V_{m,f,t}$ or $I_{mn,f,t}$ on the real and imaginary components is linearized. To obtain linear expressions, the integer number of steps is represented as a set of binary variables $bt_{mn,f,t}$ and the products $tp_{mn,f,t}V_{m,f,t}$, $tp_{mn,f,t}I_{mn,f,t}$ are substituted by the variables $V^c_{mn,f,t,k}$ and $I^c_{mn,f,t,k}$, respectively, on the real and imaginary components.

$$V^{re}_{n,f,t} = (1 - \%R_{mn})V^{re}_{m,f,t} + \sum_{k=1}^{2Tp_{mn}} \frac{\%R_{mn}}{Tp_{mn}} V^{c(re)}_{mn,f,t,k} \quad (259)$$

$$I^{re}_{km,f,t} = (1 - \%R_{mn})I^{re}_{mn,f,t} + \sum_{k=1}^{2Tp_{mn}} \frac{\%R_{mn}}{Tp_{mn}} I^{c(re)}_{mn,f,t,k} \quad (260)$$

$$\sum_{k=1}^{2Tp_{mn}} bt_{mn,f,t,k} - Tp_{mn} = tp_{mn,f,t} \tag{261}$$

$$|V^{re}_{m,f,t} - V^{c(re)}_{mn,f,t,k}| \leq \overline{V}(1 - bt_{mn,f,t,k}) \tag{262}$$

$$|V^{c(re)}_{mn,f,t,k}| \leq \overline{V} bt_{mn,f,t,k} \tag{263}$$

$$|I^{re}_{mn,f,t} - I^{c(re)}_{mn,f,t,k}| \leq \overline{I}_{mn}(1 - bt_{mn,f,t,k}) \tag{264}$$

$$|I^{c(re)}_{mn,f,t,k}| \leq \overline{I}_{mn} bt_{mn,f,t,k} \tag{265}$$

$$bt_{mn,f,t,k} \leq bt_{mn,f,t,k-1} \qquad \forall mn \in L|_{mn\exists VR}, f \in F, t \in T, k \in 1..2Tp_{mn} \tag{266}$$

Expressions (259)–(266) are linear extensions of (240)–(243), where (259) represents the calculation of the regulated voltage and (260) represents the calculation of the regulated current for the real component. Equation (261) associates the binary variable with the tap integer variable. Constraint (262) defines the auxiliary variable $V^{c}_{mn,f,d,k}$ and (263) describes its limits. In the same way, (264) defines the auxiliary variable $I^{c}_{mn,f,d,k}$ and (265) describes its limits. Expression (266) represents the sequencing of the binary variable $bt_{mn,f,d}$ in the previous tap position. For time intervals in which the binary nature of the control variables is disregarded, the equations above are not suitable. Therefore, (267) and (268) are used to calculate the relaxed value of bt for each VR/OLTC.

In other words, (259)–(266) are used to calculate the tap position in the actual time interval and, (266), (267) and (268) are constraints applied to the rest of the time period. Similar to the approximated values of the voltages, the quality of the approximated values of the currents ($I^{re*}_{mn,f,t}$ and $I^{im*}_{mn,f,t}$) depends on the EDN operator's knowledge. Expressions similar to (259)–(268) were implemented to linearize the imaginary component.

$$V^{re}_{n,f,t} = (1 - \%R_{mn})V^{re}_{m,f,t} + \sum_{k=1}^{2Tp_{mn}} bt_{mn,f,t,k} \frac{\%R_{mn}}{Tp_{mn}} V^{re*}_{n,f,t} \tag{267}$$

$$I^{re}_{km,f,t} = (1 - \%R_{mn})I^{re}_{mn,f,t} + \sum_{k=1}^{2Tp_{mn}} bt_{mn,f,t,k} \frac{\%R_{mn}}{Tp_{mn}} I^{re*}_{mn,f,t} \qquad \forall mn \in L|_{mn\exists VR}, f \in F, t \in T \tag{268}$$

4.3 TESTS AND RESULTS

To assess the proposed methodology, tests were carried out on a three-phase EDN with 34 nodes at medium voltage (24.9 kV) and 144 nodes at low voltage (480 V) shown in Fig. 30. The EDN was adapted from the IEEE 34-node test system; for further information, the complete description of the EDN used is available in (DISTRIBUTION. . . , b). The test system includes a DG unit at node 8, an ESS at node 23, a VR connected at the end-point of circuit 16-17 and a CB at node 31. Moreover, phases A, B, and C were loaded with 33%, 35%, and 32% of the total demand, respectively. The values of the parameters α and β, used to represent different types of loads in the voltage dependent model, are presented in (DISTRIBUTION..., 2014). The hourly energy costs and load variation percentages are shown in Table 8. It was assumed that EVs could arrive and depart at any time interval during the period in bold, based on the fact that this is the time window when the EV demand has a greater impact.

The DG unit energy cost $\zeta_{n,t}^{G}$ was equal to 0.045 US$/kWh, while its maximum active power was 350 kW and its minimum and maximum reactive powers were equal to -175 kVAr and 175 kVAr, respectively. Finally, the minimum power factor for the operation was 0.90.

The ESS was assumed to be owned by the EDN operator. Hence, the cost for the active power injected into the grid by the ESS ζ^{SD} was disregarded. Moreover, the ESS maximum energy capacity was 3 MWh, with a maximum charge and discharge power of 300 kW, 10% of DoD , and charging and discharging efficiencies of 100%. The expected ESS SOC at the end of the time period was set at its initial energy level. Finally, the curtailment costs ζ_{c}^{SD} was set to 100 US$/kWh.

The VR was assumed to be a three-phase VR built from three single-phase VRs. This feature offers the flexibility of controlling each phase independently. Each single-phase VR could vary the voltage with a regulation ratio of ±10%; in addition, this ratio was equally distributed across 16 tap positions (±8). Furthermore, the switchable CB capacity was 300 kVAr, divided into 6 individual modules. For these tests, the maximum number of allowable operations for both CB and VR (Δ^{cb} and Δ^{vr}, respectively) were set at unreachable values, i.e., the number of operations for each device over the time period was unlimited.

Figure 30 – 178-nodes test system.

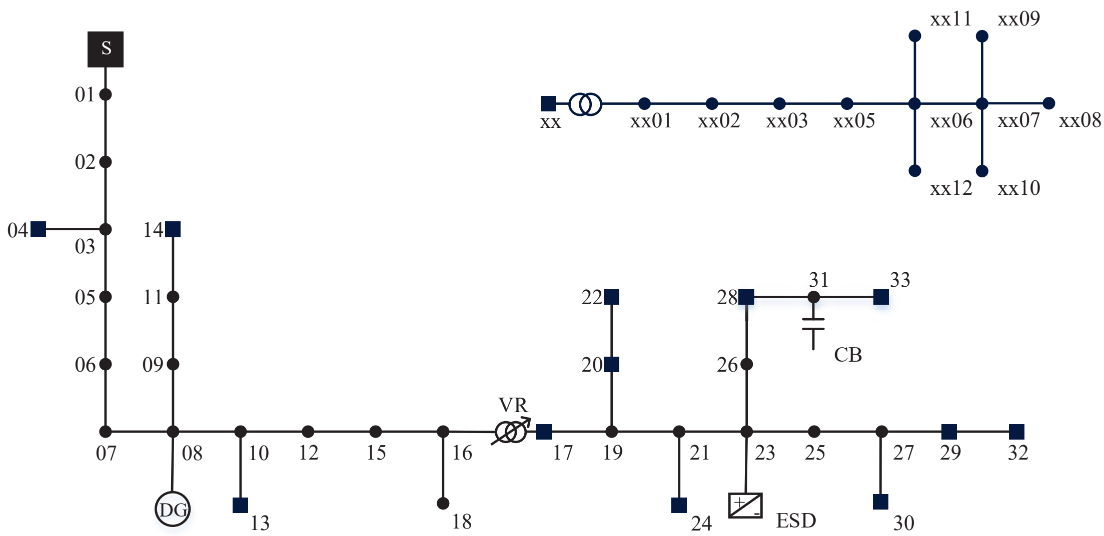

Source: Created by the author.

Table 8 – Hourly Energy Costs and Load Variations

Hour	Energy cost ($/kWh)	% of peak load	Hour	Energy cost ($/kWh)	% of peak load
08:00	0.0442	50	**20:00**	**0.0875**	**89**
09:00	0.0529	55	**21:00**	**0.0837**	**87**
10:00	0.0606	63	**22:00**	**0.0721**	**75**
11:00	0.0673	70	**23:00**	**0.0625**	**69**
12:00	0.0721	75	**00:00**	**0.0529**	**59**
13:00	0.0798	83	**01:00**	**0.0385**	**46**
14:00	0.0847	88	**02:00**	**0.0327**	**44**
15:00	0.0866	90	**03:00**	**0.0317**	**42**
16:00	0.0914	95	**04:00**	**0.0336**	**41**
17:00	0.0933	97	**05:00**	**0.0327**	**40**
18:00	**0.0962**	**100**	**06:00**	**0.0394**	**45**
19:00	**0.0895**	**91**	**07:00**	**0.0423**	**48**

Source: Created by the author.

In addition, 180 consumers with EVs were considered in the network, representing almost a 40% penetration. Two types of EVs were considered: the ‘Tesla Model S’ with a 70 kWh battery capacity and 10 kW charging power (TESLA-MOTORS, 2014), and the ‘Nissan Leaf’ with a 24 kWh battery capacity and 4 kW charging power (NISSAN, 2014). Moreover, a 100% efficiency for all EV charging stations was assumed and the curtailment the EVs ζ_c^{EV} was set to 100 US$/kWh. cost for

The proposed MILP model was written in the mathematical language AMPL (FOURER; GAY; KERNIGHAN, 2003) and solved using the commercial solver CPLEX (ILOG INC., 2009), on a computer with an Intel $i7$ 4770 processor. Tests were carried out for four different cases with the following control alternatives:

- Case I: ESS not available; VVC predefined.
- Case II: ESS enabled; VVC predefined.
- Case III: ESS not available; VVC enabled.
- Case IV: ESS enabled; VVC enabled.

For the Cases I and II, in which the VVC was predefined, the VVC devices followed preset settings. These settings are defined by the EDN operator following the daily conventional demand pattern.

Table 9 shows a summary of the results from the test cases. Case I, which includes only the control over the EVs plugged into the system, presented the worst solution, with high EV energy curtailment and expensive overall energy cost. From Case II, it can be seen how the enabling of the ESS in the grid leads to a significant reduction in the EV energy curtailment, hence, an improvement in the EVCC solution. Besides, Case II presented an increment on the overall energy costs due to a higher EV demand attended. Moreover, Case III shows how with the inclusion of the VVC, the grid is able to attend the whole EV demand, avoiding technical limit breaches. Finally, the best OF value with the lowest overall energy cost and no EV energy curtailment was obtained in Case IV, demonstrating the advantages of the proposed control methodology.

Table 9 – Summary Of The Test Cases

Case	SE Energy Cost ($)	DG Energy Cost ($)	Total Energy Cost ($)	EV Energy Curtailment (kWh)	Objective Function ($)
I	1957.69	314.98	2272.67	274	29672.67
II	1969.79	336.18	2305.97	104	12705.97
III	1905.24	279.13	2184.37	0	2184.37
IV	1852.81	287.94	2140.75	0	2140.75

Source: Created by the author.

Fig. 31 shows the active power injected into the grid by the SE, the DG unit, and the ESS for a) Case I, b) Case II, c) Case III, and d) Case IV. In addition, this figure shows, for all cases, the power demanded by the EVs and the ESS when charging (by convention, the active power due to these demands is shown in negative values). It should be noted that the methodology found an optimal schedule to recharge the EVs mainly at low-cost energy time intervals. Nevertheless, energy curtailments were presented when the grid was unable to meet the EV demand. When VVC was enabled, the EDN could completely charge the EVs during the low-cost energy time intervals, thereby achieving a better OF. On the other hand, the ESS improves the EVCC by allowing a higher number of EVs to be scheduled at the last time intervals. Furthermore, as the VVC was enabled, the total amount of power demanded in the time period decreased as well as the energy bought from the DGs.

The VVC pre-set profile and the VVC schemes for Cases III and IV are shown in Table 10. For every case, the VVC seeks to fulfill the technical constraints and determine the best economical operation of the EDN. When enabled, all the modules of the CB were plugged into the grid; this permits a greater voltage reduction at the VR, therefore, achieving a better economic performance. Although the limit for the number of switching operations was set in a very large number, the maximum number of switching operations for any VVC device over the entire time period for Cases III and IV was 30.

Fig. 32 shows the minimum voltage magnitude profiles for each time interval in the EDN, evidencing the fulfillment of voltage limits in all cases. Due to the voltage dependency of the loads, in the cases where the VVC was enabled (Cases III and IV), the minimum voltage profile was kept as close as possible to the lower boundary. This feature can be quantified by the economical operation improvement shown in Table 9. Thereby, comparing Cases I and III, there is a reduction in the overall energy cost of the EDN throughout the entire time period, even though the EVs were completely attended only

Figure 31 – Active power injected into the grid.

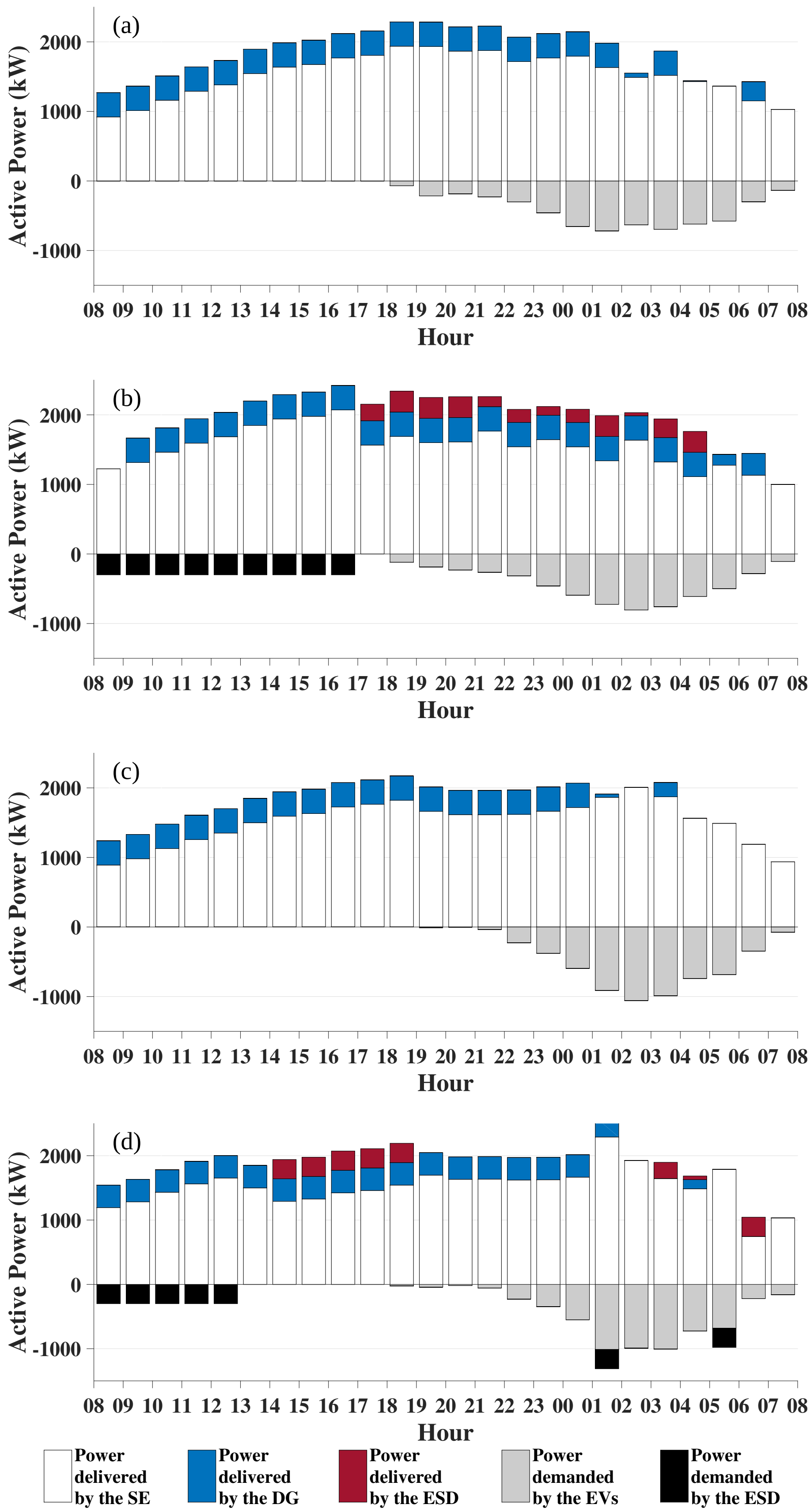

Source: Created by the author.

Table 10 – VR Tap Position Range for each Phase and CB Modules

Time intervals		07–12	13–21	22–01	02–06
Predefined Settings	A,B,C	{2}	{4}	{2}	{1}
	CB	{3}	{5}	{3}	{1}
Case III	*A*	{-6,-3}	{-3,-1}	{-4,4}	{-1,4}
	B	{-4,-2}	{-1,1}	{2,6}	{-5,5}
	C	{-6,-4}	{-3,-2}	{-1,0}	{-1,5}
	CB	{6}	{6}	{6}	{6}
Case IV	*A*	{-5,-3}	{-3,-1}	{-4,4}	{-2,3}
	B	{-4,-2}	{-1,0}	{1,5}	{-3,5}
	C	{-5,-4}	{-3,-2}	{-1,2}	{-6,4}
	CB	{6}	{6}	{6}	{6}

Source: Created by the author.

in Case III.

Figure 32 – Minimum voltage profile

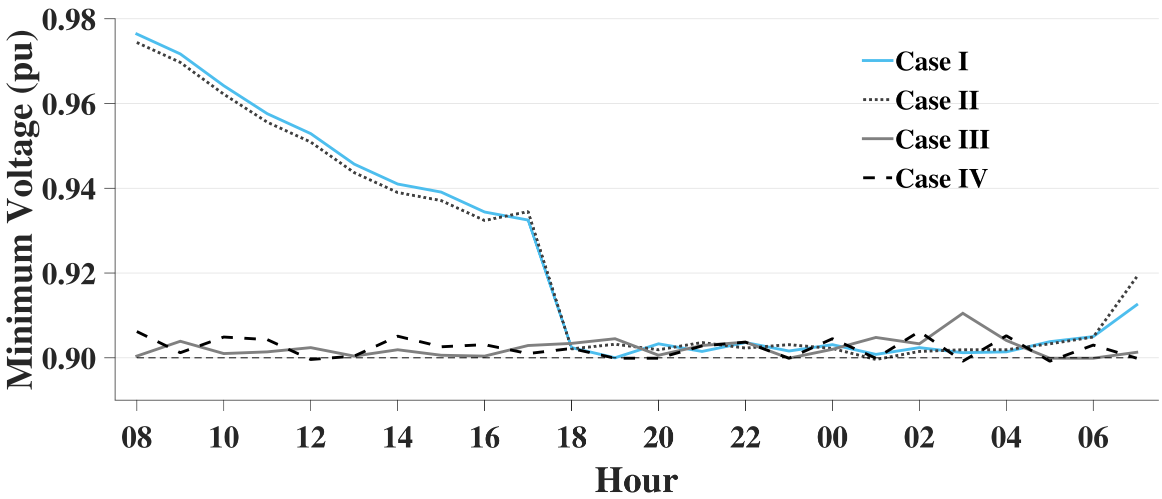

Source: Created by the author.

To properly validate the importance of the voltage dependent load model, the formulation was solved considering constant power in the load representation (i.e., $\alpha = 0$ and $\beta = 0$). A power flow considering the voltage dependent load model was later executed, fixing the control variables obtained from the constant power test. The results showed that the solutions obtained using an approach without proper load modeling breached technical limits when applied to the grid. Furthermore, the solution obtained from the constant power test not only exceeded operational constraints, but also presented higher OF.

Finally, in order to evaluate the precision of the proposed formulation, all the decision variables of the solution found by the methodology (i.e., the power delivered by each dispatchable DG unit ($P^G_{n,t}$), the number of modules connected in each CB ($B_{n,t}$), the tap position for each VR ($tp_{mn,f,t}$), the charging schedule for each EV ($y_{n,t}$), and the charging and discharging schedule for each ESS (P^{SD+}_u and P^{SD-}_u, respectively)) in

Case IV were used to solve a conventional AC power flow. Thereby, for the OF, the error found by comparing the MILP formulation and the conventional power flow was 0.023%. Moreover, the voltage magnitude error percentage obtained for all nodes at the time intervals with the highest conventional load and EV demand (hours 18:00 and 01:00, respectively), are presented in Fig. 33. It is worth noting that this error percentage does not exceed 0.005% at 18:00 hours and 0.06% at 01:00 hours. Hence, these results validate the presented MILP formulation as an accurate approximation of the EDN steady-state operation.

Figure 33 – Voltage magnitude error percentage.

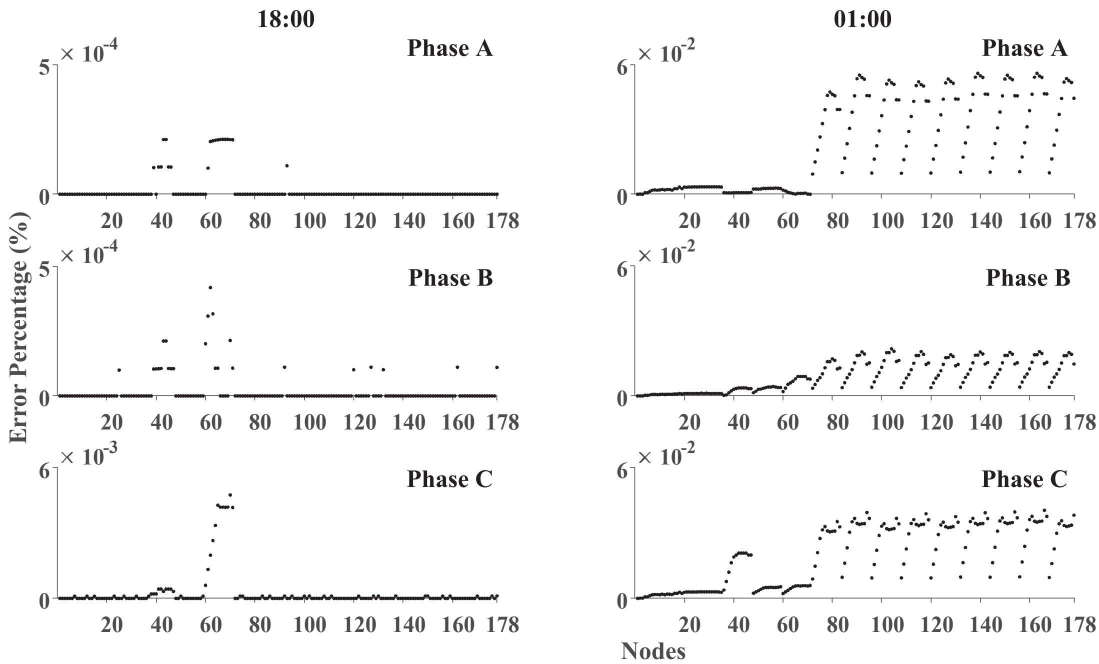

Source: Created by the author.

4.4 CHAPTER CONCLUSIONS

A new methodology based on a mixed-integer linear programming model for the electric vehicle charging coordination (EVCC) problem considering Volt VAr control (VVC), energy storage device (ESS) operation, and dispatchable distributed generation (DG) units in a three-phase unbalanced electrical distribution network (EDN), taking into account a voltage dependent load model, was presented. The proposed formulation was tested on an EDN with 34 medium–voltage nodes and 144 low–voltage nodes. The results showed that the optimized operation of the DG, ESS, VVC devices, and EV recharge represented an overall energy cost reduction and guaranteed the avoidance of technical limit violations.

The dynamic coordination was proved to be efficient, because it defines the step to be implemented and gives a broad view of the EDN state throughout the whole time period. Moreover, this methodology handles the randomness in the electric vehicle (EV) arrival and departure times, initial state of charge, battery sizes, and forecast errors.

The presented results highlight the importance of the proposed methodology, which encompasses the optimal control of the aforementioned devices. Besides, they foreground how the ESSs help in the avoidance of energy curtailment in EV recharging and how the VVC scheme becomes more suitable in order to avoid voltage limit violations in the EDN.

5 PV UNITS AND EVs IN RESIDENTIAL NETWORKS

The growing penetration of low–carbon technologies in residential networks such as photovoltaic generation (PV) units and electric vehicles (EVs) may cause technical issues on the grid. Thus, operation planning of electrical distribution networks (EDNs) should consider the inclusion of these technologies in order to avoid operational limit breaches. This chapter proposes a dynamic scheduling method for an optimal operation of PV units and EVs in unbalanced residential EDNs, considering energy storage systems (ESSs). The proposed method optimizes the joint operation of PV units and EVs, using ESSs to increase the local consumption of the renewable energy. A rolling multi–period strategy based on a mixed integer linear programming model is used to dynamically optimize a centralized decision making, determining control actions for on-load tap changers (OLTCs), ESSs, PV units, and EVs connected to the network. At each time interval, data for PV generation and EV demand is updated using actual information and historical profiles, generating an updated forecast for a one-day-ahead operation in order to properly cope with weather uncertainties and EV owner's behavior without the need of multiple scenarios. The effectiveness and robustness of this approach are verified in different cases via a 107–node test EDN.

5.1 INTRODUCTION

Low carbon technologies such as renewable DG and EVs are rapidly growing in the EDNs as a response to latter-day challenges related to world's energy consumption growth and CO2 emissions mitigation (I.E.A. INTERNATIONAL ENERGY AGENCY, 2012; U.S. DEPARTMENT OF ENERGY, 2013). In this regards, techno-economic improvements in the solar PV industry have surpassed previous expectations leading to considerable cost reductions, making the PV option stand out among other renewable energy alternatives (EUROPEAN COMMISSION, 2014). On the other hand, the use of EVs in the transport sector is expected to increase in the upcoming years which will reduce greenhouse emissions (CLEMENT-NYNS; HAESEN; DRIESEN, 2010; EUROPEAN COMMISSION, 2014). Hence, the distribution network operator will require smart control methods in order to successfully adopt these technologies.

Many studies have addressed the impacts of DG units on the EDN operation: Voltage profiles, energy losses, restoration actions, and network reinforcements, among others, are directly affected by DG inclusion. Thus, the corresponding economic and technical issues must be assessed to ensure high–quality service for each consumer (QUEZADA; ABBAD; ROMAN, 2006). PV generation, like any renewable energy source, has specific implications that have to be addressed to guarantee proper network operation. Voltage rise and increase of energy losses are some of the most common problems that appear as a result of high penetration of PV units on the EDNs (TANT et al., 2013; THOMSON; INFIELD, 2007). In order to prevent these issues, different active power control techniques aiming to avoid excessive PV power injection have been studied (TONKOSKI; LOPES; EL-FOULY, 2011; WECKX; GONZALEZ; DRIESEN, 2014).

The penetration of EVs is expected to rise in residential EDNs (CLEMENT-NYNS; HAESEN; DRIESEN, 2010). EVs recharge their batteries from the grid, i.e., they use electrical energy instead of fossil fuel. The uncontrolled charging of these batteries in a scenario with high EV penetration may cause the EDN to experience overloads, voltage limit violations, and/or excessive increase in energy losses (LIN et al., 2010; WU; ALIPRANTIS; GKRITZA, 2011). Furthermore, EV charging coordination (EVCC) has been proven to represent significant savings due to energy loss reduction and network reinforcement deferral (VERZIJLBERGH et al., 2012). Several techniques have been proposed to solve the EVCC problem (FRANCO; RIDER; ROMERO, 2015; O'CONNELL; KEANE; FLYNN, 2014; QUIRóS-TORTóS et al., 2016; SHAABAN et al., 2014; TRIPPE; MASSIER; HAMACHER, 2013). Mathematical programming formulations for charging cost reduction are presented in (FRANCO; RIDER; ROMERO, 2015; O'CONNELL; KEANE; FLYNN, 2014; TRIPPE; MASSIER; HAMACHER, 2013). In addition, a two-stage optimization process, which uses a prediction unit for the EV demand, is developed in (SHAABAN et al., 2014) to ensure effective EV charging coordination while aiming overall cost reduction. Finally in (QUIRóS-TORTóS et al., 2016), a centralized control algorithm, based on corrective and preventive approaches, is proposed to mitigate technical problems related to the connection/disconnection of EV charging points.

High penetration of both PV units and EVs in the EDN might challenge its operation due to large non-coincident renewable generation and demand. In this context, energy storage systems (ESSs) have emerged to conciliate time-difference between excessive generation and peak demand (ELNOZAHY; ABDEL-GALIL; SALAMA, 2015). Different approaches have been developed to effectively integrate the ESSs into the grid (ATZENI et al., 2013; ELNOZAHY; ABDEL-GALIL; SALAMA, 2015; MACEDO et al., 2015). A probabilistic method is proposed in (ELNOZAHY; ABDEL-GALIL; SALAMA, 2015) to maximize the benefits related to ESS allocation in residential EDNs; furthermore, it is also established that ESSs must be installed downstream of each distribution transformer to alleviate overloading due to excessive PV generation and EV demand peak. A demand-side management approach using a day-ahead optimization process for the scheduling of both ESSs and DG units is developed in (ATZENI et al., 2013); nevertheless, the economic and operational constraints of the EDN are disregarded. A control scheme based on a mathematical programming model, which considers ESSs and renewable DG units connected in medium voltage networks, is presented in (MACEDO et al., 2015); however, this method is based on a single-phase formulation that does not consider dynamic control.

This work proposes a dynamic scheduling method for the joint optimal operation of EVs and PV units in unbalanced residential EDNs with ESSs. The adopted optimization strategy allows a dynamic centralized decision–making, which takes into account an updated forecast for both EV demand and PV generation. Thereby, uncertainties related to weather conditions and EV owner's behavior are considered, avoiding the complexity associated with a decision–making based on a large set of scenarios. The proposed method makes it possible to find an optimal scheduling for the on-load tap changer (OLTC), PV units, EV charging, and ESS charging/discharging, not only mitigating technical issues associated with high PV generation and peak demand, but also encouraging the local consumption of the renewable energy produced by the PV units connected to residential EDNs.

Although there is a fair share of researches tackling problems related to the EDN operation, to the best of the authors' knowledge, there is no approach considering an online control for PV units and EVs, using ESSs, that takes into account low voltage (LV), medium voltage (MV), transformers constraints, and the substation OLTC in unbalanced residential EDNs. Supporting this statement, Table 11 shows a summary of works related to this topic. The main characteristics of those approaches were described, while the differences with the proposed method were highlighted.

The main contribution of this work is an online control method for the joint optimal operation of EVs and PV units in unbalanced residential EDNs, which considers ESSs and OLTCs to enforce the grid operational limits (e.g., voltage and thermal limits) through a dynamic scheduling based on an optimal power flow. This can be apportioned into: 1) the adoption of a rolling multi-period optimization strategy (which has been utilized in other applications within the EDN (O'CONNELL; KEANE; FLYNN, 2014; SHAABAN et al., 2014)) for the joint optimal operation of EVs and PV units, embedded in the concept of high resolution and accuracy in the problem formulation for the near-term modelling; 2) a Mixed Integer Linear Programming (MILP) formulation that considers the EDN complexity of unbalance, multiple voltage levels, the service transformers, and low voltage networks (features typically disregarded in aforementioned approaches for this matter (AREFIFAR; ORDONEZ; MOHAMED, 2017; GAO et al., 2014; WANG et al., 2015)); and 3) a novel centralized control method for the operation of the EDN which guarantees the fulfillment of technical limits in MV and LV networks, controlling OLTCs, ESSs, EVs and PV units.

Table 11 – Literature review summary

Reference	Uncontrolled	Controlled	Controlled	Uncontrolled	Controlled	Imbalance	MV	LV	Voltage	Thermal	Centralized	Decentralized	Real-time
	PVs		ESS	EVs		EDN	Grid		Limits		Control		
(CLEMENT-NYNS; HAESEN; DRIESEN, 2010)					x	x		x	x		x		
(THOMSON; INFIELD, 2007)		x	x			x		x	x				
(FRANCO; RIDER; ROMERO, 2015)					x	x	x	x	x	x	x		
(O'CONNELL; KEANE; FLYNN, 2014)					x	x		x	x	x	x		x
(SHAABAN et al., 2014)		x			x		x		x		x		x
(QUIRóS-TORTóS et al., 2016)					x	x		x	x		x		x
(ELNOZAHY; ABDEL-GALIL; SALAMA, 2015)	x		x	x			x	x	x	x	x		
(MACEDO et al., 2015)	x		x				x		x	x	x		
(GAO et al., 2014)					x						x		x
(WANG et al., 2015)	x				x		x		x	x	x		x
(AREFIFAR; ORDONEZ; MOHAMED, 2017)	x		x		x		x				x		
(APPEN et al., 2014)		x	x									x	x
(ANTUNEZ et al., 2016b)					x	x	x		x	x	x		x
(BADAWY; SOZER, 2017)	x		x	x								x	x
(WEI et al., 2017)	x		x									x	x
(LIU et al., 2015)	x				x						x		x
(ALAM, 2013)		x		x							x		x
(SCHURMANN; TIMPNER; WOLF, 2017)					x						x		x
(ALAM; MUTTAQI; SUTANTO, 2016)	x				x			x	x			x	x
(MARRA et al., 2013)	x				x			x	x			x	x
(WECKX; DRIESEN, 2015)		x			x	x		x			x	x	x
(AKHAVAN-REZAI et al., 2017)	x				x	x	x		x	x	x		x
(CHENG; CHANG; HUANG, 2015)	x				x		x		x	x	x	x	x
(GUNTER; AFRIDI; PERREAULT, 2013)	x		x		x								
(YANG et al., 2017)	x		x		x							x	x
(RIFFONNEAU et al., 2011)	x		x									x	
(PEREZ et al., 2013)	x		x									x	x
(YAO et al., 2015)	x		x								x		
(TELEKE et al., 2010)	x		x									x	
(MOKHTARI; NOURBAKHSH; GHOSH, 2013)	x		x				x		x	x	x	x	x
(AKHTAR et al., 2017)	x		x	x				x	x			x	x
Proposed approach													
		x	x		x	x	x	x	x	x	x		x

Source: Created by the author.

5.2 DYNAMIC SCHEDULING METHOD

This section describes the method proposed to dynamically control EDNs with high penetration of PV units and EVs. Considerations and descriptions in regard to the EDN and the aforementioned devices will also be addressed.

The control method is based on an optimization problem that determines the optimal operation of the OLTC, ESSs, PV units and EV charging schedule. These optimal settings are defined considering a one-day ahead operation (divided into time intervals) and a rolling multi-period optimization strategy, as shown in Fig. 34. The optimization algorithm requires forecast profiles for the available PV generation and EV demand along the one-day ahead period. The creation of these forecast profiles will be further detailed later in this section.

The solution of the optimization problem (MILP model) will define, for the considered time period, the OLTC tap positions, the optimal charging/discharging schedule for the ESSs, the power exchange between the PV units and the grid, and the optimal charging schedule for the EVs. These control actions are mathematically represented through integer variables.

At each time step of the rolling multi-period optimization process (t_1, t_2, t_3, ...), the corresponding optimization problem is solved considering a one–day–ahead period, as shown in Fig. 35. This time horizon makes it possible to define an optimal charging/discharging schedule for the ESSs taking into account forecasted PV generation and EV demand. Therefore, the operation of the devices connected to the grid is optimized, as dynamic schedules for EVs and ESSs are constructed.

Due to the integer nature of the variables involved in this multi-period process, a high computational effort is required. In order to reduce the processing time, the time period is divided into 25 time intervals with a duration of 15 minutes for the first one (current time) and one–hour for the remaining 24. Furthermore, considering that only the settings of the current time interval will be implemented, the integer nature of the control variables is disregarded for all time intervals but the first one, i.e., it is assumed that they are continuous. These approximations reduce the complexity of the optimization model without compromising the quality of the solution.

Figure 34 – Rolling multi-period optimization flow chart.

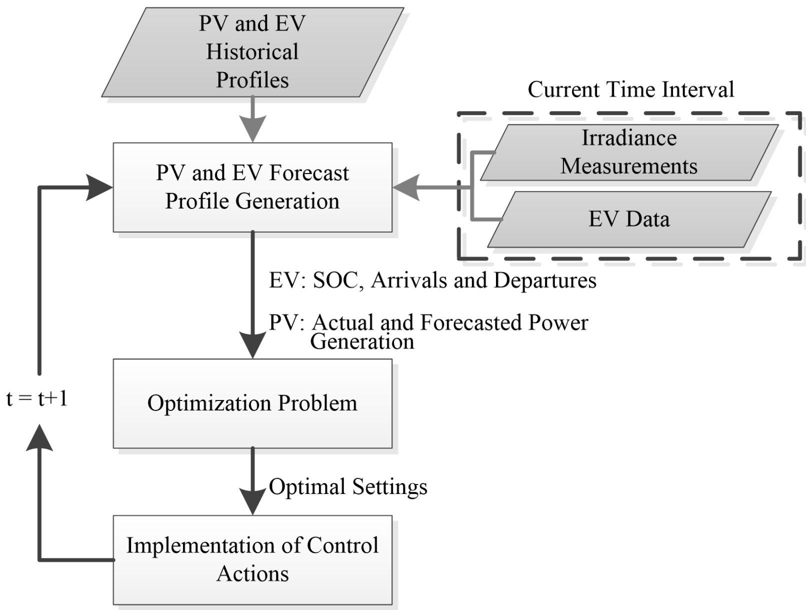

Source: Created by the author.

The proposed method models a residential feeder with medium voltage (MV) and low voltage (LV) nodes, including an OLTC at the substation (i.e., at the beginning of the feeder), MV/LV transformers, ESSs installed downstream from the MV/LV transformers, single-phase PV units, and single-phase EV charging points at the households. In addition, the proposed control scheme takes advantage of communication infrastructure offered

Figure 35 – Time intervals considered at each step of the optimization.

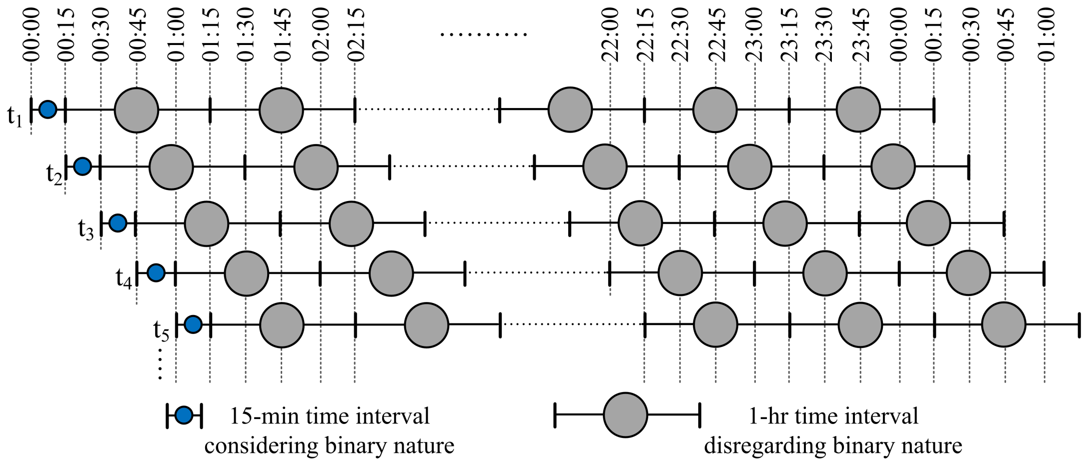

Source: Created by the author.

by future smart residential grids in order to implement the defined control actions (SCHAUDER, 2016), (SOJOUDI; LOW, 2011).

High PV generation may cause an energy surplus in the EDN. This energy surplus can be exported to the main grid (WANG et al., 2016). In this energy trade-off, the selling price is usually smaller than the buying price in order to encourage the self-consumption of the locally produced PV power (APPEN et al., 2014).

In order to determine the control actions to be executed by the controlled devices, several considerations must be adopted, which are explained as follows.

5.2.1 PV Power Generation

For each PV unit, the algorithm will identify at every time interval the maximum active power that it may inject into the grid without causing operational issues. If in a given time, a PV unit is able to generate more power than the aforementioned limit, that difference will be considered as a power curtailment. It is assumed that all PV units are connected to the low-voltage network, operate with unity power factor, and their power output is controlled by smart power inverters (SCHAUDER, 2016). Furthermore, the PV penetration is defined as the percentage of LV customers with a PV unit connected to the grid (the same definition is used for EV penetration).

The decision–making requires a one–day–ahead PV generation forecast, which can be obtained using historical information and the forecasted weather condition. Several PV generation profiles, classified by a Clearness Index (CI), might be used. The CI represents the concentration of intercepting agents that reduce the amount of radiation over the panel (DUSABE; MUNDA; JIMOH, 2009); therefore, it can be used to calculate the net radiation in terms of the total radiation at clear sky and, consequently, the corresponding PV generation. Typical one–day–long PV generation profiles were divided into the following CI classifications: Clear day ($CI_{avg} \geq 65\%$), cloudy day ($45\% \leq CI_{avg} \leq 65\%$), and dark day ($CI_{avg} \leq 45\%$). These profiles were obtained using the PV simulation tool presented in (RICHARDSON; THOMSON, 2011).

The PV power generation forecast is built using historical data that considers an estimation for the CI average along the current day (e.g., clear, cloudy, or dark). This forecast is used for all the time intervals but the first one, for which the higher value between the forecast and the average PV generation over the last minutes is used. It is important to remark that for the first time interval, the constructed forecast does not aim to precisely predict weather conditions but to anticipate any issue related to high PV generation. The adopted approach for the PV forecast, along with the rolling multi–period optimization strategy, permits to find solutions that cope with the uncertain behavior of the PV generation.

5.2.2 EV Battery Charging

The control method will determine the charging schedule for each EV, i.e., it will define its status (charging/idle) for every time interval. For this charging schedule (solution to the EVCC problem), it is assumed that the initial State of Charge (SOC) of every vehicle is known when it is plugged into the grid and the batteries can be controlled in each time interval. Moreover, each EV user may provide a departure time when its vehicle is plugged in; otherwise, it will be assumed that the EV will remain plugged in until a probable time determined by the EV historical departure time.

The EVs may arrive and depart in any time interval of the time period. Therefore, the charging agenda will be generated between arrival and departure, ideally dispatching fully charged batteries. If an EV does not depart with a completely charged battery, the related unserved energy will be considered as a curtailment on the EV battery. Furthermore, the parameters (SOC, arrival and departure times) of already connected EVs are known; in addition, the control method uses a forecast to take into account EVs that might be plugged into the grid in future time intervals. Thus, to account for the random behavior of EV owners, several techniques can be applied to forecast initial SOC, arrival, and departure times (MELO; CARRENO; PADILHA-FELTRIN, 2014; QUIRóS-TORTóS; OCHOA; LEES, 2015). The forecast used in this work is based on the probability distribution functions shown in (QUIRóS-TORTóS; OCHOA; LEES, 2015).

In order to model the energy transference between an EV battery and the grid, a binary variable is used to represent the EV battery state (charging/idle). This variable ($y_{e,t}$) has a value of 1, if at time interval t the EV e is charging at its maximum power P_e^{EV}, and a value of 0, if EV e remains idle.

5.2.3 Energy Storage Management

Similar with the EVs, the control method will construct a charging schedule for the ESSs, determining their state at every time interval, i.e., if they will charge, discharge, or remain idle. It is assumed that the ESSs are owned by the EDN utility and can be controlled through communication devices in order to define their charging states. The ESS state of charge should be always maintained over its specified Depth of Discharge (DoD). In order to model the power injected into the grid by an ESS, a continuous variable $P^{SD}_{u,t}$ represents the amount of power injected by ESS u at time interval t. This variable is limited by the maximum ESS active power ($\bar{P}^{SD}_{u}$).

5.3 MATHEMATICAL FORMULATION OF THE OPTIMIZATION PROBLEM

The method presented in Section 5.2 defines a dynamic coordination of the devices connected to the smart grid by solving an optimization problem. In this section, a mixed integer nonlinear programming (MINLP) model for this optimization problem is proposed. Due to the complexity of the MINLP model (i.e., nonconvex nature), an easier–to–solve MILP formulation is then developed. The convexity of the MILP model makes it possible to use efficient classical optimization techniques, which guarantee finding the optimal solution. The steady state operation of an unbalanced EDN is represented through a three phase formulation (FRANCO; RIDER; ROMERO, 2015), which takes into account the coupling between phases as well as the unbalance of loads and PV units.

The proposed formulations consider the sets EV, F, L, N, PV, SD, and T to represent electric vehicles, phases, circuits, nodes, PV units, ESSs, and time intervals, respectively, while $TR \subseteq N$ represents the set of nodes where a transformer is installed. Furthermore, $V^{re/im}_{n,f,t}$ are the real/imaginary parts of the voltage at node n, phase f and time interval t, while $I^{Gre/im}_{n,f,t}$ and $I^{Dre/im}_{n,f,t}$ are the real/imaginary parts of the generated and demanded currents. $P^{G/D}_{n,f,t}$ and $Q^{G/D}_{n,f,t}$ are the generated/demanded active and reactive powers. In addition, $I^{re/im}_{mn,f,t}$ represents the real/imaginary parts of the current through the circuit connecting nodes m and n, while $B_{mn,f}$ is its the shunt susceptance for phase f. The real/imaginary parts of the currents corresponding to the PV unit h, ESS u and EV e are defined as $I^{PVre/im}_{h,t}$, $I^{SDre/im}_{u,t}$, and $I^{EVre/im}_{e,t}$, respectively. Finally, $R_{mn,f,h}$ and $X_{mn,f,h}$ are the resistance and reactance for circuit mn between phases f and h.

In order to obtain an MILP model, linearization techniques (e.g., Taylor's approximation, linear constraints limiting the feasible region, and piecewise linearization) and some approximations are applied to all nonlinear expressions from the MINLP formulation. This transformation enables the utilization of classic optimization methods and commercial solvers, ensuring optimality in the solution found for the MILP model. In this sense, consider the superscript $^{re^*/im^*}$ in any voltage as the real/imaginary value of the voltage operation point; replacing the actual voltage variable, this approximation is applied to several equations in order to avoid nonlinearities.

The mathematical problem (MILP model) optimizes an objective fuction, while keeping the state variables (EDN's real and imaginary parts of voltages and currents) in values such that the operational limits are satisfied, determining optimal values for the control variables of the devices connected to the grid. In this context, the control variables for the MILP model are: the maximum active power injection allowed for each PV unit; the charging status (charging/idle) for each EV; the active power interaction (injected/drawn) for each ESS; and the tap position for the OLTC.

5.3.1 Objective Function

The optimization problem aims to minimize the overall costs related to energy generation and curtailments on the controlled devices, as well as to encourage the local consumption of renewable energy provided by the PV units, as shown in (269),

$$min\ CIE - CEE + CEPV + PenPV + PenEV \tag{269}$$

where:

$$CIE = \sum_{t \in T} \sum_{f \in F} \alpha^{B}_{S,t} P^{G+}_{S,f,t} \Delta_t$$

$$CEE = \sum_{t \in T} \sum_{f \in F} \alpha^{S}_{S,t} P^{G-}_{S,f,t} \Delta_t$$

$$CEPV = \sum_{t \in T} \sum_{h \in PV} \alpha^{PV}_{h,t} P^{PVin}_{h,t} \Delta_t$$

$$PenPV = \sum_{t \in T} \sum_{h \in PV} \zeta^{PV} PV^{curt}_{h,t} \Delta_t$$

$$PenEV = \sum_{e \in EV} \zeta^{EV} E^{EVcurt}_{e}$$

Here, the non-negative variables $P^{G+}_{S,f,t}$, $P^{G-}_{S,f,t}$ are the importing and exporting active powers at the substation (node S) at time interval t, which has a duration equal to Δ_t. Moreover, $\alpha^{B}_{S,t}$ and $\alpha^{S}_{S,t}$ are the buying and selling energy prices at the substation, while the price of the energy generated and the power injection of the PV unit h are represented by $\alpha^{PV}_{h,t}$ and $P^{PVin}_{h,t}$. Finally, ζ^{PV}, and ζ^{EV}, are penalizations for curtailments associated to PV units and EVs, which in turn are represented by $PV^{curt}_{h,t}$, and E^{EVcurt}_{e}.

5.3.2 Steady State Operation Constraints

The set of equations (270)–(276) models the steady state operation of an unbalanced EDN. The application of the first Kirchhoff's Law for the real and imaginary parts of the currents is represented by (270) and (271), respectively. Equation (272) determines the direction of the power flow at the substation (i.e., if the grid operator is selling or buying from/to the main grid). Constraints (273) and (274) define the demanded currents (related to conventional loads), while (275) and (276) represent the voltage drop on the circuits,

$$I^{Gre}_{m,f,t} + \sum_{h\in PV} I^{PVre}_{h,t}\gamma_{h,m,f} + \sum_{km\in L} I^{re}_{km,f,t} - \sum_{mn\in L} I^{re}_{mn,f,t} - \left(\sum_{km\in L} B_{km,f} + \sum_{mn\in L} B_{mn,f}\right)\frac{V^{im}_{m,f,t}}{2} =$$
$$I^{Dre}_{m,f,t} + \sum_{e\in\Xi} I^{EVre}_{e,t}\gamma_{e,m,f} + \sum_{u\in SD} I^{SDre}_{u,t}\gamma_{u,m,f} \tag{270}$$

$$I^{Gim}_{m,f,t} + \sum_{h\in PV} I^{PVim}_{h,t}\gamma_{h,m,f} + \sum_{km\in L} I^{im}_{km,f,t} - \sum_{mn\in L} I^{im}_{mn,f,t} - \left(\sum_{km\in L} B_{km,f} + \sum_{mn\in L} B_{mn,f}\right)\frac{V^{re}_{m,f,t}}{2} =$$
$$I^{Dim}_{m,f,t} + \sum_{e\in\Xi} I^{EVim}_{e,t}\gamma_{e,m,f} + \sum_{u\in SD} I^{SDim}_{u,t}\gamma_{u,m,f} \tag{271}$$

$$P^{G+}_{S,f,t} - P^{G-}_{S,f,t} = V^{re^*}_{S,f,t} I^{Gre}_{S,f,t} + V^{im^*}_{S,f,t} I^{Gim}_{S,f,t} \tag{272}$$
$$I^{Dre}_{n,f,t} = (P^D_{n,f,t}V^{re}_{n,f,t} + Q^D_{n,f,t}V^{im}_{n,f,t})/({V^{re}_{n,f,t}}^2 + {V^{im}_{n,f,t}}^2) \tag{273}$$
$$I^{Dim}_{n,f,t} = (P^D_{n,f,t}V^{im}_{n,f,t} - Q^D_{n,f,t}V^{re}_{n,f,t})/({V^{re}_{n,f,t}}^2 + {V^{im}_{n,f,t}}^2) \tag{274}$$
$$V^{re}_{m,f,t} - V^{re}_{n,f,t} = \sum_{h\in F}(R_{mn,f,h}I^{re}_{mn,h,t} - X_{mn,f,h}I^{im}_{mn,h,t}) \tag{275}$$
$$V^{im}_{m,f,t} - V^{im}_{n,f,t} = \sum_{h\in F}(X_{mn,f,h}I^{re}_{mn,h,t} + R_{mn,f,h}I^{im}_{mn,h,t}) \tag{276}$$
$$\forall mn \in L, \forall n \in N, f \in F, t \in T$$

where $\gamma_{x,m,f}$ is a binary parameter that takes a value of 1 if the device x is connected at node m and phase f.

Note that (273) and (274) are nonlinear functions; therefore, consider $g(P^D_{n,f,t}, Q^D_{n,f,t}, V^{re}_{n,f,t}, V^{im}_{n,f,t})$ and $h(P^D_{n,f,t}, Q^D_{n,f,t}, V^{re}_{n,f,t}, V^{im}_{n,f,t})$ as the right part of (273) and (274), respectively. Hence, (277) and (278) show the first-order Taylor's approximation around an estimated operation point $(V^{re^*}_{n,f,t}, V^{im^*}_{n,f,t})$ for (273) and (274), respectively.

$$I^{Dre}_{n,f,t} = g^* + \left.\frac{\partial g}{\partial V^{re}}\right|^* (V^{re}_{n,f,t} - V^{re^*}_{n,f,t}) + \left.\frac{\partial g}{\partial V^{im}}\right|^* (V^{im}_{n,f,t} - V^{im^*}_{n,f,t}) \tag{277}$$
$$I^{Dim}_{n,f,t} = h^* + \left.\frac{\partial h}{\partial V^{re}}\right|^* (V^{re}_{n,f,t} - V^{re^*}_{n,f,t}) + \left.\frac{\partial h}{\partial V^{im}}\right|^* (V^{im}_{n,f,t} - V^{im^*}_{n,f,t}) \tag{278}$$

5.3.3 EDN operational limits

Equations (279)–(283) represent the technical limits that must be fulfilled in the EDN in order to provide high–quality service to the consumer. Here, (279) and (280) define the voltage and current magnitude limits, respectively. Equations (281) and (282) calculate, for transformer $\wp$ at time interval t, the active ($P^{TR}_{\wp,t}$) and reactive ($Q^{TR}_{\wp,t}$) powers in terms of the real and imaginary voltages ($V^{re/im}_{\wp,f,t}$) and currents ($I^{re/im}_{\wp,f,t}$) at the secondary windings. Equation (283) represents the apparent power limit for each transformer,

$$\underline{V_n}^2 \leq {V^{re}_{n,f,t}}^2 + {V^{im}_{n,f,t}}^2 \leq \overline{V_n}^2 \tag{279}$$

$$f(I^{re}_{mn,f,t}, \bar{I}_{mn}, \Lambda) + f(I^{im}_{mn,f,t}, \bar{I}_{mn}, \Lambda) \leq \bar{I}^2_{mn} \tag{280}$$

$$P^{TR}_{\wp,t} = \sum_{f \in F} V^{re*}_{\wp,f,t} I^{re}_{\wp,f,t} + V^{im*}_{\wp,f,t} I^{im}_{\wp,f,t} \tag{281}$$

$$Q^{TR}_{\wp,t} = \sum_{f \in F} -V^{re*}_{\wp,f,t} I^{im}_{\wp,f,t} + V^{im*}_{\wp,f,t} I^{re}_{\wp,f,t} \tag{282}$$

$$f(P^{TR}_{\wp,t}, \overline{S^{TR}_{\wp,t}}, \Lambda) + f(Q^{TR}_{\wp,t}, \overline{S^{TR}_{\wp,t}}, \Lambda) \leq \overline{S^{TR}_{\wp,t}}^2 \tag{283}$$

$$\forall \wp \in TR, \forall mn \in L, \forall n \in N, f \in F, t \in T$$

where $\underline{V_n}$ and $\overline{V_n}$ are the upper and lower voltage limits for node n, respectively; $\bar{I}_{mn}$ is the current limit through circuit mn; and, $\overline{S^{TR}_{\wp,t}}^2$ is the maximum apparent power for transformer $\wp$.

Equations (284) and (285) are linear approximations for the upper and lower voltage limits presented in (279), improving the approximation shown in (FRANCO; RIDER; ROMERO, 2015). Constraint (284) represents a set of $2 * \ell$ line segments that approximate the upper voltage limit. Where, $\varphi^+_{n,f,i} = \theta^*_{n,f} + \ell_i \phi$; $\varphi^-_{n,f,i} = \theta^*_{n,f} + (\ell_i - 1)\,\phi$; $\theta^*_{n,f}$ is the operation angle for bus n in phase f; ℓ_i is the i-element from the set of line segments; and ϕ is the angle of the arc corresponding to each line segment. Likewise, (285) approximates the lower voltage limit. Where, $\varphi^{o+}_{n,f,i} = \theta^*_{n,f} + \phi$; and $\varphi^{o-}_{n,f,i} = \theta^*_{n,f} - \phi$.

$$V^{im}_{n,f,t} \leq \frac{\sin(\varphi^+_{n,f,i}) - \sin(\varphi^-_{n,f,i})}{\cos(\varphi^+_{n,f,i}) - \cos(\varphi^-_{n,f,i})} \left[V^{re}_{n,f,t} - \bar{V}\cos(\varphi^-_{n,f,i})\right] + \bar{V}\sin(\varphi^-_{n,f,i}) \tag{284}$$

$$V^{im}_{n,f,t} \leq \frac{\sin(\varphi^{o+}_{n,f}) - \sin(\varphi^{o-}_{n,f})}{\cos(\varphi^{o+}_{n,f}) - \cos(\varphi^{o-}_{n,f})} \left[V^{re}_{n,f,t} - \underline{V}\cos(\varphi^{o+}_{n,f})\right] + \underline{V}\sin(\varphi^{o+}_{n,f}) \tag{285}$$

$$\forall i \in -\ell ... \ell, n \in N, f \in F, t \in T$$

Finally, the nonlinear expressions (280) and (283) are linearized as shown in the Section 2.11.

5.3.4 PV Unit Constraints

The operation of the PV units is defined by (286)–(288). The active and reactive powers of the PV unit h in time interval t are represented in terms of its voltage and currents and are shown in (286) and (287), while (288) calculates the power curtailment ($PV_{h,t}^{cut}$) in terms of the available PV generation ($P_{h,t}^{PV}$) and the actual power injection ($P_{h,t}^{PVin}$).

$$P_{h,t}^{PVin} = V_{h,t}^{re^*} I_{h,t}^{PVre} + V_{h,t}^{im^*} I_{h,t}^{PVim} \tag{286}$$

$$0 = -V_{h,t}^{re^*} I_{h,t}^{PVim} + V_{h,t}^{im^*} I_{h,t}^{PVre} \tag{287}$$

$$P_{h,t}^{PVcut} = P_{h,t}^{PV} - P_{h,t}^{PVin} \qquad \forall h \in PV, t \in T \tag{288}$$

5.3.5 EV Constraints

Equations (289) and (290) represent the active and reactive powers demanded by the EV charging points; they are written in terms of the maximum charging power (P_e^{EV}) and the status ($y_{e,t}$) of the EV charging point. Furthermore, (291) determines the energy curtailment on each EV (E_e^{EVcurt}), taking into account the allowable maximum SOC ($\bar{E}_e^{EV}$), while (292) calculates the corresponding energy at departure (E_e^{EV}) in terms of the initial SOC (E_e^{ini}), P_e^{EV}, and the charging point efficiency (η_e).

$$P_e^{EV} y_{e,t} = V_{e,t}^{re^*} I_{e,t}^{EVre} + V_{e,t}^{im^*} I_{e,t}^{EVim} \tag{289}$$

$$0 = -V_{e,t}^{re^*} I_{e,t}^{EVim} + V_{e,t}^{im^*} I_{e,t}^{EVre} \tag{290}$$

$$\bar{E}_e^{EV} = E_e^{EV} + E_e^{EVcurt} \tag{291}$$

$$E_e^{EV} = E_e^{ini} + \sum_{t \in T} \Delta_t P_e^{EV} y_{e,t} \eta_e \qquad \forall e \in \Xi, t \in T \tag{292}$$

5.3.6 ESS Constraints

Equations (293) and (294) represent the active and reactive power demanded or injected by each ESS from/to the grid. In order to model the ESS instant power at each time interval ($P_{u,t}^{SD}$), two non-negative variables that represent the ESS charging and discharging powers (P_u^{SD+} and P_u^{SD-}, respectively) are used, as shown in (295). Furthermore, (296) defines the energy stored on each ESS at each time interval ($E_{u,t}^{SD}$) in terms of the ESS initial SOC (E_u^{SDi}) and the energy charged on previous time intervals. Constraint (297) maintains this energy level between the storage system maximum capacity ($\bar{E}_u^{SD}$) and the pre-established DoD. Finally, (298) defines the limits for the ESS charging and discharging powers.

$$P_{u,t}^{SD} = V_{u,t}^{re^*} I_{u,t}^{SDre} + V_{u,t}^{im^*} I_{u,t}^{SDim} \tag{293}$$

$$0 = -V_{u,t}^{re^*} I_{u,t}^{SDim} + V_{u,t}^{im^*} I_{u,t}^{SDre} \tag{294}$$

$$P_{u,t}^{SD} = P_u^{SD+} - P_u^{SD-} \tag{295}$$
$$E_{u,t}^{SD} = E_u^{SDi} + \sum_{k \in T, k \leq t} \Delta_k P_{u,k}^{SD} \tag{296}$$
$$\bar{E}_u^{SD} DoD \leq E_{u,t}^{SD} \leq \bar{E}_u^{SD} \tag{297}$$
$$0 \leq P_u^{SD+}, P_u^{SD-} \leq \bar{P}_u^{SD} \qquad \forall u \in SD, f \in F, t \in T \tag{298}$$

5.3.7 OLTC Constraints

The OLTC at the beginning of the feeder is modeled in (299) and (300). These constraints represent the real and imaginary parts of the regulated voltage at the secondary windings of the transformer ($V_{S,f,t}^{re}$ and $V_{S,f,t}^{im}$, respectively) in terms of the voltage at the primary windings ($\hat{V}_{f,t}^{re/im}$), the nominal transformation ratio (a_S^{ratio}), the regulation percentage of the OLTC ($\%R_{oltc}$), and an integer variable limited between 0 and the maximum tap ($\tau_t \in \{0, \bar{\tau}\}$) which models the OLTC tap position.

$$V_{S,f,t}^{re} = (1 - \%R_{oltc} + \tau_t \frac{\%R_{oltc}}{\bar{\tau}}) \hat{V}_{f,t}^{re} a_S^{ratio} \tag{299}$$
$$V_{S,f,t}^{im} = (1 - \%R_{oltc} + \tau_t \frac{\%R_{oltc}}{\bar{\tau}}) \hat{V}_{f,t}^{im} a_S^{ratio} \qquad \forall f \in F, t \in T \tag{300}$$

5.3.8 MILP Formulation

In consequence, the complete MILP formulation is given by:

min (269)

Subject to: (270)–(272), (275)–(278), and (280)–(300).

5.4 CASE STUDY

The effectiveness of the proposed method was studied considering different test cases in a 107–node EDN. The operation of the EDN in each time interval, after the definition of the control variables by the dynamic scheduling method, was assessed using a conventional power flow. For all test cases, a one–day–long time period was evaluated from 8 a.m. to 8 a.m. of the following day.

The rolling multi-period method was written in the mathematical language AMPL (FOURER; GAY; KERNIGHAN, 2003) and the MILP model was solved using CPLEX (ILOG INC., 2009). The time limit for the solution process in each interval was 120s.

5.4.1 Test system

The 107–node test system (an extension of the IEEE 13-node test feeder), used to study the efficiency of the proposed method, has 11 medium-voltage nodes and 96 low-voltage nodes. The topology of the EDN for both MV and LV networks is shown in Fig. 36. Moreover, the EDN complete description per feeder is available on (DISTRIBUTION. . . , 2014). The EDN has 6 three-phase and 2 one-phase radial LV feeders, and supplies 663 users following a residential load pattern based on the diversified demand presented in Quirós-Tortós et al. (2016). The whole conventional demand is 238.5 kVA (35.94%), 220.35 kVA (33.21%), and 204.65 kVA (30.85%), connected to phases A, B, and C, respectively. The hourly energy cost and load variation percentages are shown in Fig. 37.

Moreover, important features for the controlled devices connected to the grid are described as follows. Adopted considerations are similar to those presented on well-known references regarding control strategies for specific devices; e.g., (WECKX; GONZALEZ; DRIESEN, 2014) for PV units, (QUIRóS-TORTóS et al., 2016) for EVs, and (ELNOZAHY; ABDEL-GALIL; SALAMA, 2015) for ESSs.

Figure 36 – Topology of the test system: a) MV network; b) LV network.

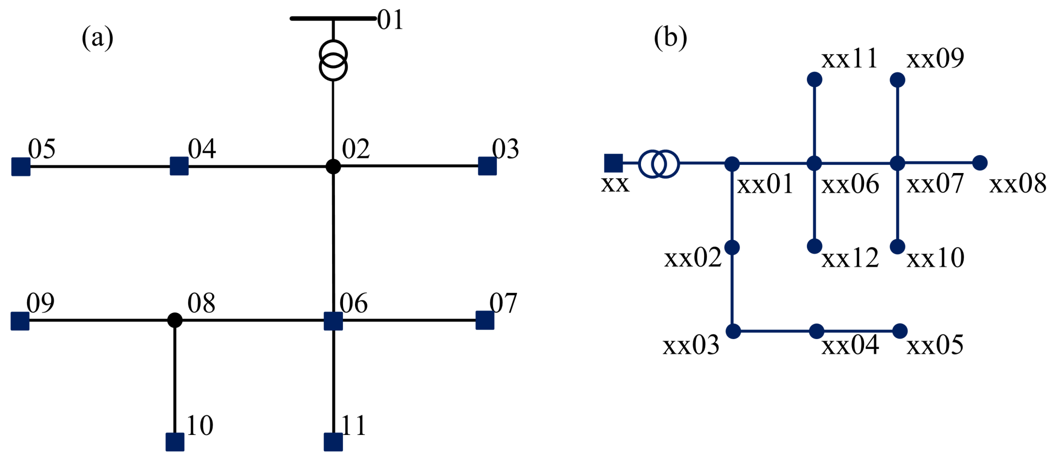

Source: Created by the author.

PV units

A penetration of 60% was considered for the PV units, i.e., 60% of the users connected to the EDN own a PV unit. This represents 400 PV units connected to the grid. Moreover, it was assumed that the nominal power PV units was 5 kW and α^{PV} was set at 20 ¢/kWh. When not managed, the PV units were assumed to inject all the available power generation into the grid.

Given that operational issues caused by PV penetration appear mainly on days with high PV generation, a clear–day profile was used for the available PV generation in

Figure 37 – Hourly energy costs and load variation.

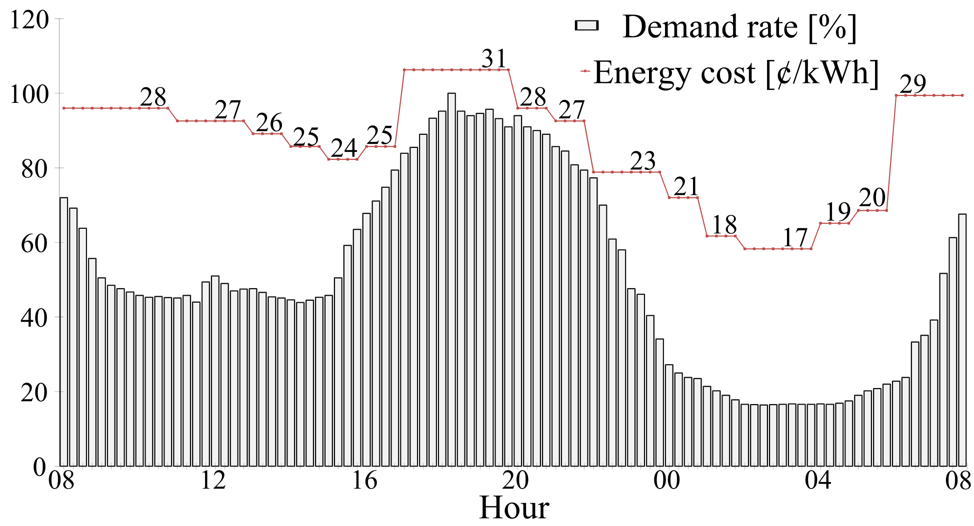

Source: Created by the author.

all test cases. This profile, as well as the average PV generation profile for clear days, is shown in Fig. 38.

EVs

A penetration of 40% was considered for the EVs. It was assumed that the EVs are 'Nissan Leaf' with a battery capacity of 24 kWh. Due to the focus on residential networks, the slow charging mode was only considered, i.e., chargers with a constant charging power of 3.6 kW and 83.33% efficiency (NISSAN, 2014). When no control was available over an EV, it was assumed that the battery will continuously charge until it reaches its full capacity or is disconnected by the owner.

ESSs

All ESSs were assumed to have DODs equal to 10% and located downstream from the MV/LV distribution transformers (ELNOZAHY; ABDEL-GALIL; SALAMA, 2015). Three different sizes for ESSs were considered: 1 MWh/150 kW (in the LV feeder at node 6); 500 kWh/50 kW ESSs (in the LV feeders at nodes 3, 4, 5, 7, and 11); and 100 kWh/15 kW ESSs (in the LV feeders at nodes 9 and 10).

OLTC

The OLTC installed at the HV/MV substation transformer, could vary the voltage with a regulation ratio of ±5%; in addition, this ratio was equally distributed across 9 tap positions. When not managed, a pre–set control, which defines a -2.5% voltage regulation from 08:00 a.m. to 16:00 p.m. and a +2.5% voltage regulation in any other time of the day, was established. These settings were defined to reduce the voltage at the beginning of the feeder during high PV generation time intervals and to increase it at low PV generation and high–demand time intervals. By these means, voltage limit violations are avoided.

Figure 38 – PV generation profile.

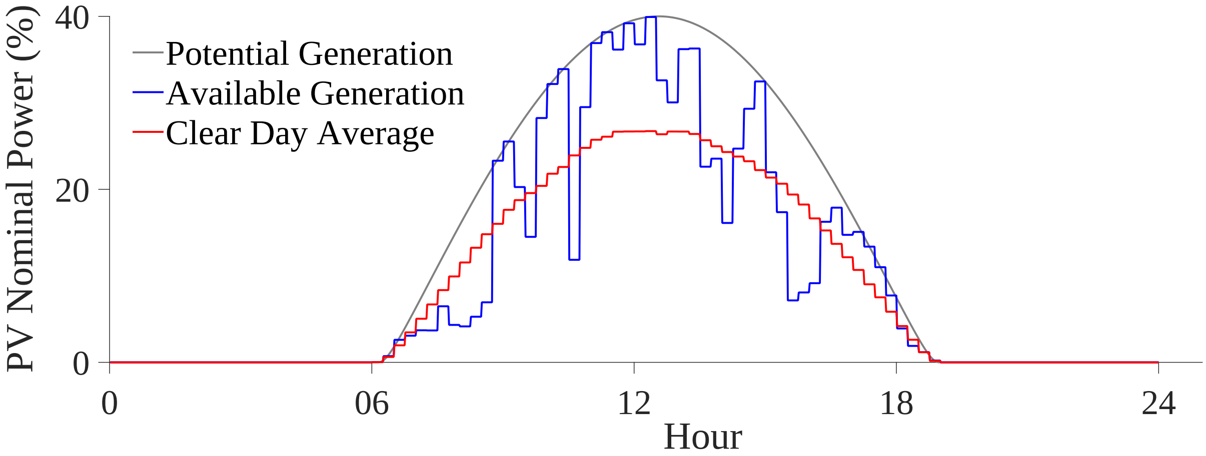

Source: Created by the author.

5.4.2 Test Cases

Tests were carried out for four different cases. Table 12 summarizes, for each case, the control availability over the PV units, EVs, ESSs, and OLTC.

Base Case

No management is enabled for PV units and EVs, the ESSs were not installed, and the OLTC follows the pre-set control settings; i.e., no management is done and the results reflect the operation of the EDN for the demand and PV generation profiles in Figs. 37 and 38.

Case I

No management is enabled for PV units and EVs; on the other hand, it is assumed that ESSs were installed and their control enabled in the EDN, and the OLTC management is also available. Due to the disabling of the management over PV units and EVs for this case, conservative lower and upper voltage limits (0.92 p.u. and 1.08 p.u.) were used in order to guarantee the fulfillment of the operational constraints regarding random changes on the PV generation.

Case II

The management over the PV units, the EVs, and the OLTC is enabled; notwithstanding, it is assumed that no ESSs were installed in the EDN.

Case III

All managements were enabled.

A summary of the results for all test cases is presented in Table 13. The cost of the imported energy (CIE) and the cost of the exported energy (CEE), related to the power exchange between the EDN and the external grid, are presented in columns 2 and

3, respectively. This power exchange is better illustrated along the entire time period in Fig. 39, where the active power flow through the HV/MV transformer installed in the substation node is shown. By convention, when the EDN is importing power from the main grid, the flow is positive; when the EDN is exporting, the flow is negative. Furthermore, column 4 shows the cost paid to the PV unit owners (CEPV) due to the energy produced, while columns 5 and 6 present the average SOC at departure for all EVs ($\tilde{E}_e^{EV}$) and the percentage of the available PV energy that was curtailed (PVEC), respectively. Finally, column 7 shows the maximum loading in the substation transformer in the evaluated time period; showing how the application of the control method not only improves the economic operation and encourages the self-consumption of renewable distributed generation, but also conveys to the fulfillment of the operational constraints in the EDN. It can be seen, how the overloading in the substation transformer shown in Case I was reduced by more than 40% in Case II, while Case III and Case IV do not present violations.

Table 12 – Control availability for test cases

Case	PV Units	EVs	ESSs	OLTC
Base	X	X	X	Pre-set
I	X	X	✓	✓
II	✓	✓	X	✓
III	✓	✓	✓	✓

Source: Created by the author.

Table 13 – Summary for test cases

Case	CIE ($)	CEE ($)	CEPV ($)	$\tilde{E}_e^{EV}$ (%)	PVEC (%)	HV/MV max loading (%)
Base	151.05	94.58	234.6	100	0	152.78
I	75.46	58.15	234.6	100	0	111.36
II	136.96	69.44	196.1	100	16.41	95.18
III	66.65	45.20	215.79	100	8.02	92.45

Source: Created by the author.

The maximum loading of all transformers in the EDN along the studied time period are presented in Fig. 40. The HV/MV substation transformer loading and the maximum loading among the MV/LV distribution transformers are shown, evidencing overloading in the EDN at high PV generation (Base Case and Case I). Furthermore, the maximum and minimum voltage magnitude profiles in the EDN are shown in Fig. 41. It can be seen that there were no voltage limit breaches, not even in the Base Case, hence the preset control defined for the OLTC is enough to cope with potential voltage limit outstrips.

The results of the control decisions defined by the rolling multi–period method for the ESSs, PV units, and EVs are illustrated in Figs. 42–44. The energy level of the ESSs along the time period is shown, for Cases I and III, in Fig. 42. The energy injected into the ENS by the PV units without PV generation control (Base Case and Case I) and with PV management (Cases II and III) can be observed in Fig. 43. Likewise, Fig. 44 shows the EV demand along the time period without control (Base Case and Case I) and when the EV control was enabled (Cases II and III).

Figure 39 – HV/MV transformer active power flow.

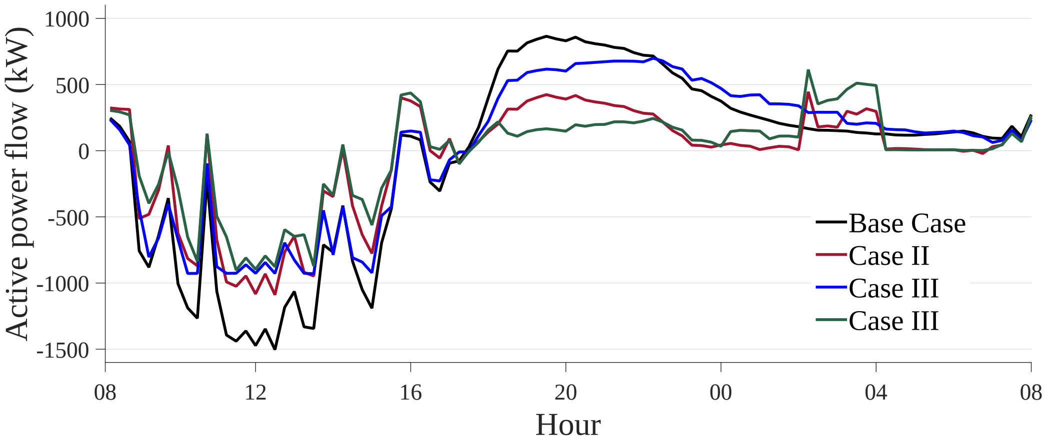

Source: Created by the author.

Centralized control optimization avoids voltage and thermal limit issues in every phase of the feeders in the EDN, as shown in Figs. 40 and 41. It can be seen how the sole inclusion of ESSs, without any management over PV units and EVs (Case I), not only eliminates thermal violations at the HV/MV transformer, but also reduces thermal breaches in the MV/LV transformers in about 50% of the nominal capacity.

All cases get a lower value of CIE in comparison with the Base Case, as shown in Table 13. Nevertheless, Cases I and III show better results due to the enabling of the ESSs. These devices permit a better exploitation of the PV energy, as they charge in high PV generation time intervals and discharge in load peak time intervals; this fact is clearly shown in Fig. 42 in which all the ESSs follow a similar charging/discharging pattern. Hence, the active power flow magnitude is reduced in both the high PV generation time intervals and load peak time interval for the aforementioned cases (Fig. 39).

Moreover, when the EV control is enabled, the EV demand is shifted to beneficial time intervals, avoiding the overlap of EV load peaks and conventional demand. By this means, the EVs are charged at low-cost energy time intervals, while overloads due to peak demand are prevented.

The best operation for the EDN was found when all managements were enabled (Case III). The results show how the joint optimization of PV units, EVs, and ESSs in a centralized control lead to an improved operation of the EDN. This case presented the lowest values of CIE and CEE, which means an improvement in the economic operation and an upturn in the self-consumption of the PV generation. Furthermore, it avoids all technical breaches, attending to all EV users and presenting the lowest curtailments on the PV units.

Figure 40 – Transformer loadings.

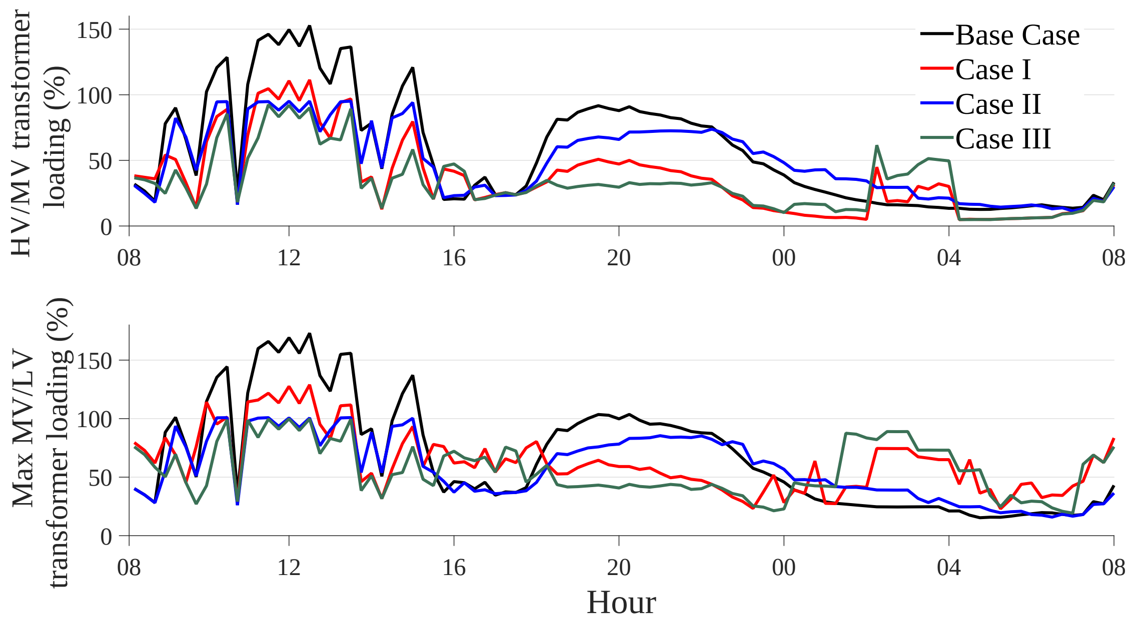

Source: Created by the author.

Figure 41 – Maximum and minimum voltages in the EDN.

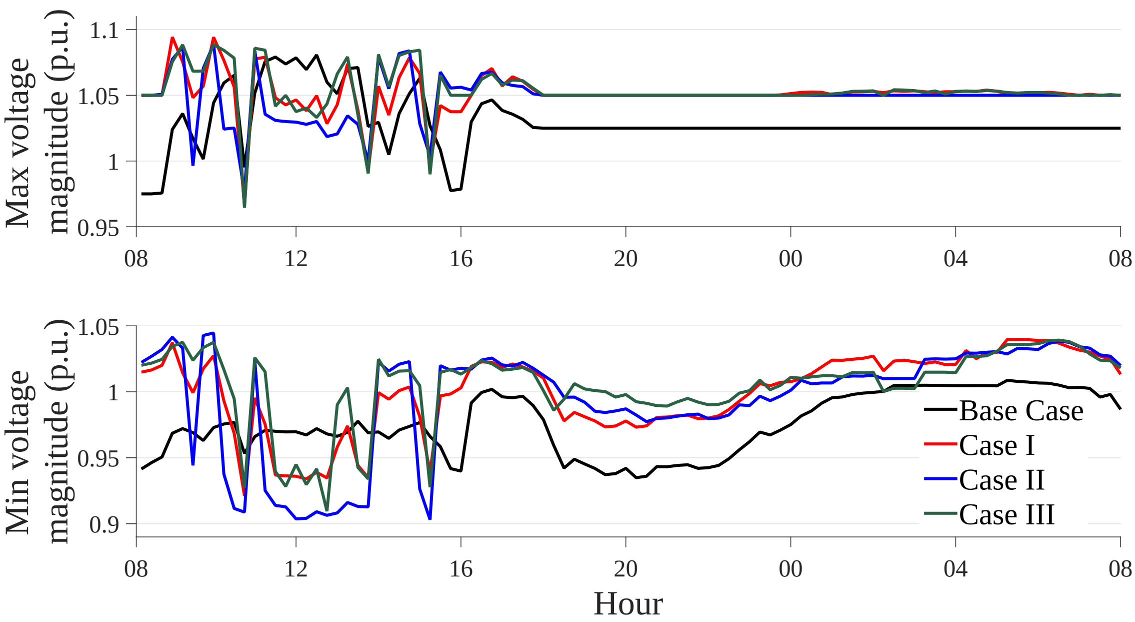

Source: Created by the author.

5.5 DISCUSSION

Although a traditional EV charging schedule was proposed in this work (i.e., the method define a charging or an idle state for the EVs), further advantages regarding the energy interaction between EVs and the EDN can be considered. It is important to remark that the proposed EV charging scheme was selected as a nowadays suitable control for residential EV chargers, where the implementation of complex and more elaborated chargers is yet uncertain. Nevertheless, with the advances on EV smart

Figure 42 – ESS energy level.

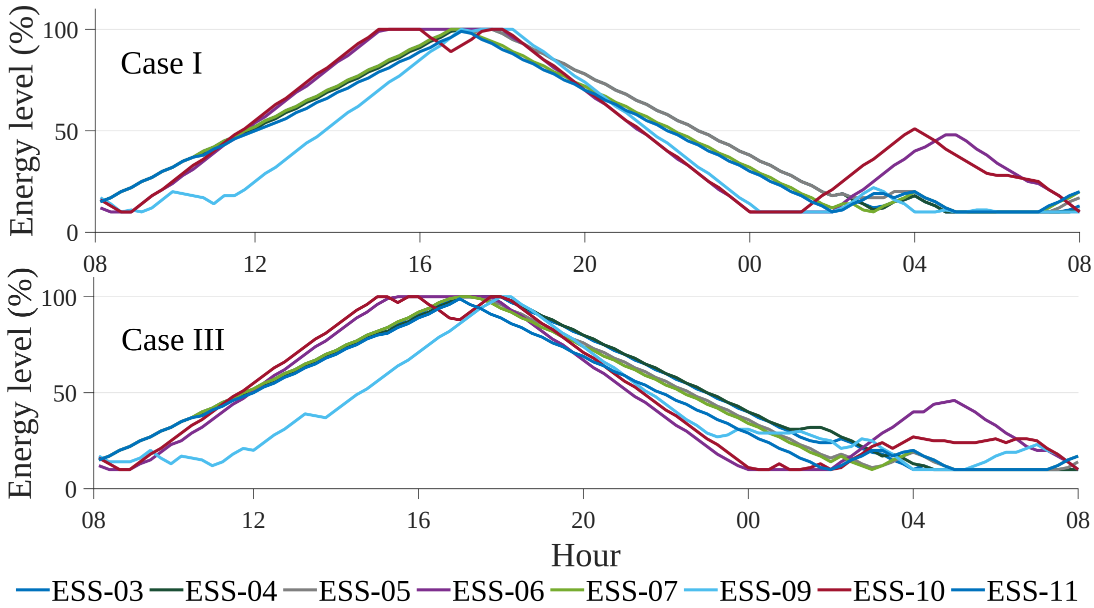

Source: Created by the author.

Figure 43 – PV power generation.

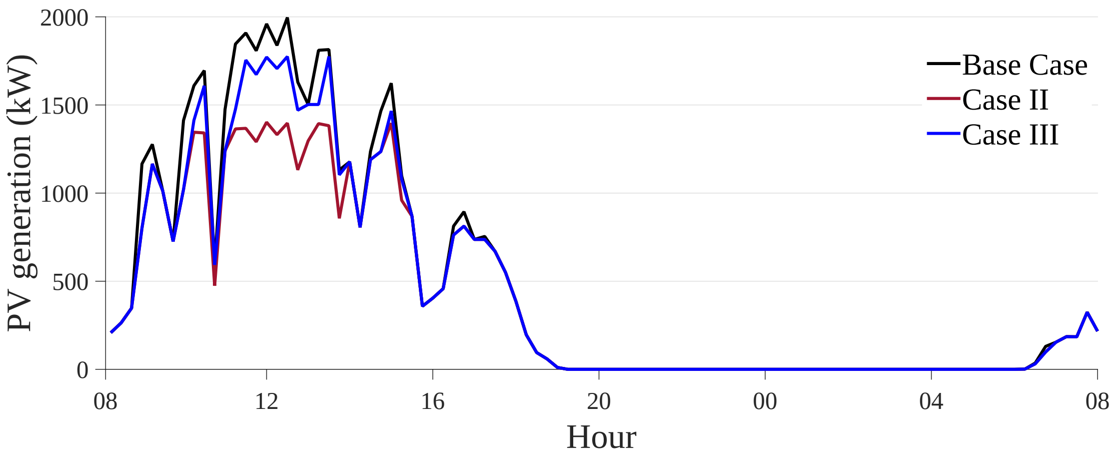

Source: Created by the author.

Figure 44 – EV power demand.

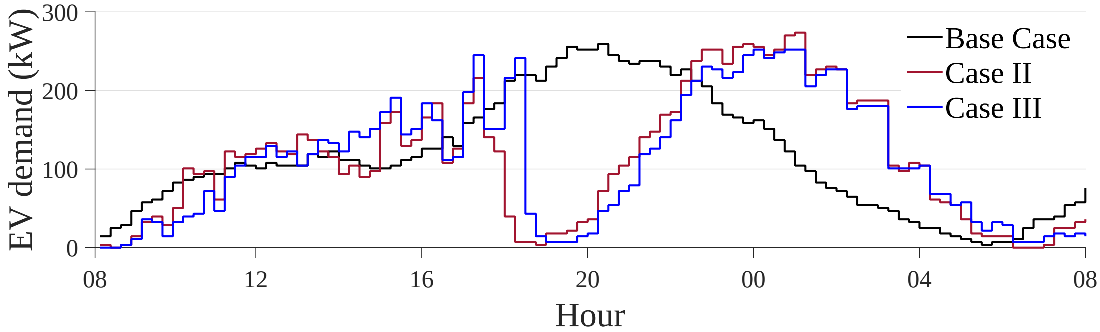

Source: Created by the author.

charging technologies, improvements in EV flexibility services can be taken into account in future approaches. This features, also known as EV ancillary services, can be included within charging strategies in order to achieve technical or economic objectives. The V2G feature, which can be defined as the purveyance of energy from an EV to the grid, stands out as a well-studied EV ancillary service (AL-AWAMI; SORTOMME, 2012). Hence, the presented framework can be easily adapted to include V2G, adopting the EV mathematical representation proposed in (ANTUNEZ et al., 2016b).

The results obtained demonstrate that the rolling multi–period optimization based on a MILP model provides a suitable controlled operation for the unbalanced three phase EDN. Therefore, technical issues that commonly appear on EDNs with high penetration of PV units and EVs were avoided, coping with uncertainties related to weather and EV owner's behavior without the need of multiple scenarios. Nevertheless, large real–time deviations, which can potentially happen between time intervals (e.g., lingering cloud passages or a simultaneous disconnection of EVs in several households), may affect and/or disrupt the execution of the optimal schedule. Hence, further studies can be undertaken to adopt probabilistic methods (e.g., (ELNOZAHY; ABDEL-GALIL; SALAMA, 2015) and (PROCOPIOU; QUIROS-TORTOS; OCHOA, 2017) employed for the maximization of ESS benefits and EV control, respectively) within the presented approach.

Finally, the proposed approach requires a smart grid environment for its proper implementation in residential EDNs. Hence, a communication infrastructure which allows data exchange between a programmable unit, hosting the decision-making algorithm, and the controlled devices is essential. Nevertheless, when several EVs and PV units are simultaneously operated by a centralized control, an outsized control signaling overhead might jeopardize the algorithm efficiency. Therefore, future works must address this issue to avoid possible communication issues.

5.6 CHAPTER CONCLUSIONS

A dynamic scheduling method for the joint optimal operation of EVs and PV units in unbalanced residential EDNs has been presented, taking into account installed ESSs and OLTC. The proposed formulation was tested on an 107-node distribution system (11 medium–voltage nodes and 96 low–voltage nodes). The proposed method makes it possible to find an optimal scheduling for the OLTC, EVs, PV units, and ESSs, thus mitigating all technical issues associated with high PV generation and peak demand.

By using an updated forecast, built using similar days historical data and the average PV generation of the last minutes, within a rolling multi–period optimization strategy, the methodology was capable of coping with uncertainties related to weather conditions and EV owner's; avoiding the complexity associated with the commonly used decision–making based on a large set of scenarios. A mixed-integer linear programming model was developed to define the OLTC tap positions, the optimal charging/discharging schedule for the ESSs, the power exchange between the PV units and the grid, and the optimal charging schedule for the EVs. Hence, the proposed method gives a broad view of the EDN operation state throughout a whole day–ahead.

Besides avoiding the technical limit breaches presented on an uncoordinated EDN, the results showed that the proposed centralized control method reduces the costs of energy imported from the main grid. Hence, the self-consumption of the PV energy generated as distributed generation in the EDN is encouraged, conciliating, by these means, the time difference between excessive generation and peak demand.

6 Conclusions & Future Works

This chapter presents conclusive remarks regarding the mathematical framework and the control algorithms presented. Besides, new lines of research are suggested to continue in the improvement of the electric distribution network mathematical representation.

6.1 Conclusions

A mathematical framework for optimization analysis of the electric distribution network (EDN) operation, which makes it possible to formalize decision-making processes, has been presented. Two mathematical formulations for the steady-state operation of EDN that consider the unbalance of three-phase networks were developed, considering mathematical representations for the operational limits and several smart-grid-related devices (e.g., electric vehicles, energy storage systems (ESS), voltage regulators (VR/OLTC), and capacitor banks).

Results showed that both representations of the steady-state operation of the EDN offer a good accuracy. Built as linear programming formulations, objectives related to technical and/or economic aspects can be pursued within the framework, using commercial solvers to find the global optimum of the problem.

Several algorithms were developed addressing the importance of the integration of EV charging points, renewable DG, ESSs, Volt-VAr control devices, and a grid interface. Unified control schemes in EDNs will enhance the hosting capability of the grid, while avoiding technical limit breaches. The proposed methods can be used on unbalanced EDNs, specially over residential feeders with high penetration of PV units and EV charging points. Nevertheless, the implementation of these approaches entail a smart grid environment; i.e., the grid must offer technological requirements such as:

- ESSs and Volt-VAr devices installed in the grid that can be managed by the EDN operators.
- A simple market scheme in which the EDN is enable to control the charging states of the EVs and the power injection of PV units in the households.
- A communication infrastructure, proper of smart grids, that enables the data exchange between the EDN operator and the controlled devices along the grid. Therefore, at each time interval a EDN operator will receive/send the inputs/outputs required to develop the proposed centralized decision–making scheme.

A step-by-step methodology was presented to solve the optimal charging coordination of EV in unbalanced EDN considering vehicle-to-grid (V2G) technology. The proposed method can be used to define optimal charging schedules in order to avoid operational concerns associated with uncontrolled EV recharging. The methodology was proven to efficiently handle EV load imbalance; randomness in EVs' arrival and departure times, and initial state of charge; different battery sizes; and forecast uncertainties. In addition, the charging schedules satisfied operational constraints, taking into account the imbalance of the system circuits and loads; they also achieved a better economical operation of the EDN.

A methodology for the electric vehicle charging coordination (EVCC) problem considering Volt-VAr control (VVC), ESS operation, and dispatchable distributed generation (DG) units in a three-phase unbalanced electrical distribution network (EDN), taking into account a voltage dependent load model, was presented. Moreover, this methodology handles the randomness in the electric vehicle (EV) arrival and departure times, initial state of charge, battery sizes, and forecast errors. The results showed that the optimized operation of the DG, ESD, VVC devices, and EV recharge represented an overall energy cost reduction and guaranteed the avoidance of technical limit violations. The dynamic coordination was proved to be efficient, because it defines the step to be implemented and gives a broad view of the EDN state throughout the whole time period.

A dynamic scheduling method for the joint optimal operation of EVs and photovoltaic (PV) units in unbalanced residential EDNs has been presented, taking into account installed ESSs and OLTC. The proposed method makes it possible to find an optimal scheduling for the OLTC, EVs, PV units, and ESSs, thus mitigating all technical issues associated with high PV generation and peak demand. Besides avoiding the technical limit breaches presented on an uncoordinated EDN, the results showed that the proposed centralized control method reduces the costs of energy imported from the main grid. Hence, the self-consumption of the PV energy generated as distributed generation in the EDN is encouraged, conciliating, by these means, the time difference between excessive generation and peak demand.

6.2 Future Works

The proposed approaches employ an unbalanced representation of the EDNs, which is crucial to enforce voltage limits. Nevertheless, the proposed framework can be extended to consider further features associated to the system unbalance (e.g., the minimization of the voltage unbalance factor). This potential improvement represents the next challenge regarding the mathematical representation of the grid.

Further studies can be undertaken to adopt probabilistic methods within the presented approaches. This can improve the robustness of the solutions found by algorithms developed using the optimization framework presented.

Finally, future works may target a different scalability within EDNs. Decision-making processes can be decentralized in order to operate in EDNs that do not offer a complete communication infrastructure. Besides, methods in which the combination of metaheuristics with mathematical optimization for linear and nonlinear models is exploited, can be studied.

Bibliography

ACKERMANN, T.; ANDERSSON, G.; SÖDER, L. Distributed generation: A definition. *Electric Power Systems Research,* Lausane, v. 57, n. 3, p. 195–204, 2001. Cited on page 51.

AGHAEI, J. et al. Distribution expansion planning considering reliability and security of energy using modified PSO algorithm. *Energy,* Stanford, v. 65, p. 398 – 411, 2014. ISSN 0360-5442. Cited on page 20.

AHMADI, H.; MARTÍ, J. R.; DOMMEL, H. W. A framework for volt-var optimization in distribution systems. *IEEE Trans. Smart Grid,* Piscataway, v. 6, n. 3, p. 1473–1483, May 2015. Cited 5 times on pages 44, 58, 97, 98, and 102.

AKHAVAN-REZAI, E. et al. Managing demand for plug-in electric vehicles in unbalanced LV systems with photovoltaics. *IEEE Trans. Ind. Informat.,* Piscataway, v. 13, n. 3, p. 1057–1067, Jun. 2017. Cited on page 121.

AKHTAR, Z. et al. Smart loads for voltage control in distribution networks. *IEEE Trans. Smart Grid, Piscataway*, v. 8, n. 2, p. 937–946, Mar. 2017. Cited on page 121.

AL-AWAMI, A. T.; SORTOMME, E. Coordinating vehicle-to-grid services with energy trading. *IEEE Trans. Smart Grid*, Piscataway, v. 3, n. 1, p. 453–462, Mar. 2012. ISSN 1949-3053. Cited 3 times on pages 49, 70, and 138.

ALAM, M. J.; MUTTAQI, K. M.; SUTANTO, D. Effective utilization of available PEV battery capacity for mitigation of solar PV impact and grid support with integrated V2G functionality. *IEEE Trans. Smart Grid,* Piscataway, v. 7, n. 3, p. 1562–1571, May 2016. Cited on page 121.

ALAM, M. S. Conceptual framework of a solar PV based high voltage battery charging strategyfor PHEVs and EVs. *American Journal of Electrical Power and Energy Systems,* Guildoford, v. 2, n. 6, p. 137, Nov. 2013. Cited on page 121.

ALEIXO, L. et al. *A general framework for active distribution network planning*. In: .[S.l.: s.n.], 2013. p. 1–8. Cited 2 times on pages 16 and 51.

ANGLANI, N.; FATTORI, F.; MULIERE, G. Electric vehicles penetration and grid impact for local energy models. In: In: INTERNATIONAL ENERGY CONFERENCE AND EXHIBITION (ENERGYCON), 2012, Florence. *Proceedings...* Pistacaway: IEEE, 2012. p. 1009–1014. Cited 2 times on pages 48 and 68.

ANTUNEZ, C. S. et al. Optimal volt–var control operation for energy cost reduction in distribution systems considering a voltage dependent load model. In: TRANSMISSION DISTRIBUTION CONFERENCE AND EXPOSITION–LATIN AMERICA. *Proceedings...* Pistacaway: IEEE, 2016. p. 1–6. Cited 2 times on pages 22 and 24.

ANTUNEZ, C. S. et al. A new methodology for the optimal charging coordination of electric vehicles considering vehicle-to-grid technology. *IEEE Trans. Sust. Energy,* Piscataway, v. 7, n.2, p. 596–607, Apr. 2016. Cited 4 times on pages 24, 48, 121, and 138.

APPEN, J. von et al. Local voltage control strategies for PV storage systems in distribution grids. *IEEE Trans. Smart Grid*, Pistacaway, v. 5, n. 2, p. 1002–1009, Mar. 2014. ISSN 1949-3053. Cited 2 times on pages 121 and 123.

APS, M. *The MOSEK optimization tools manual - version 6.0.* Copenhagen, 2009. Cited on page 18.

AREFIFAR, S. A.; ORDONEZ, M.; MOHAMED, Y. A. R. I. Energy management in multi-microgrid systems - development and assessment. *IEEE Trans. Power Syst.*, Piscataway, v. 32, n2, p. 910–922, Mar. 2017. Cited 2 times on pages 120 and 121.

ATWA, Y. M. et al. Optimal renewable resources mix for distribution system energy loss minimization. *IEEE Trans. Power Syst.*, Piscataway, v. 25, n. 1, p. 360–370, Feb 2010. Cited on page 54.

ATZENI, I. et al. Demand-side management via distributed energy generation and storage optimization. *IEEE Trans. Smart Grid*, Piscataway, v. 4, n. 2, p. 866–876, Jun. 2013. ISSN 1949-3053. Cited 2 times on pages 98 and 119.

BADAWY, M. O.; SOZER, Y. Power flow management of a grid tied PV-Battery system for electric vehicles charging. *IEEE Trans. Ind. Appl.*, Piscataway, v. 53, n. 2, p. 1347–1357, Apr. 2017. Cited on page 121.

BARAN, M. E.; HSU, M.-Y. Volt/var control at distribution substations. *IEEE Trans. Power Systems*, Piscataway, v. 14, n. 1, p. 312–318, Feb. 1999. ISSN 0885-8950. Cited 2 times on pages 97 and 100.

BEVIS, T. et al. A review of phev grid impacts. In: NORTH AMERICAN POWER SYMPOSIUM, 41., 2009, [S. l.]. *Proceedings…* Pistacaway: IEEE, 2009. p. 1–6. Cited on page 68.

BISERICA, M. et al. Neural networks to improve distribution state estimation volt var control performances. *IEEE Trans. Smart Grid*, Piscataway, v. 3, n. 3, p. 1137–1144, Sep. 2012. ISSN 1949-3053. Cited 2 times on pages 97 and 98.

BOLLEN, M.; HASSAN, F. *Integration of distributed generation in the power system.* [S.l.: s.n.], 2011. Cited on page 51.

BONAMI, P.; LEE, J. *BONMIN Users' manual.* [S.l.], 2007. Cited on page 18.

BORGES, M. C. O.; FRANCO, J. F.; RIDER, M. J. Optimal reconfiguration of electrical distribution systems using mathematical programming. *Journal of Control Automation and Electrical Systems*, [S. l.], v. 25, n. 1, p. 103–111, Cited on page 21.

BOROZAN, V.; BARAN, M. E.; NOVOSEL, D. Integrated volt/var control in distribution systems. In: POWER ENG. SOC. WINTER MEETING. CONFERENCE PROCEEDINGS (Cat. No.01CH37194). *Proceedings…* [S.l.: s.n.], 2001. v. 3, p. 1485–1490. Cited on page 97.

BOYD, S. P. et al. Distributed optimization and statistical learning via the alternating direction method of multipliers. *Foundations and Trends in Machine Learning*, Hanover, v. 3, n. 1, p. 1–122, 2011. Cited on page 22.

BYRD, R. H.; NOCEDAL, J.; WALTZ, R. A. Knitro: An integrated package for nonlinear optimization. In: ______. *Large–scale nonlinear optimization*. Boston: Springer, 2006. p. 35–59. Cited 2 times on pages 18 and 20.

CESPEDES, R. G. New method for the analysis of distribution networks. *IEEE Trans. Power Del.*, Pistacaway, v. 5, n. 1, p. 391–396, Jan. 1990. Cited on page 25.

CHENG, L.; CHANG, Y.; HUANG, R. Mitigating voltage problem in distribution system with distributed solar generation using electric vehicles. *IEEE Trans. Sustain. Energy*, Pistacaway, v. 6, n. 4, p. 1475–1484, Oct. 2015. Cited on page 121.

CIVANLAR, S.; GRAINGER, J. J. Volt/var control on distribution systems with lateral branches using shunt capacitors and voltage regulators part i: The overall problem. *IEEE Trans. Power App. and Syst.*, Pistacaway, PAS-104, n. 11, p. 3278–3283, Nov. 1985. ISSN 0018-9510. Cited on page 97.

CLEMENT-NYNS, K.; HAESEN, E.; DRIESEN, J. The impact of charging plug-in hybrid electric vehicles on a residential distribution grid. *IEEE Trans. Power Syst.*, Pistacaway, v. 25, n. 1, p. 371–380, Feb. 2010. ISSN 0885-8950. Cited 4 times on pages 48, 118, 119,and 121.

DABIC, V. et al. Bc hydro's experience on voltage var optimization in distribution system. In: TRANSMISSION AND DISTRIBUTION CONFERENCE AND EXPOSITION, 2010, New Orleans. *Proceedings*... Pistacaway: IEEE, 2010. p. 1–7. Cited on page 102.

DANDENO, P. L. et al. System load dynamics–simulation effects and determination of load constants. *IEEE Trans. Power Del.*, Pistacaway, PAS-92, n. 2, p. 600–609, Mar. 1973. Cited on page 44.

DAS, R. et al. Mathematical modeling for economic evaluation of electric vehicle to smart grid interaction. *IEEE Trans. Smart Grid*, Pistacaway, v. 5, n. 2, p. 712–721, Mar. 2014. ISSN 1949-3053. Cited on page 98.

DEILAMI, S. et al. Real-time coordination of plug-in EV charging in smart grids to minimize power losses and improve voltage profile. *IEEE Trans. Smart Grid*, Pistacaway, v. 2, n. 3, p. 456–467, Sep. 2011. ISSN 1949-3053. Cited 3 times on pages 69, 98, and 99.

DELGADO, G. M. noz; CONTRERAS, J.; ARROYO, J. M. Joint expansion planning of distributed generation and distribution networks. IEEE Trans. Power Syst., Pistacaway, v. 30, n. 5, p. 2579-2590, 2015. ISSN 1932-5517. Cited on page 20.

DISTRIBUTION Test systems, 109 bus test system. Disponível em: <http://tinyurl.com/oeojrkr>. Cited on page 131.

DISTRIBUTION test systems, 33 bus test system with secondary network. Disponível em: <http://tinyurl.com/oeojrkr>. Cited 2 times on pages 110 and 111.

DUSABE, D.; MUNDA, J.; JIMOH, A. Modelling of cloudless solar radiation for PV module performance analysis. *Journal of Electrical Engineering*, Manchester, v. 60, n. 4, p. 192–197, 2009. Cited on page 123.

ELNOZAHY, M.; ABDEL-GALIL, T. K.; SALAMA, M. Probabilistic ESS sizing and scheduling for improved integration of PHEVs and PV systems in residential distribution systems. *Electric Power Systems Research*, Lausanne, v. 125, p. 55 – 66, 2015. ISSN 0378-7796. Cited 6 times on pages 55, 119, 121, 131, 132, and 138.

ENERGY, U. D. of. *What is the smart grid?* [S. l.: s. n.], 2016. Disponível em: <www.smartgrid. gov>. Cited on page 16.

EUROPEAN COMMISSION. *EU Energy, transport and GHG emissions: Reference Scenario 2013*. 2014. Cited on page 118.

FOURER, R.; GAY, D. M.; KERNIGHAN, B. W. *AMPL: A modeling language for mathematical programming*. 2. ed. Pacific Grove: CA: Brooks/Cole-Thomson Learning, 2003. Cited 7 times on pages 20, 21, 36, 82, 93, 112, and 130.

FRANCO, J. F. et al. A mixed-integer lp model for the reconfiguration of radial electric distribution systems considering distributed generation. *Electric Power Systems Research*, Lausanne, v. 97, p. 51–60, Apr. 2013. Cited 2 times on pages 22 and 63.

FRANCO, J. F.; RIDER, M. J.; ROMERO, R. A mixed-integer quadratically-constrained programming model for the distribution system expansion planning. *International Journal of Electrical Power & Energy Systems*, Oxford, v. 62, p. 265 – 272, 2014. ISSN 0142-0615. Disponível em: <//www.sciencedirect.com/science/article/pii/S0142061514002439>. Cited 2 times on pages 19 and 20.

FRANCO, J. F.; RIDER, M. J.; ROMERO, R. A mixed-integer linear programming model for the electric vehicle charging coordination problem in unbalanced electrical distribution systems. *IEEE Trans. Smart Grid*, Pistacaway, v. 6, n. 5, p. 2200–2210, Sep. 2015. ISSN 1949-3053. Cited 8 times on pages 22, 28, 73, 109, 119, 121, 125, and 128.

GANGULY, S.; SAHOO, N. C.; DAS, D. Recent advances on power distribution system planning: a state-of-the-art survey. *Energy Systems*, Piscataway, v. 4, n. 2, p. 165–193, 2013. ISSN 1868-3975. Disponível em: <http://dx.doi.org/10.1007/s12667-012-0073-x>. Cited on page 19.

GAO, S. et al. Integrated energy management of plug-in electric vehicles in power grid with renewables. *IEEE Trans. Veh. Technol.*, Pistacaway, v. 63, n. 7, p. 3019–3027, Sep. 2014. Cited 2 times on pages 120 and 121.

GOMEZ, J. F. et al. Ant colony system algorithm for the planning of primary distribution circuits. *IEEE Transactions on Power Systems*, Pistacaway, v. 19, n. 2, p. 996–1004, May 2004. ISSN 0885-8950. Cited on page 20.

GONCALVES, R.; ALVES, P. R.; RIDER, M. J. Um modelo linear inteiro misto para o planejamento da operacao de redes de distribuicao de energia eletrica. In: CONGRESSO BRASILEIRO DE AUTOMATICA – CBA, 2012, [S. l.]. *Anais...* [S.l.: s.n.], 2012. *Cited on page 21.*

GONCALVES, R. dos R. *Modelos de programacao linear inteira mista para resolver problemas de otimizacao de sistemas de distribuicao de energia elétrica radiais*. Tese (Doutorado) Faculdade de Engenharia - UNESP, Ilha Solteira - SP, 2013. Cited on page 20.

GONEN, T.; RAMIREZ-ROSADO, I. J. Review of distribution system planning models: a model for optimal multistage planning. *IEE Proceedings C - Generation, Transmission and Distribution*, Piscataway, v. 133, n. 7, p. 397–408, Nov. 1986. Cited on page 20.

GUNTER, S. J.; AFRIDI, K. K.; PERREAULT, D. J. Optimal design of grid-connected pev charging systems with integrated distributed resources. *IEEE Trans. Smart Grid*, Pistacaway, v4, n. 2, p. 956–967, Jun. 2013. Cited on page 121.

HAFFNER, S. et al. Multistage model for distribution expansion planning with distributed generation part I: problem formulation. *IEEE Trans. Power Del.*, Pistacaway, v. 23, n. 2, p. 915–923, Apr. 2008. ISSN 0885-8977. Cited on page 20.

HAN, S.; HAN, S.; SEZAKI, K. Development of an optimal vehicle-to-grid aggregator for frequency regulation. *IEEE Trans. Smart Grid*, Pistacaway, v. 1, n. 1, p. 65–72, Jun. 2010. ISSN 1949-3053. Cited 2 times on pages 70 and 92.

HE, Y.; VENKATESH, B.; GUAN, L. Optimal scheduling for charging and discharging of electric vehicles. *IEEE Trans. Smart Grid*, Pistacaway, v. 3, n. 3, p. 1095–1105, Sep. 2012. ISSN 1949-3053. Cited 2 times on pages 70 and 98.

INTERNATIONAL ENERGY AGENCY. – I.E.A. *World Energy Outlook*. [S. l.], 2012. Cited on page 118.

IEEE task force on load representation for dynamic performance. Bibliography on load models for power flow and dynamic performance simulation. *IEEE Trans. Power Sys.*, Pistacaway, v. 10, n. 1, p. 523–538, Feb. 1995. Cited 2 times on pages 45 and 102.

IEEE/PES. *Distribution Test Feeders, 123-bus Feeder.* Piscataway, 2012, Disponível em: <http://ewh.ieee.org/soc/pes/dsacom/testfeeders.> Access in: Mar 2018, Cited 3 times on pages 36, 80, and 92.

ILOG INC. *IBM ILOG CPLEX V12.1 User's manual for CPLEX*. Incline Village, 2009. Cited 7 times on pages 18, 21, 36, 82, 93, 112, and 130.

INC., G. O. *Gurobi optimizer reference manual.* [S.l.], 2014. Disponível em: <Www.Gurobi.Com>. Access in: Mar. 2018. Cited on page 18.

JABR, R. A. Polyhedral formulations and loop elimination constraints for distribution network expansion planning. *IEEE Trans. on Power Sys.*, Pistacaway, v. 28, n. 2, p. 1888–1897, May 2013. ISSN 0885-8950. Cited on page 20.

KARFOPOULOS, E. L.; HATZIARGYRIOU, N. D. A multi-agent system for controlled charging of a large population of electric vehicles. *IEEE Trans. Power Systems*, Pistacaway, v. 28, n. 2, p. 1196–1204, May 2013. ISSN 0885-8950. Cited on page 69.

KEMPTON, W.; TOMIC, J. Vehicle-to-grid power fundamentals: Calculating capacity and net revenue. *Journal of Power Sources*, Lausanne, v. 144, n. 1, p. 268–279, Jun. 2005. Cited on page 70.

KORUNOVIC, L. M. et al. Processing of load parameters based on existing load models. In: IEEE PES INNOVATIVE SMART GRID TECHNOLOGIES EUROPE (ISGT EUROPE), 3rd., 2012, [S. l.]. *Proceedings*… [S. l.: s. n.], 2012. p. 1–6. Cited 2 times on pages 45 and 102.

KUMAR, K. N. et al. V2g capacity estimation using dynamic ev scheduling. *IEEE Trans. Smart Grid*, Pistacaway, v. 5, n. 2, p. 1051–1060, Mar. 2014. Cited on page 70.

LAVORATO, M. et al. Imposing radiality constraints in distribution system optimization problems. *IEEE Trans. Power Sys.*, Pistacaway, v. 27, n. 1, p. 172–180, Feb. 2012. ISSN 0885-8950. Cited 2 times on pages 20 and 21.

LIN, S. et al. Impact of plug-in hybrid electric vehicles on distribution systems. In: POWER SYSTEM TECHNOLOGY (POWERCON), 2010 INTERNATIONAL CONFERENCE ON., 2010, [S. l.]. *proceedings...* [S. l.: s.n.], 2010. p. 1–5. Cited 3 times on pages 68, 98, and 119.

LIU, L. et al. Economic assessment of lithium-ion batteries in terms of V2G utilisation. In: INTERNATIONAL CONFERENCE AND EXPOSITION ON ELECTRICAL AND POWER ENGINEERING, 2012, [S. l.]. *Proceedings...* [S.l.: s.n.], 2012. p. 934–938. Cited 2 times on pages 70 and 89.

LIU, N. et al. A heuristic operation strategy for commercial building microgrids containing EVs and PV system. *IEEE Trans. Ind. Electron.*, Pistacaway, v. 62, n. 4, p. 2560–2570, Apr. 2015. Cited on page 121.

LOJOWSKA, A. et al. Stochastic modeling of power demand due to EVs using copula. *IEEE Trans. Power Syst.*, Pistacaway, v. 27, n. 4, p. 1960–1968, Nov. 2012. ISSN 0885-8950. Cited 2 times on pages 73 and 103.

LOPES, J. A. P. et al. Integrating distributed generation into electric power systems: A review of drivers, challenges and opportunities. *Electric Power Systems Research*, v. 77, Lausanne, v. 77, n. 9, p. 1189–1203, 2007. Cited on page 51.

MACEDO, L. H. et al. Optimal operation of distribution networks considering energy storage devices. *IEEE Trans. Smart Grid*, Pistacaway, v. 6, n. 6, p. 2825–2836, Nov. 2015. ISSN 1949-3053. Cited 5 times on pages 21, 98, 119, 120, and 121.

MARRA, F. et al. Improvement of local voltage in feeders with photovoltaic using electric vehicles. *IEEE Trans. Power Syst.*, Pistacaway, v. 28, n. 3, p. 3515–3516, Aug. 2013. Cited on page 121.

MELGAR, O. D. et al. Planejamento da operacao de sistemas eletricos de distribuicao usando programacao conica. In: SOCIEDADE BRASILEIRA DE AUTOMATICA, 20., 2014, Belo Horizonte. *Anais...* Belo Horizonte: [s. n.], 2014. p. 2845-2852. Cited 2 times on pages 20 and 21.

MELO, J. D.; CARRENO, E. M.; PADILHA-FELTRIN, A. Spatial-temporal simulation to estimate the load demand of battery electric vehicles charging in small residential areas. *Journal of Control, Automation and Electrical Systems*, [S. l.], v. 25, n. 4, p. 470–480, 2014. ISSN 2195-3899. Cited 4 times on pages 73, 86, 103, and 124.

MOKHTARI, G.; NOURBAKHSH, G.; GHOSH, A. Smart coordination of energy storage units (ESUs for voltage and loading management in distribution networks. *IEEE Trans. Power Syst.*, Pistacaway, v. 28, n. 4, p. 4812–4820, Nov. 2013. Cited on page 121.

MOMOH., J. A. *Electric power system applications of optimization*. 2. ed. [S.l.]: CRC , 2009. Cited 2 times on pages 16 and 19.

NISSAN. Nissan specifications. [S.l.]. Disponível em: <http://www.nissanusa.com/electric-cars/leaf/>. access in: Nov. 2014, Cited 3 times on pages 80, 112, and 132.

NYKVIST, B.; NILSSON, M. Rapidly falling costs of battery packs for electric vehicles. [S. l.], *Nature Climate Change*, v. 5, n. 4, p. 329–332, Mar. 2015. Cited on page 90.

O'CONNELL, A.; KEANE, A.; FLYNN, D. Rolling multi-period optimization to control electric vehicle charging in distribution networks. In: *2014 IEEE PES General Meeting | Conference Exposition*. [S.l.: s.n.], 2014. p. 1–1. ISSN 1932-5517. Cited 6 times on pages 48, 69, 98, 119, 120, and 121.

PADILHA-FELTRIN, A.; QUIJANO, D.; MANTOVANI, J. R. Volt-var multiobjective optimization to peak-load relief and energy efficiency in distribution networks. *IEEE Trans. Power Del.*, Pistacaway, v. 30, n. 2, p. 618–626, Apr. 2015. Cited 6 times on pages 44, 58, 97, 98, 101, and 102.

PADILHA, L. N. *Analise comparativa de estrategias para regulacao de tensao em sistemas de distribuicao de energia eletrica na presenca de geradores distribuidos.* Dissertacao (Mestrado em Engenharia Eletrica) Escola de Engenharia de Sao Carlos, Universidade de Sao Paulo, Sao Carlos, 2010. Cited on page 20.

PAPADOPOULOS, P. et al. Coordination of the charging of electric vehicles using a multi-agent system. *IEEE Trans. Smart Grid*, Pistacaway, v. 4, n. 4, p. 1802–1809, Dec. 2013. ISSN 1949-3053. Cited on page 69.

PEREZ, E. et al. Predictive power control for PV plants with energy storage. *IEEE Trans. Sustain. Energy*, Pistacaway, v. 4, n. 2, p. 482–490, Apr. 2013. Cited on page 121.

PROCOPIOU, A. T.; QUIROS-TORTOS, J.; OCHOA, L. F. HPC-based probabilistic analysis of LV networks with EVs: Impacts and control. *IEEE Trans. Smart Grid*, Pistacaway, v. 8, n. 3, p. 1479–1487, May 2017. Cited on page 138.

QIAN, K. et al. Modeling of load demand due to ev battery charging in distribution systems. *IEEE Trans. Power Syst.*, Pistacaway, v. 26, n. 2, p. 802–810, May 2011. ISSN 0885-8950. Cited 2 times on pages 73 and 103.

QIAN, K. et al. Analysis of the environmental benefits of distributed generation. In: IEEE POWER AND ENERGY SOCIETY, 21th., 2008 , [S. l.]. *Proceedings...* Pistacaway: IEEE, 2008. p. 1-8. Cited on page 51.

QUEZADA, V. H. M.; ABBAD, J. R.; ROMAN, T. G. S. Assessment of energy distribution losses for increasing penetration of distributed generation. *IEEE Trans. Power Syst.*, Pistacaway, v. 21, n. 2, p. 533–540, May 2006. Cited on page 119.

QUIRóS-TORTóS, J. et al. Control of EV charging points for thermal and voltage management of LV networks. *IEEE Trans. Power Syst.*, Pistacaway, v. 31, n. 4, p. 3028–3039, Jul. 2016. Cited 3 times on pages 119, 121, and 131.

QUIRóS-TORTóS, J.; OCHOA, L. F.; LEES, B. A statistical analysis of EV charging behavior in the UK. In: INNOVATIVE SMART GRID TECHNOLOGIES LATIN AMERICA (ISGT LATAM), 2015, Montevideo. *Proceedings...* Pistacaway: IEEE PES, 2015. p. 445–449. Cited on page 124.

RAHIMI, S.; MARINELLI, M.; SILVESTRO, F. Evaluation of requirements for volt/var control and optimization function in distribution management systems. In: INTERNATIONAL ENERGY CONFERENCE AND EXHIBITION (ENERGYCON), 2012, Florence. *Proceedings...* Pistacaway: IEEE, 2012. p. 331–336. Cited on page 101.

RAMIREZ-ROSADO, I. J.; GONEN, T. Pseudodynamic planning for expansion of power distribution systems. *IEEE Trans. on Power Syst.*, Pistacaway, v. 6, n. 1, p. 245–254, Feb. 1991. ISSN 0885-8950. Cited on page 20.

RAVADANEGH, S. N.; ROSHANAGH, R. G. On optimal multistage electric power distribution networks expansion planning. *International Journal of Electrical Power & Energy Systems*, Oxford, v. 54, p. 487 – 497, 2014. ISSN 0142-0615. Cited on page 20.

RESENER, M. et al. Mixed-integer LP model for volt-var control and energy losses minimization in distribution systems. *Electric Power Systems Research*, Lausanne, v. 140, p. 895 –905, 2016. Cited on page 21.

RICHARDSON, I.; THOMSON, M. *Integrated domestic electricity demand and PV micro-generation model*. 2011. Disponível em: <https://dspace.lboro.ac.uk/dspace-jspui/handle/2134/7773>. access in: May, 2017. Cited on page 124.

RIFFONNEAU, Y. et al. Optimal power flow management for grid connected PV systems with batteries. *IEEE Trans. Sustain. Energy*, Pistacaway, v. 2, n. 3, p. 309–320, Jul. 2011. Cited on page 121.

ROBBINS, B. A.; DOMINGUEZ-GARCIA, A. D. Optimal reactive power dispatch for voltage regulation in unbalanced distribution systems. *IEEE Trans. Power Sys.*, Pistacaway, v. 31, n. 4, p. 2903–2913, Jul. 2016. ISSN 0885-8950. Cited on page 22.

ROMAIS, R.; BORGES, M. C.; RIDER, M. J. Reconfiguracao de sistemas de distribuicao de energia eletrica utilizando um modelo de programacao conica de segunda ordem. In: SIMPOSIO BRASILEIRO DE SISTEMAS ELETRICOS – SBSE, 2014, Foz do Iguaçu. *Anais...* Foz do Iguaçu: [s. N], 2014. Cited on page 22.

ROSS, M. et al. Analysis of energy storage sizing and technologies. In: EPEC 2010 -IEEE ELECTRICAL POWER AND ENERGY CONFERENCE: SUSTAINABLE ENERGY FOR AN INTELLIGENT GRID, 2010, Halifax. *Proceedings...* Pistacaway: IEEE, 2010. p. 1-6. Cited on page 55.

ROY, J. V.; BREUCKER, S. D.; DRIESEN, J. Analysis of the optimal battery sizing for plug-in hybrid and battery EVs on the power consumption and v2g availability. In: INTERNATIONAL CONFERENCE ON INTELLIGENT SYSTEM APPLICATIONS TO POWER SYSTEMS, 16th., 2011, Hersonissos. *Proceedings...* Pistacaway: IEEE, 2011. p. 1–6. Cited on page 70.

ROYTELMAN, I.; WEE, B. K.; LUGTU, R. L. Volt/var control algorithm for modern distribution management system. *IEEE Trans. Power Syst.*, Pistacaway, v. 10, n. 3, p. 1454–1460, Aug. 1995. Cited on page 97.

RUEDA-MEDINA, A. C. et al. A mixed-integer linear programming approach for optimal type, size and allocation of distributed generation in radial distribution systems. *Electric Power Systems Research*, Lausanne, v. 97, p. 133–143, 2013. Cited 3 times on pages 51, 52, and 53.

SABILLON-ANTUNEZ, C. et al. Volt-var control and energy storage device operation to improve the electric vehicle charging coordination in unbalanced distribution networks. *IEEE Trans. Sust. Energy*, Pistacaway, v. 8, n. 4, p. 1560–1570, Oct. 2017. Cited 3 times on pages 24, 44, and 55.

SCHAINKER, R. B. Executive overview: energy storage options for a sustainable energy future. In: POWER ENGINEERING SOCIETY GENERAL MEETING, 2004, Denver. *Proceedings...* Pistacaway: IEEE, 2004. p. 2309–2314. Cited on page 98.

SCHAUDER, C. *Advanced inverter technology for high penetration levels of PV generation in distribution systems.* [S.l.], 2016. Cited on page 123.

SCHNEIDER, K. P.; WEAVER, T. F. A method for evaluating volt-var optimization field demonstrations. *IEEE Trans. Smart Grid*, Pistacaway, v. 5, n. 4, p. 1696–1703, Jul. 2014. ISSN 1949-3053. Cited 2 times on pages 97 and 98.

SCHURMANN, D.; TIMPNER, J.; WOLF, L. Cooperative charging in residential areas. *IEEE Trans. Intell. Transp. Syst.*, Pistacaway, v. 18, n. 4, p. 834–846, Apr. 2017. Cited on page 121.

SHAABAN, M. F. et al. Real-time PEV charging/discharging coordination in smart distribution systems. *IEEE Trans. Smart Grid*, Pistacaway, v. 5, n. 4, p. 1797–1807, Jul. 2014. ISSN 1949-3053. Cited 4 times on pages 69, 119, 120, and 121.

SHAHNIA, F.; A, A.; LEDWICH, G. *Electric distribution network planning.* [S.l.]: Springer, 2018. Cited on page 24.

SHIRMOHAMMADI, D. et al. A compensation-based power flow method for weakly meshed distribution and transmission networks. *IEEE Trans. on Power Syst.*, Pistacaway, v. 3, n. 2, 753–762, May 1988. Cited on page 25.

SOJOUDI, S.; LOW, S. H. Optimal charging of PHEV in smart grids. In: POWER AND ENERGY SOCIETY GENERAL MEETING, 2011, Detroit. *Proceedings...* Pistacaway: IEEE, 2011. p. 1–6. Cited 3 times on pages 68, 69, and 123.

SOUZA, B. A. de; ALMEIDA, A. M. F. de. Multiobjective optimization and fuzzy logic applied to planning of the volt/var problem in distributions systems. *IEEE Trans. Power Syst.*, Pistacaway, v. 25, n. 3, p. 1274–1281, Aug. 2010. Cited on page 20.

TABARES, A. et al. Multistage long-term expansion planning of electrical distribution systems considering multiple alternatives. *IEEE Trans. Power Syst.*, Pistacaway, v. 31, n. 3, p. 1900–1914, May 2016. ISSN 0885-8950. Cited on page 19.

TANG, Y. Power distribution system planning with reliability modeling and optimization. *IEEE Trans. Power Sys.*, Pistacaway, v. 11, n. 1, p. 181–189, Feb 1996. ISSN 0885-8950. Cited on page 20.

TANT, J. et al. Multiobjective battery storage to improve PV integration in residential distribution grids. *IEEE Trans. Sust. Energy*, Pistacaway, v. 4, n. 1, p. 182–191, Jan. 2013. ISSN 1949-3029. Cited on page 119.

TELEKE, S. et al. Rule-based control of battery energy storage for dispatching intermittent renewable sources. *IEEE Trans. Sustain. Energy*, Pistacaway, v. 1, n. 3, p. 117–124, Oct. 2010. Cited on page 121.

TESLA-MOTORS. *Model specifications.* [S.l.], 2014. Disponível em: <http://www.teslamotors. com/models/specs>. Access in: 05 May 2014. Cited 3 times on pages 80, 92, and 112.

THOMSON, M.; INFIELD, D. G. Impact of widespread photovoltaics generation on distribution systems. *IET Renewable Power Generation*, Pistacaway, v. 1, n. 1, p. 33–40, Mar. 2007. ISSN 1752-1416. Cited 2 times on pages 119 and 121.

TONKOSKI, R.; LOPES, L. ; EL-FOULY, T. Coordinated active power curtailment of grid connected PV inverters for overvoltage prevention. *IEEE Trans. Sust. Energy*, Pistacaway, v. 2, n. 2, p. 139–147, Apr. 2011. Cited 2 times on pages 55 and 119.

TRIPPE, A.; MASSIER, T.; HAMACHER, T. Optimized charging of EVs with regard to battery constraints - case study: Singaporean car park. In: ENERGYTECH, 2013, Cleveland. *Proceedings...* Pistacaway: IEEE, 2013. p. 1–6. Cited 2 times on pages 69 and 119.

UNDA, I. et al. Management of electric vehicle battery charging in distribution networks with multi-agent systems. *Electric Power Systems Research*, Lausanne, v. 110, p. 172–179, May 2014. Cited 2 times on pages 69 and 92.

U.S. DEPARTMENT OF ENERGY. *International energy outlook 2013*. Washington DC, 2013. Cited 2 times on pages 43 and 118.

VERZIJLBERGH, R. A. et al. Network impacts and cost savings of controlled EV charging. *IEEE Trans. Smart Grid*, Pistacaway, v. 3, n. 3, p. 1203–1212, Sep. 2012. ISSN 1949-3053. Cited on page 119.

WANG, G. et al. Ergodic energy management leveraging resource variability in distribution grids. *IEEE Trans. Power Syst.*, Pistacaway, v. 31, n. 6, p. 4765–4775, Nov. 2016. Cited on page 123.

WANG, G. et al. Dispatch strategy of PHEVs to mitigate selected patterns of seasonally varying outputs from renewable generation. *IEEE Trans. Smart Grid*, Pistacaway, v. 6, n. 2, p. 627–639, Mar. 2015. Cited 2 times on pages 120 and 121.

WECKX, S.; DRIESEN, J. Load balancing with EV chargers and PV inverters in unbalanced distribution grids. *IEEE Trans. Sustain. Energy*, Pistacaway, v. 6, n. 2, p. 635–643, Apr. 2015. Cited on page 121.

WECKX, S.; GONZALEZ, C.; DRIESEN, J. Combined central and local active and reactive power control of PV inverters. *IEEE Trans. Sust. Energy*, Pistacaway, v. 5, n. 3, p. 776–784, Jul. 2014. Cited 3 times on pages 55, 119, and 131.

WEI, Q. et al. Adaptive dynamic programming-based optima control scheme for energy storage systems with solar renewable energy. *IEEE Trans. Ind. Electron.*, Pistacaway, v. 64, n. 7, p. 5468–5478, Jul. 2017. Cited on page 121.

WU, D.; ALIPRANTIS, D. C.; GKRITZA, K. Electric energy and power consumption by light-duty plug-in electric vehicles. *IEEE Trans. Power Syst.*, Pistacaway, v. 26, n. 2, p. 738–746, May 2011. Cited 4 times on pages 48, 68, 69, and 119.

YANG, X. et al. Optimal energy flow control strategy for a residential energy local network combined with demand-side management and real-time pricing. *Energy and Buildings*, Lausanne, v. 150, p. 177–188, 2017. Cited on page 121.

YAO, E. et al. Residential demand side management under high penetration of rooftop photovoltaic units. *IEEE Trans. Smart Grid*, Pistacaway, v. 7, n. 3, p. 1597–1608, May 2015. Cited on page 121.

ZHU, J. Operation of smart grid. In: ______. *Optimization of power system operation*. [S.l.]: Wiley-IEEE, 2015. p. 664–. Cited on page 15.